

THE EFFECT OF DUAL PARTICLE SIZE SIC REINFORCEMENTS AND HEAT TREATMENT ON MICROSTRUCTURE, MECHANICAL AND TRIBOLOGICAL PROPERTIES OF A357 COMPOSITES

Thesis

Submitted in partial fulfillment of the requirements for the Degree of

DOCTOR OF PHILOSOPHY

By

AVINASH L



**DEPARTMENT OF MECHANICAL ENGINEERING
NATIONAL INSTITUTE OF TECHNOLOGY KARNATAKA,
SURATHKAL, MANGALORE -575025**

JUNE, 2021

DECLARATION

I hereby declare that the Research Thesis entitled “**THE EFFECT OF DUAL PARTICLE SIZE SIC REINFORCEMENTS AND HEAT TREATMENT ON MICROSTRUCTURE, MECHANICAL AND TRIBOLOGICAL PROPERTIES OF A357 COMPOSITES**” which is being submitted to the **National Institute of Technology Karnataka, Surathkal** in partial fulfillment of the requirements for the award of the Degree of **Doctor of Philosophy** in **Department of Mechanical Engineering** is a *bonafide report of the research work carried out by me*. The material contained in this Research Thesis has not been submitted to any other Universities or Institutes for the award of any degree.

Register Number: **135064ME13P05**

Name of the Research Scholar: **AVINASH L**

Signature of the Research Scholar: 

Department of Mechanical Engineering

Place: NITK, Surathkal

Date: 03-06-2021

CERTIFICATE

This is to certify that the Research Thesis entitled “**THE EFFECT OF DUAL PARTICLE SIZE SIC REINFORCEMENTS AND HEAT TREATMENT ON MICROSTRUCTURE, MECHANICAL AND TRIBOLOGICAL PROPERTIES OF A357 COMPOSITES**” submitted by **Mr. AVINASH L (Register Number: 135064ME13P05)** as the record of the research work carried out by him, *is accepted as the Research Thesis submission* in partial fulfillment of the requirements for the award of the Degree of **Doctor of Philosophy**.

Research Guide



Dr. Srikanth Bontha

Associate Professor

Department of Mechanical Engineering

National Institute of Technology Karnataka, Surathkal



Chairman-DRPC

Date: 08/06/2021



Dedicated to

- ❖ *“God Muneshwara, Idagunji Ganapathi and Shree Sigandur Chowdeshwari”*
- ❖ *My beloved Grandmother Late Smt. Komala*
- ❖ *My beloved parent’s Smt. Hemalatha G and Sri. Lakshmikanthan M*
- ❖ *My beloved in-laws Smt. Chandrakala M and Sri. Manjunath DH*
- ❖ *My beloved wife Kirti M*
- ❖ *All my Teachers and Professors who taught and encouraged me with positive thoughts*

ACKNOWLEDGEMENTS

With a deep sense of gratitude, I wish to express my sincere thanks to my supervisor **Dr. Srikanth Bontha**, Associate Professor, Department of Mechanical Engineering, National Institute of Technology Karnataka (N.I.T.K), Surathkal, for his excellent guidance and support throughout the work. I received very useful, encouraging, and excellent academic feedback from him, which has stood in good stead while writing this thesis. I profoundly thank him.

I take this opportunity to thank **Prof. Kulkarni S. M.**, Professor and Head, Department of Mechanical Engineering for his continuous and timely suggestions. Thanks are due to **Prof. Prasad Krishna**, Professor, Department of Mechanical Engineering, *N.I.T.K, Surathkal*, for his moral support during my research work. I wish to express my sincere gratitude to all former HOD's, faculty members, technical and administrative staff of the Department of Mechanical Engineering, N.I.T.K, for their unbiased appreciation, support throughout this research work.

I sincerely thank my RPAC members, **Dr. Ramesh M.R.**, Associate Professor, Department of Mechanical Engineering, N.I.T.K and **Dr. Ravishankar K.S.**, Associate Professor, Department of Metallurgical and Materials Engineering, N.I.T.K for providing valuable suggestions and also for the support extended to me on all occasions. I am grateful to **Dr.T Ramprabhu**, *Defence Research and Development Organization, Bangalore, India* , **Dr. Krishna M**, *RV College of Engineering, Bangalore, India* , **Dr. Manoj Gupta**, *National University of Singapore, Singapore* and **Dr. U Sai Babu**, *Indian Institute of Science, Bangalore, India* for their valuable inputs on my research work in many ways, especially towards the completion of this thesis.

I owe my deepest gratitude to my teachers Dr. PL Srinivas Murthy and Dr. R Chandrashekar, *RIT, Bangalore*, Dr. H N Reddappa and Dr. Nagaraja C Reddy, *BIT, Bangalore*, Dr. N Mohan, *Dr. AIT, Bangalore*, Dr. R Suresh, *MSRUAS, Bangalore*. Without their enthusiasm, encouragement, support, and continuous optimism this thesis would hardly have been completed.

I would like to express my sincere thanks to management of Nitte Meenakshi Institute of Technology (NMIT) for the support extended to me all these years. Thanks are due to Prof N R Shetty, Dr. H C Nagaraj, Prof P G Mukunda, Dr. Sudheer Reddy J, Dr. P B Shetty and Dr. Kiran Aithal S for their support and encouragement throughout my research work. I thank my colleagues of NMIT for the support extended to me whenever I needed their help during my research work.

I also, like to express my sincere thanks to all of my friends in PhD, Dr. Mallikarjuna B, Dr. Rakesh K R, Dr. Manjunath P, Dr. Muralidhar A, Dr. Vijay Kumar T, Dr. Vinyas M, Dr. Pradeep BV, and Dr. Sarvana B; in MTech Mr. Nagendra G and Dr. Karthik R, in BTech, Mr. Varun, Mr. Nagaraj , Mr. Mohan, Mr. Pavan , Dr. Bharath VG ; in Intermediate, Mr. Darshan D, Mr. Harsha N ; and in schooling, Mr. Suhas NS, Dr. Vinayaka N, Dr. Chandan, Dr. Tejas V, Mr. Nishank, Mrs. Puneetha S and Mrs. Uma S for their help and support in my life.

I want to share this moment of happiness with my parents, Smt. Hemalatha G, and Sri. Lakshmikanthan M, who always encouraged me to read and advised to acquire a higher degree due to which only I think what I am today. I would like to express my special thanks of gratitude to my In-laws, Smt. Chandrakala M and Sri. Manjunath D H for their encouragement in all my endeavors. At this point, I find no words to express the support and encouragement received from my wife, Smt. Kirti M and also for her patience endured during all these years. Last but not least, my deep and sincere gratitude to my grandparents, Late Smt. Komala, Sri. Gopinath, Late Smt. Rangamma, Late Sri. Muniswamaiah, my aunt Smt. Suman, my brother Mr. Abhilash L, my uncles Mr. Amaresh N, Mr. Manjunath M, and relatives for their tremendous encouragement ,support ,and I dedicate this milestone to them.

The list goes on and there are many others I should mention. There are people who have helped me all the way and provided me support when I didn't even realize I needed it, or needed it now, or needed it constantly. Listing all of them would fill a book itself, so I merely will have to limit myself to a few words: I THANK YOU ALL.....!

AVINASH L

ABSTRACT

The demand for light-weight materials is increasing in the automobile industry due to the increasing cost of fuel. In particular, there is a huge demand for high-strength and wear-resistant materials for engine cylinder applications. Al-Si-Mg series alloys such as A357 alloy would be an ideal choice for such applications owing to their low density, excellent castability, high strength and wear resistance.

Enhancing the strength of any material can be achieved by work hardening, heat treatment, or reinforcing with a hard phase. The present work focused on development of A357 composites wherein the A357 alloy was reinforced with dual-size SiC particles. In the current work, two different sizes of SiC particles (coarse ($140 \pm 10\mu\text{m}$) and (fine ($30 \pm 5 \mu\text{m}$)) were used to reinforce A357 alloy. Stir casting was used to develop A357 composites, with different weight ratios of the two sizes of SiC powders, keeping the total weight fraction at 6%. Three composites were cast in finger moulds; DPS1 (coarse: fine;1:1), DPS2 (coarse: fine;2:1), and DPS3 (coarse: fine; 1:2). The cast A357 alloy as well as the composites were subjected to heat treatment as per T6 temper conditions. The effect of varying solution temperature (500°C to 540°C in steps of 20°C for 9h and keeping aging temperature constant at 150°C for 6 h) and aging temperature (160°C to 200°C in steps of 20°C for 6h and keeping solution temperature constant at 540°C for 9h) were studied for both A357 alloy and the developed composites. Both A357 alloy and dual-size SiC reinforced composites were subjected to microstructural analysis using optical, scanning, and transmission electron microscopy techniques. Hardness and tensile testing were carried on the A357 alloy and its DPS composites before and after heat treatment. Tribological properties namely wear rate was assessed by conducting dry-sliding wear test using a pin-on-disc machine. In the wear test, the effect of varying load on wear rate was studied by keeping sliding velocity and sliding distance constant. Worn surface analysis was carried out using SEM to study the wear mechanisms operating in both untreated and heat-treated alloy and composites.

Mechanical testing results showed improved hardness, yield, and tensile strength values for DPS composites when compared with that of A357 alloy. The strengthening of A357 composites is based on the addition of hard phase like SiC particles to the A357

alloy. The strengthening mechanisms that contributed to improvement in properties were effective load transfer, precipitation hardening and dislocation strengthening due to thermal mismatch. Precipitation hardening occurs for the A357 alloy and its composites because of T6 heat treatment. Formation of β'' phase and Mg_2Si precipitates were primarily responsible for strengthening after heat treatment. Wear rate of composites was found to be less than that of A357 alloy. Prohibition of direct contact between the two mating surfaces by presence of dual-size SiC particles was one of the primary reasons for low wear rate in composites.

The key conclusions from this work include: Among the three developed composites, hardness, and wear resistance of DPS2 composite before and after heat treatment was found to be significantly higher than the other two composites (DPS1 and DPS3). Also, the tensile and yield strength values of DPS3 composite before and after heat treatment was found to be significantly higher when compared to the other two composites (DPS1 and DPS2). Lastly, the ratio of coarse particles to fine particles has an effect on the mechanical and tribological properties. Presence of more fine particles was found to be good for strength and ductility whereas more coarse particles were found to be good for hardness and wear resistance.

Keywords: *Stir Casting; Dual Particle Size (DPS) composites; Microstructure; Mechanical properties; Wear; T6 Heat Treatment; Solutionizing temperature; Aging temperature*

TABLE OF CONTENTS

	Page No
DECLARATION	
CERTIFICATE	
ACKNOWLEDGEMENTS	
ABSTRACT	
CONTENTS	i
LIST OF FIGURES	vii
LIST OF TABLES	xiii
ABBREVIATIONS	xv
1 INTRODUCTION	1
1.1 Composite materials	1
1.2 Classification of composite materials	1
1.2.1 Classification of composites based on matrix material	2
1.2.2 Classification of composite materials based on various reinforcement materials	3
1.2.2.1 Classification of MMC's based on reinforcements	4
1.3 Classification based on various metals/alloys available as matrix materials	5
1.4 Particulates used to reinforce the metal matrices	7
1.5 Importance of metal matrix composites	7
1.5.1 Aluminium metal matrix composites (AMMC's)	9
1.6 Cast aluminium alloys	9
1.6.1 Cast aluminium alloy A357	11
1.7 Dual particle size (DPS) composites and their advantages	12
1.8 Applications of Al-Si alloys	13
1.8.1 Potential application of Al-based MMC's	14

1.9	Fabrication techniques of Al-based MMC's	15
1.9.1	Liquid state fabrication	15
1.9.2	Solid state fabrication	17
1.9.3	Gaseous state fabrication	18
1.10	Factors influencing the mechanical performance of composite materials	18
1.10.1	Interfacial bonding	19
1.10.2	Orientation	19
1.10.3	Material	20
1.10.4	Wettability	20
1.11	Heat treatment	21
1.11.1	Temper designations used in heat treatment	21
1.12	Heat treatment of aluminium alloys (Precipitation hardening)	22
1.13	Effect of heat treatment on mechanical behaviour and strengthening mechanisms	24
1.14	Wear behaviour	25
2.	LITERATURE SURVEY	27
2.1	Mechanical properties of Al-based MMC's	27
2.2	Tribological properties of Al-based MMC's	32
2.3	Dual particle size (DPS) composites	35
2.4	Summary of literature review	43
2.5	Objectives of present research	44
2.6	Organization of the thesis	45
3.	EXPERIMENTAL DETAILS AND METHODOLOGY	47
3.1	Material selection	49
3.2	Processing set up	51

3.2.1	Composite fabrication	52
3.3	Heat treatment	54
3.4	Density measurement	59
3.5	Sample preparation for metallographic studies	60
3.6	Microstructural characterization	61
3.7	Evaluation of mechanical properties	63
3.7.1	Hardness testing	63
3.7.2	Tensile testing	64
3.8	Wear testing	64
3.8.1	Three-dimensional surface topography measurement	66
4.	RESULTS AND DISCUSSION: Effect of dual particle size (DPS) SiC reinforcements on microstructure, physical, mechanical and wear properties of A357 composites	67
4.1	Density of A357 alloy and the developed DPS composites	67
4.2	Microstructural analysis of A357 alloy	68
4.3	Microstructural analysis of the developed DPS composites	70
4.4	Hardness results	72
4.5	Tensile strength	73
4.6	Tensile fracture surface analysis	76
4.7	Graphical interpretation of wear rate	77
4.8	Wear behaviour	79
4.9	Worn surface analysis	80
4.10	Three-dimensional surface topographies of worn surfaces	81
4.11	Wear debris analysis	85

5.	RESULTS AND DISCUSSION: Effect of solutionizing temperature on microstructure, physical, mechanical and wear properties of dual particle size SiC reinforced A357 composites	89
5.1	Density of A357 alloy and the developed DPS composites	89
5.2	Microstructural analysis of the A357 alloy	90
5.3	Microstructural analysis of the developed DPS composites	93
5.4	TEM analysis of A357 alloy and the developed DPS composites	96
5.5	Tensile strength	97
5.6	Tensile fracture surface analysis	101
5.7	Hardness results	103
5.8	Specific wear rate	105
5.9	Worn surface analysis	106
5.10	Three-dimensional surface topographies of worn surfaces	110
5.11	Wear debris analysis	112
6.	RESULTS AND DISCUSSION: Effect of aging temperature on microstructure, physical, mechanical and wear properties of dual particle size SiC reinforced A357 composites	115
6.1	Density of A357 alloy and the developed DPS composites	115
6.2	Microstructural analysis of the A357 alloy	116
6.3	Microstructural analysis of the developed DPS composites	118
6.4	TEM analysis of A357 alloy and the developed DPS composites	120
6.5	Tensile strength	122
6.6	Tensile fracture surface analysis	125
6.7	Hardness results	127
6.8	Specific wear rate	128
6.9	Worn surface analysis	130
6.10	Three-dimensional surface topographies of worn surfaces	132

6.11	Wear debris analysis	134
7	CONCLUSIONS AND FUTURE WORK	137
7.1	Conclusions	137
7.1.1	Effect of dual particle size (DPS) SiC reinforcements on microstructure, mechanical and wear properties of A357 alloy and the developed composites	138
7.1.2	Effect of solutionizing temperature on microstructure, mechanical and wear properties of A357 alloy and the developed DPS composites	139
7.1.3	Effect of varying aging temperature on microstructure, mechanical and wear properties of A357 alloy and the developed DPS composites	141
7.2	Future work	142
	REFERENCES	143
	LIST OF PUBLICATIONS BASED ON PHD RESEARCH WORK	170
	BIODATA	171

LIST OF FIGURES

Figure No.	Description	Page No
Figure 1.1	Flowchart showing the broad classification of composite materials	2
Figure 1.2	Applications of Al-based MMC's	15
Figure 1.3	Schematic of stir casting technique	17
Figure 1.4	Schematic of commonly used temper designations in heat treatment	21
Figure 1.5	Schematic of precipitation hardening (Temperature vs Time diagram)	22
Figure 1.6	Precipitation sequence of Al-Si-Mg alloy	23
Figure 3.1	Flowchart of the work (Processing, characterization, and testing) carried out in this research	48
Figure 3.2	Aluminium A357 ingots	49
Figure 3.3	Morphology of SiC particles. Where (a) SiC powder sample (fine size), (b) Morphology of fine size SiC particles with EDS analysis, (c) SiC powder sample (coarse size), and (d) Morphology of coarse size SiC particles with EDS analysis	50
Figure 3.4	Details of fabrication of A357-DPS composites. Where (a) Stir casting set up (bottom pouring technique), (b) Line diagram of stir casting setup, and (c) Cast iron permanent mould	51
Figure 3.5	Process flowchart for fabrication of A357 composite reinforced with dual size SiC particles	53
Figure 3.6	Images of Cast Sample	53
Figure 3.7	Muffle furnace with a temperature controller	55
Figure 3.8	Precipitation heat treatment (T6-Cycle) for varying solutionizing temperature at constant aging temperature	56
Figure 3.9	Precipitation heat treatment (T6-Cycle) for varying aging temperature at constant solutionizing temperature	58
Figure 3.10	Steps involved in sample preparation for metallographic studies	60
Figure 3.11	Optical microscope	61
Figure 3.12	Scanning Electron Microscope (Courtesy: BMSCE)	62

Figure 3.13	Transmission Electron Microscope (Courtesy: PSGCT)	62
Figure 3.14	(a) Vickers hardness tester and (b) Schematic of specimen used for hardness testing	63
Figure 3.15	(a) Universal testing machine and (b) Schematic of specimen used for tensile testing	64
Figure 3.16	(a) Pin-on-disc tribometer and (b) Schematic of wear test specimen	65
Figure 3.17	3D - Optical- profiler (Courtesy: IISC)	66
Figure 4.1	Micrographs of (a) A357 alloy showing dendritic structure, (b) A357 alloy showing inter dendritic region, (c) SEM image of A357 alloy at higher magnification, and (d) EDAX spectra taken on A357 alloy	69
Figure 4.2	Optical micrographs of (a) DPS1 composite, (b) DPS2 composite, (c) DPS3 composite and (d) DPS2 composite at higher magnification	71
Figure 4.3	EDAX spectra taken on DPS1 composite confirming the presence of SiC	72
Figure 4.4	Hardness test results of A357 alloy and the developed DPS composites	73
Figure 4.5	Tensile strength of A357 alloy and the developed DPS composites	74
Figure 4.6	Percent elongation (%) of A357 alloy and the developed DPS composites	75
Figure 4.7	Fractographs of (a) A357 alloy, (b) DPS1 composite, (c) DPS2 composite, and (d) DPS3 composite	77
Figure 4.8	Graphical interpretation of wear rate for A357 alloy and DPS2 composite (a) A357 alloy at 10N, (b) A357 alloy at 30N, (c) DPS2 composite at 10N, and (d) DPS2 composite at 30N	78
Figure 4.9	Effect of load on wear rate (mm^3/m) of A357 alloy and the developed DPS composites	79
Figure 4.10	Wear tracks of (a) and (b) A357 alloy, (c) and (d) DPS1 composite, (e) and (f) DPS2 composite, and (g) and (h) DPS3 composite at loads of 10N and 30N, respectively	82
Figure 4.11	EDAX analysis of selected area on worn surface of DPS2 composite at a load of 30N	83

Figure 4.12	Three-dimensional surface topographies of worn surfaces of (a) A357 alloy, (b) DPS1 composite, (c) DPS2 composite, and (d) DPS3 composite at a loads of 30N	84
Figure 4.13	Wear debris of (a) and (b) A357 alloy, (c) and (d) DPS1 composite, (e) and (f) DPS2 composite, and (g) and (h) DPS3 composite at loads of 10 N and 30 N, respectively	86
Figure 4.14	EDAX analysis of selected area on wear debris of DPS2 composite at a load of 30 N	87
Figure 5.1	(a) and (b) shows optical and SEM micrograph of A357 alloy solutionized at 500°C, (c) and (d) shows optical and SEM micrograph of A357 alloy solutionized at 520°C, and (e) and (f) shows optical and SEM micrograph of A357 alloy solutionized at 540°C.	92
Figure 5.2	Optical micrographs of the developed DPS composites solutionized at 540°C. Where (a) DPS1 composite, (b) DPS2 composite, (c) DPS3 composite, and (d) DPS2 composite at higher magnification showing interfacial bonding	94
Figure 5.3	EDAX of DPS 1 composite solutionized at 540°C. Where (a) EDAX spectrum taken exactly on SiC particle, (b) EDAX spectrum taken on DPS1 composite and (c) EDAX spectrum taken at Al/SiC interface.	95
Figure 5.4	Bright-field TEM images of (a) A357 alloy, (b) DPS1 composite, (c) DPS2 composite, and (d) DPS3 composite, after heat treatment at solutionizing temperature of 540°C	96
Figure 5.5	(a) Yield and (b) Ultimate tensile strengths of A357 alloy and the developed DPS composites at different solutionizing temperatures	98
Figure 5.6	Percent elongation (%) of A357 alloy and the developed DPS composites at varying solutionizing temperatures	100
Figure 5.7	Fractographs of (a), (b), and (c) A357 alloy, (d), (e), and (f) DPS1 composite, (g), (h), and (i) DPS2 composite, (j), (k), and (l) DPS3 composite solutionized at 500 °C, 520 °C, and 540 °C respectively	102
Figure 5.8	Hardness test results of A357 alloy and its DPS composites at different solutionizing temperatures.	104

Figure 5.9	Effect of solutionizing temperature on the wear rate of A357 alloy and the developed DPS composites	105
Figure 5.10	Wear tracks of (a), (b), and (c) A357 alloy, (d), (e), and (f) DPS1 composite, (g), (h), and (i) DPS2 composite, (j), (k), and (l) DPS3 composite solutionized at 500 °C, 520 °C, and 540 °C respectively	108
Figure 5.11	Three-dimensional surface topographies of worn surfaces of (a) and (b) A357 alloy, (c) and (d) DPS1 composite, (e) and (f) DPS2 composite, (g) and (h) DPS3 composite, solutionized at 520°C and 540°C, respectively	111
Figure 5.12	Wear debris of (a), (b), and (c) A357 alloy, (d), (e), and (f) DPS1 composite, (g), (h), and (i) DPS2 composite, (j), (k), and (l) DPS3 composite aged at 500 °C, 520 °C, and 540 °C respectively	114
Figure 6.1	(a) and (b) shows optical and scanning electron micrographs of A357 alloy aged at 180°C, (c) and (d) shows optical and scanning electron micrograph of A357 alloy aged at 200°C and (e) EDS spectrum of A357 alloy taken on Al-Si interface at 180°C	117
Figure 6.2	Optical Micrographs of (a) DPS1 composite, (b) DPS2 composite, (c) DPS3 composite, all aged at 180°C, (d) EDS spectrum taken on DPS2 composite particle, and (e) EDS spectrum at Al/SiC interface	119
Figure 6.3	Bright-field TEM images of (a) A357 alloy, (b) DPS1 composite, (c) DPS2 composite, (d) DPS3 composite, and (e) Modified Si particles with twins in DPS2 composite after heat treatment at aging temperature of 180°C	121
Figure 6.4	(a) Yield and (b) Ultimate tensile strengths of A357 alloy and the developed DPS composites at different aging temperatures	123
Figure 6.5	Percent elongation (%) of A357 alloy and the developed DPS composites at varying aging temperatures	124
Figure 6.6	Fractographs of (a), (b), and (c) A357 alloy, (d), (e), and (f) DPS1 composite, (g), (h), and (i) DPS2 composite, (j), (k), and (l) DPS3 composite, aged at 160 °C, 180 °C, and 200 °C respectively	126
Figure 6.7	Hardness results of A357 alloy and the developed DPS composites at varying aging temperatures	127
Figure 6.8	Effect of aging temperature on wear rate of A357 alloy and the developed DPS composites	129

- Figure 6.9** Wear tracks of (a), (b), and (c) A357 alloy, (d), (e), and (f) DPS1 composite, (g), (h), and (i) DPS2 composite, (j), (k), and (l) DPS3 composite, aged at 160 °C, 180 °C, and 200 °C respectively 131
- Figure 6.10** Three-dimensional surface topographies of worn surfaces of (a) and (b) A357 alloy, (c) and (d) DPS1 composite, (e) and (f) DPS2 composite, (g) and (h) DPS3 composite, aged at 180°C and 200°C respectively 133
- Figure 6.11** Wear debris of (a), (b) and (c) A357 alloy, (d), (e) and (f) DPS1 composite, (g), (h) and (i) DPS2 composite, (j), (k) and (l) DPS3 composite aged at 160 °C, 180 °C, and 200 °C respectively 136

LIST OF TABLES

Table No.	Description	Page No
Table 1.1	Classification of reinforcements	5
Table 1.2	Properties of particulate reinforcements	7
Table 1.3	Designation of cast Al alloys	10
Table 1.4	Applications of Al-based MMC's	14
Table 2.1	Dual particle size combinations used in different studies	42
Table 3.1	Chemical composition of A357	49
Table 3.2	Physical properties of A357 (Al-7.4Si-0.55Mg)	49
Table 3.3	Chemical composition of SiC particles	50
Table 3.4	Physical properties of SiC particles	51
Table 3.5	Process parameters used for stir casting of composites	54
Table 3.6	Reinforcement combination of A357 alloy and its DPS composites	54
Table 3.7	Designation of A357 alloy and the developed DPS composites heat-treated by varying solutionizing temperature at constant aging temperature	57
Table 3.8	Designation of A357 alloy and the developed DPS composites heat-treated by varying aging temperature at constant solutionizing temperature	59
Table 3.9	Chemical composition of EN-32 steel disc	65
Table 4.1	Theoretical and experimental densities of A357 alloy and the developed DPS composites	67
Table 5.1	Theoretical and experimental densities of A357 alloy and the developed DPS composites at varying solutionizing temperatures.	89
Table 6.1	Theoretical and experimental densities of A357 alloy and the developed DPS composites at varying aging temperatures.	115

ABBREVIATIONS

MMC's	:	Metal Matrix Composites
PMC's	:	Polymer Matrix Composites
CMC's	:	Ceramic Matrix Composites
Al	:	Aluminium
AMMCs	:	Aluminium- Based Metal Matrix Composites
HT	:	Heat Treatment
SHT	:	Solution Heat Treatment
AT	:	Aging Heat Treatment
CTE	:	Coefficient of Thermal Expansion
CVD	:	Chemical Vapor Deposition
PVD	:	Physical Vapor Deposition
ASTM	:	American Society for Testing and Materials
DPS	:	Dual Particle Size
SPS	:	Single Particle Size
EDAX	:	Energy Dispersive X-ray Analysis
GP zone	:	Guinier–Preston zone
OM	:	Optical Microscopy
RSM	:	Response Surface Methodology
SEM	:	Scanning Electron Microscopy
TEM	:	Transmission Electron Microscopy
HV	:	Vickers Hardness
% EL	:	Percentage of Elongation
YS	:	Yield Strength
UTS	:	Ultimate Tensile Strength

CHAPTER 1

1. INTRODUCTION

This chapter provides a brief background on composite materials, their constituents, and their classification. Since the present research is focused on metal-matrix composites (MMC's), especially Aluminum-based MMC's they are discussed in detail. Next, the different matrix materials and particulates used in Al-based MMC's are discussed. The processing techniques for Al-based MMC's are also documented. A brief overview of dual particle size composites, heat treatment of Al alloys, and temper designations used in heat treatment are also herewith included. Finally, the factors influencing the mechanical and wear properties of Al-based MMC's are discussed.

1.1 Composite materials

Composite materials are engineering materials made by a mixture of different constituents that are distinct from each other and offer several properties which are unattainable by its individual constituents (Vencl et al. 2004; Chawla et al. 2006). In composite materials, the continuous phase is known as the matrix phase while the reinforcing phase is generally discontinuous and can have different forms based upon its aspect ratio. Based on the inputs of a design engineer the composite material can be tailored to fit the requirements by opting for appropriate materials (Surappa et al. 2003).

1.2 Classification of composite materials

Composite materials can be classified based on the matrix and reinforcement materials. Based on the morphology of the reinforcements, the composites can be classified as fiber, particulate, whisker, or flake. Based on the type of matrix, composite materials are classified metal-matrix composites (MMC's), ceramic matrix composites (CMC's) and polymer matrix composites (PMC's) (Hull and Clyne, 1996;

Matthews and Ralwings, 1994; Mohamed et al. 2018; Thostenson et al. 2001). Broad classification of composite materials is shown in Figure. 1.1.

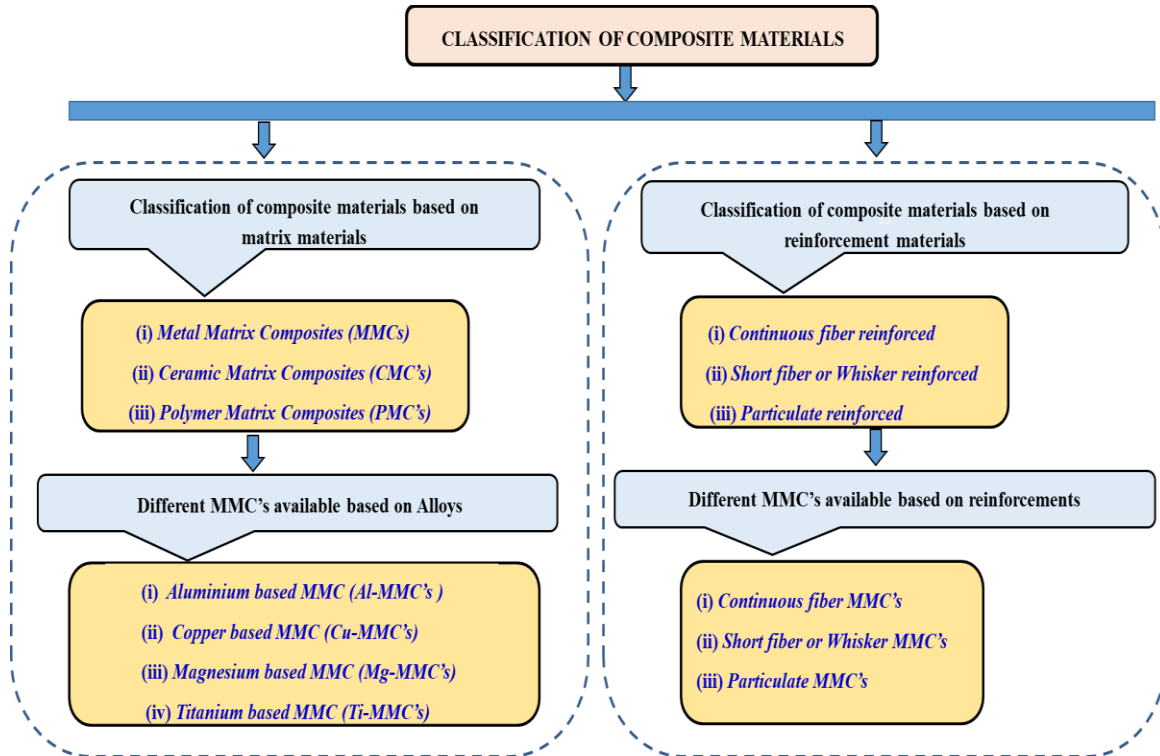


Figure 1.1: Flowchart showing the broad classification of composite materials.

1.2.1 Classification of composites based on matrix material

Based on the matrix material used, composite materials are classified as follows:

Metal matrix composites (MMC's)

Metal matrix composites consist of two main components. The first is metal/alloy matrix which is the continuous phase and second is the reinforcement which is discontinuous phase and can have different morphology. Commonly used metals and alloys are aluminium, nickel, copper, steel, titanium, and magnesium for numerous applications spanning from electrical wire to automobile parts. With respect to

PMC's, MMC's offer, high specific strength, high wear resistance, ability to deform plastically, better joining characteristics and enhancement of strength by various methods.

Ceramic matrix composites (CMC's)

Non-metallic solids having strong ionic bonding are generally known as ceramics and are crystalline in nature. Ceramics possess high temperature operating capability, high chemical inertness, high compressive strength, and high hardness. However, due to their poor fracture toughness they are not suitable for structural applications. In order to improve their fracture toughness, ceramics are reinforced with fibers (Al_2O_3 , ZrO_2 , BN , Si_3N_4), whiskers (Glass, TiB_2 , SiC , Si_3N_4) and particulates (Al_2O_3 , TiC , SiC). Ceramic matrix composites are used for making cutting tool inserts, aircraft engines, brake disks, turbine blades, exhaust ducts, heat exchanger tubes and bearings.

Polymer matrix composites (PMC's)

Here an organic polymer matrix is reinforced by different types of continuous or short fibers or sometimes even nanoparticles. Two different categories of polymer matrix composites namely reinforced plastics and advanced polymer composites have been developed. These two polymer composites are distinguished on the basis of the achieved strength and stiffness. Polymers themselves are classified as thermoplastics (PEEK, polyetherimide and liquid crystal) and thermosets (polyamides, epoxy, and polyester). On the other hand, reinforcements like continuous fibers (Aramid, glass, and carbon) and nanoparticles (TiO_2 , Al_2O_3 and CaSiO_3) are used to reinforce polymers. Common examples include non-structural parts such as exterior panels, structural parts such as leaf spring for vehicles, moulded propeller assemblies in naval industry, lampposts, helicopter rotor blades, golf club shafts and highway culverts for construction applications.

1.2.2 Classification of composite materials based on reinforcement material.

Reinforcements are the materials used to strengthen the matrix phase by various strengthening mechanisms. These are used to reinforce the matrix because of its

advantages, such as low density, thermal stability, high stiffness, high hardness, and high strength (Miyajima et al. 2003). Generally, reinforcements are classified as continuous fibers, whiskers, or particulates based upon their aspect ratio and morphology. Based on the application, the reinforcements having similar property profile are chosen to make a part/component. Fibers are quite popular owing to their high strength, high aspect ratio, and a high degree of flexibility. Various fibers such as glass fibers (E/C/S glass), boron fibers, Aramid fibers, carbon fibers, SiC fibers and α -alumina fibers are used as reinforcements (Chou et al. 1985). Monofilament fibers have high elastic modulus while carbide fibers possess both high specific modulus and strength. SiO₂ and SiC based multifilament fibers possess very high specific strength when compared to that of specific modulus. On the other hand, whiskers are monocrystalline which means they have no grain boundaries due to which they possess very high strength, high stability and are not degradable. However, their main drawback is the lack in uniform dimensions. Another major drawback of whiskers is poor bonding with the matrix materials; for example, Al₂O₃ whiskers have difficulties in bonding with metal matrix. Among all available whiskers, silicon carbide and silicon nitride whiskers are quite popular for reinforcing metal matrices. However, one should note that whiskers are known to be health hazardous causing serious problems. Since MMC's with particulate reinforcements cost much less than MMC's with continuous fiber reinforcements, the particulate composites are more popular. From the processing point of view the particulates can be blended more efficiently with the metal matrices when compared with that of whiskers or fibers. Ceramic based particulate materials are quite popular owing to their low density, high strength, thermal stability, and good mechanical compatibility (Kainer et al. 2006; Kaw et al. 2006).

1.2.2.1 Classification of MMC's based on reinforcements

Continuous fiber MMC's

Here the reinforcing phase is continuous fiber whose aspect ratio is more than 1000 and whose diameter can vary from 3 to 150 μm . Example of continuous fiber MMC's

are Al-SiC, Al-B, Ti-6Al-4V-SiC, Al-Li-Al₂O₃, Mg-Al₂O₃ and Mg-C composites (Christensen, 2005).

Short fiber or whisker MMC's

Here the reinforcing phase is a short fiber or a whisker whose aspect ratio is usually over 10 and whose diameter can be in the range of 0.01 to 1 μm . Examples of short fiber/whisker MMC's are AlSi12CuMgNi/Al₂O₃ short fibers, AlSi12CuMgNi/SiC whisker and Al/SiC whisker composites (Christensen, 2005).

Particulate MMC's

Here the reinforcing phase is a particle whose aspect ratio lies in the range of 1 to 4 with size varying from nanometre to micrometre. Common examples of particulate MMC's are Mg/SiC, Pb/Al₂O₃, AlMgSiCu/Al₂O₃, Al-4Cu-2Mg/SiC and Al-12Si-Mg/SiC composites (Hutching, 1987; Husking et al. 1982; Debda et al. 2005).

Table 1.1: Classification of reinforcements (Christensen, 2005; Kainer 2006)

Reinforcement type	Aspect ratio	Examples of reinforcements
Continuous fibers	> 1000	Carbon, Glass, Boron, SiC, Kevlar, Steel, Wood fibers, Carbon nanotubes, Al ₂ O ₃ , Si ₃ N ₄ , NbTi
Whiskers/flakes	> 10	Mica, Graphite, BN, SiC, Al ₂ O ₃ , TiB ₂ , Al ₂ O ₃ +SiO ₂
Particulates	1 - 4	SiC, WC, TiC, B ₄ C, TiO ₂ , Al ₂ O ₃ , Flash

1.3 Classification based on various metals/alloys available as matrix materials

There are various types of metals or alloys available which can be used as matrix materials for making MMC's and this depends upon the applications. A brief

discussion on different matrix materials used to develop MMC's is provided below, (Kaw et al. 2006; Surappa et al. 2003; Czerwinski et al. 2008).

Aluminium and its alloys

Aluminium and its alloys are widely used because of their low density ($\approx 2.7 \text{ g/cm}^3$) and reasonable mechanical properties such as good strength and corrosion resistance. The alloys series like Al2xxx, Al6xxx and Al7xxx hold special significance when subjected to heat treatment. After heat treatment these alloys exhibit good strength and toughness which make them probable candidate materials for automotive and aircraft industries.

Copper and its alloys

Copper has a density of 8.9 g/cm^3 . This high density rules out its application in automotive or aircraft industries as structural members. But what are more important is its physical properties such as electrical and thermal conductivity. Due to its high ductility, Cu can be easily cast and worked using secondary processing techniques. In its pure state, it is used for thermal management and electrical applications like heat sinks, power cables, bus bars and other electrical components.

Magnesium and its alloys

This is one of the lightest metals whose density (1.8 g/cm^3) is less than that of aluminium. It possesses high specific strength, good damping properties and good electrical conductivity. Further, it can be cast or formed easily due to which it is seen as an attractive material for large volume applications.

Titanium and its alloys

The density of titanium is 4.5 g/cm^3 , which is lower than iron. Ti exhibits a high melting point than steel. Titanium alloys are preferred for structural applications where the temperature ranges from 425 to 595°C (Donachie 2015). This metal is passive to almost all mineral acids and chlorides, thereby providing high degree of

corrosion resistance. Microstructure and chemical composition are the two important factors which decide the properties of titanium alloys. Applications of titanium and its alloys range from compressor blades and armor vehicles to hip implants.

1.4 Particulates used to reinforce the metal matrices

Hard particulate materials such as borides, nitrides, oxides, and carbides are used to reinforce the metal matrices. Table 1.2 shows the various reinforcements along with their crystal structure, density, melting point, and physical properties. It can be seen from Table 1.2 that these reinforcements are having very low density but high melting point and elastic modulus. These economically produced ceramic reinforcements are currently being used in polishing and grinding industries (Hutching, 1987; Husking et al. 1982; Debdas et al. 2005).

Table 1.2: Properties of particulate reinforcements (Kainer 2003)

Reinforcement	Crystal structure	Density (g/cm ³)	Melting point (°C)	Elastic modulus (GPa)	Coefficient of thermal expansion (10 ⁻⁶ K ⁻¹)
BN	Hexagonal	2.25	3000	90	3.8
B ₄ C	Rhombohedral	2.52	2450	450	5.4
AlN	Hexagonal	3.25	2300	350	6.0
Al ₂ O ₃	Hexagonal	3.90	2050	410	8.3
SiC	Hexagonal	3.21	2300	410	4.9
TiC	Cubic	4.93	3140	320	7.4

1.5 Importance of metal matrix composites

Day by day increasing concerns on environment, depletion of fossil fuels and need for advanced engineering materials have posed a big challenge to researchers across the world. The live examples from nature and continuous efforts have led to development of composite materials. The basic components of composite material are the matrix phase, which is continuous and the reinforcement, which is discontinuous . Both the

phases are chemically distinct and capable of imparting new range of properties which otherwise are not achieved by individual constituents of the composite material. Here, this new class of material can be distinguished based upon the type of reinforcement or matrix material. The MMC's offer competitive advantages such as improved specific strength, specific stiffness, high toughness, high surface durability, improved joining characteristics and thermal stability (Mazahery and Ostadshabani, 2011; Ibrahim et al. 1991). Initially MMC's found applications in the aerospace industry followed by their expansion into non-military fields such as the transportation industry (Davis ,1993) For example, stainless steel fiber reinforced aluminium composites were used for making connecting rods for automobiles (Bindumadhavan et al. 2001; Pavan Kumar et al. 2014). Some companies went ahead with making of tennis racket frame and golf club using silicon carbide reinforced aluminium composites. Apart from this, some special applications of MMC's include superconducting magnets made from copper reinforced Nb-Ti filaments and oil drilling inserts made up of tungsten carbide reinforced cobalt composites.

It is well known that the matrix material in a MMC's is either a metal or alloy, while the reinforcement could be either ceramic or metal. Most commonly preferred metal matrices are based on aluminium, copper, cobalt, magnesium, nickel, silver, titanium, and zinc. Here aluminium and magnesium are quite popular in aerospace and automotive industries due to their low densities. (Bindumadhavan et al. 2001; Pavan Kumar et al. 2014). Due to their high thermal and electrical conductivity, copper and silver are used in thermal management applications and superconductors. On the other hand, the reinforcement is classified based upon the aspect ratio and morphology such as particulates, whiskers, short and continuous fibers (Ghandvar et al. 2015). But it is most important to note that the ceramic based reinforcements are quite popular for reinforcing MMC's because of their high service temperature, high strength, and elastic modulus. The reinforcements in the form of particulates are most preferred compared to continuous fibers as the cost of these high modulus fibers is very high. On the other hand, particulates like silicon carbide also have a modulus of about 410 GPa along with low density of 3.21 g/cm³. In addition to this, particulates are

produced by very inexpensive technique like crushing. Based upon the application point of view, both matrix and reinforcement are chosen judiciously to meet the design engineer requirements for an application. Apart from the selection of constituents of a composite material, their fabrication also plays prominent role in dictating the properties as well as its affordability in the commercial market. There are various techniques available for fabrication right from conventional liquid metallurgy and powder metallurgy to newer techniques like thermal spray and accumulative roll bonding (Nick Tucker and Kevin Lindsey, 2002). However, economical fabrication of composites is very crucial in realizing the advantages offered by them and to compete with other engineering materials. As of now, they are restricted to few applications such as the automotive industries, where high strength to weight ratio is concerned.

1.5.1 Aluminium metal matrix composites (AMMC's)

Al-based MMC's are one of the promising materials for applications in automotive and aerospace industries as they exhibit low density, high specific strength, and good wear resistance. (Kumar et al. 2018; Mirjavadi et al. 2018; Sethuram et al. 2018; Mirjavadi et al. 2017). Aluminium alloys such as Al-Si, Al-Mg-Si, Al-Zn-Mg, Al-Cu, and Al-Cu-Mg have been used as matrix materials in developing of AMMC's. The addition of reinforcements (Al_2O_3 , TiC, SiC, etc.) to aluminium matrix helps in deflecting the crack at the interface and thereby ceases it from propagating, resulting in a increase in its toughness. In addition, the reinforcement material may help in bridging the cracks, thereby improving the performance of the aluminium matrix. Out of all reinforcements, SiC particulate is quite popular because of high-temperature stability, high strength, and stiffness (Kassim et al. 1999; Gomes et al. 2005; Zhou et al. 1997).

1.6 Cast aluminium alloys

Cast aluminium alloys are strengthened by the same alloying elements and by the same mechanisms as that of wrought aluminium alloys (Kopeliovich, 2012). Cast aluminium alloys are classified into heat treatable and non-heat treatable alloys with same temper conditions. In general, aluminium alloys are identified by three or four

number designation systems with or without decimal point in between them. Wrought and cast alloy system are differentiated by the decimal point. There is a decimal point after three numbers in the designation of cast alloys while there is no decimal point in the designation of wrought alloy system. The numbering system is based upon the alloying constituents and is preceded by letter “A” which represents Aluminium. The designation of cast aluminum alloys is shown in Table 1.3.

Table 1.3: Designation of cast Al alloys (Kopeliovich, 2012).

S/No	Designations	Alloying elements
1	1xx.x	Unalloyed aluminium
2	2xx.x	Al alloyed with Cu
3	3xx.x	Al alloyed with Si (Traces of Cu, Mg)
4	4xx.x	Binary Al-Si
5	5xx.x	Al alloyed with Mg
6	7xx.x	Al alloyed with Zn (Traces of Mg, Cr and Cu)
7	8xx.x	Al alloyed with Sn

The 6xxx series of aluminium wrought alloys are used extensively, whereas the cast alloys of 6xx.x and 9xx.x series are rarely used. Cast alloys contain large weight percentage of alloying elements which results in a heterogeneous structure when compared to wrought alloys (Hatch, 1984). However, the addition of alloying elements to aluminium needs a detailed study as they can result in brittle phase formation. The brittle phase has sharp morphology which is capable of creating internal notches. These in turn facilitate crack nucleation under loading conditions. Proper selection of alloying elements and good processing conditions can prevent such defect formation. Since the present work employs cast aluminium alloys as matrix material, detailed information from structure to physical properties is provided in the upcoming sections.

1.6.1 Cast aluminium alloy A357

In order to make any component or a part for an instrument or heavy machinery, a material with good castability or formability is often preferred. In case of cast aluminium alloys, the Al-Si-Mg alloys are well known for their excellent castability due to which they are quite popular in the automotive industry. It is interesting to note that up to 85% of cast aluminum products are made up of Al-Si alloys. Hence these alloys are extremely important in casting industries related to aluminium (Wang and Davidson, 2001; Polmear, 1995) The Al-Si alloys are generally designated as A3xx.x family. Among these, Al-Si hypoeutectic (<11%-Si) alloys such as A356 and A357 are quite popular. In particular, the structural components of automobiles like frames, housings, brackets, and car wheels are made up of cast Al-Si alloys like A357. Further, A357 alloy is replacing cast iron-based components like cylinder liners due to their high wear resistance and physical characteristics (Davis, 1993). A357 alloy is a cast aluminium alloy composed of 6-7.5% of silicon, 0.4 - 0.7% of magnesium, 0.04 - 0.07% of beryllium, 0.12% of iron and 0.10% of copper. Here the addition of each element has its own significance: Si improves the fluidity, Mg is added as precipitation hardener, Ni is added to increase tensile strength, copper increases the high temperature properties and Mn is added to modify Fe intermetallics. Its microstructure consists of α -Al phase, primary Si, Cu rich phases like CuAl_2 or Cu-Al-Si-Mg, and Al-Si eutectic.

The element Be is added to both alter the morphology of insoluble Al-Mg-Fe-Si phase to nodular form and also to modify the chemistry of such insoluble phase to exclude magnesium ensuring its availability for precipitation hardening. Since it is a heat treatable alloy, the strength, fatigue, and corrosion resistance are enhanced significantly after heat treatment using T6 temper. Further, the melt is treated with grain refiners like Al-3Ti-B, Al-5Ti-B or Al-Ti-C master alloys (Geoffrey et al. 2007). Melt modification along with heat treatment changes the morphology of silicon from coarse acicular to fibrous one due to which its properties are enhanced.

The strength and wear resistance of A357 alloy are increased with the addition of ceramic particulates. To this end, efforts have been made to reinforce A357 with graphite fibers, TiB_2 and Al_2O_3 particles to modify modulus, electrical and thermal properties (Li et al. 1990; Jacquesson et al. 2004). Due to its good mechanical and tribological characteristics, A357 alloy is chosen as matrix material to develop dual size composites in the present research.

1.7 Dual particle size (DPS) composites and their advantages

It is well known that the properties such as wear resistance of MMC's largely depend on interfacial bonding, matrix properties, type of reinforcement, particle weight, volume fraction and particle size. Few researchers have reported that the MMC's containing smaller size particles have shown higher wear resistance when compared to the MMC's with large size particles. Taking a cue from this several research studies have been carried out to study the effect of dual particle size (DPS) on the mechanical and tribological behavior of MMC's. The size difference between these particles will be quite large like; for example, the large particle size will be several hundred micrometres while smaller particle size will be few micrometres or in some case it will be submicron size. The most explored particulates for DPS composites are SiC (2/163 μm), TiC (2 μm /100 nm), B_4C (3 μm /50 nm), Al_3BC (5/300 nm), Al_2O_3 (100/150 μm) and ZrSiO_4 (20/125 μm). The idea of using two different sizes of particles in composites is get the benefit from their size difference. The addition of different size particles has significant effect on grain size and orientation and also the intensities of texture components changes. For instance, during wear testing, the larger particles not only carry the greater amount of load applied on the composites but also protect the smaller particles from being removed. On the other hand, small size particles not only help in reducing the plastic flow, i.e., by minimizing the plastic deformation but also preventing the adhesive transfer of material during wear test. These dual size particles have shown that they can bring coordinated improvements in mechanical properties such as strength, ductility, and hardness. An important property such as creep resistance of composites was also improved by 3 to 6 times for dual particle reinforced composites when compared to single reinforcement composites

and alloys. Most of the dual size particles were used to reinforce, pure aluminium, Al-3Cu, Al2124, Al6061, Al6063, LM13 piston alloy, magnesium, and copper.

1.8 Applications of Al-Si alloys

There has been steady growth in utilizing aluminium alloy castings for both aircraft and automotive applications after second world war. During this time, the United States of America made P-51 aircrafts which had the fuselage entirely made up of aluminium for weight reduction. Further, decrease in weight of P-51 engine was achieved by employing Duralumin alloy to make cylinder block, pistons, and crankcase. In present days, the Al-Si alloys are employed in making complex substructure's using investment casting process for aerospace industry. For example, Winglet substructure made of F357 alloy for Embraer Phenom is made up of a single block. The rear frame avionics bracket and tail rotor gearbox are made up of D357 alloy using precision sand casting technique. Further, Al-Si alloys are used for making powertrain components in the automotive industry by replacing gray cast iron. In making a V8 engine block, if Al-Si alloy are used then the overall weight of block is 32 kg whereas if gray cast iron is used then it weighs 68 kg. So, there is considerable amount of weight reduction by opting for Al-Si alloys in place of gray cast iron. Also, lot of efforts have been dedicated by North American automotive industry to replace iron engine blocks and cylinder heads with the cast Al-Si alloys. For example, Chrysler and Ford uses Al-Si alloy for making cylinder heads (C351) using semi-permanent casting technique. On the other hand, General Motors uses aluminium alloys to produce wheel rim by permanent casting. Chevrolet Corvette uses Al alloys for making engine blocks by sand casting process. Many minivans, cross-over vehicles, cars, and trucks employ aluminium alloys for making door handles or roof brackets (Robles Hernandez et al. 2017; Ye, 2003).

1.8.1 Potential application of Al-based MMC's

Table. 1.4 lists applications of Al-based MMC's used in different industries (Automotive, aerospace, sports, and construction). Figure. 1.2 shows the applications of Al-based MMC's used in automotive industry.

Table 1.4: Applications of Al-based MMC's (Hitesh Bansal, 2011)



Potential and existing applications 	Benefits 							
		<i>Wear resistance</i>	<i>Stiffness</i>	<i>Thermal conductivity</i>	<i>Tailorable Coefficient of Thermal Expansion (CTE)</i>	<i>Corrosion resistance</i>	<i>Corrosion to radiation</i>	<i>High strength</i>
<i>Bearings</i>	+	+				+		+
<i>Brake rotors</i>	+	+						
<i>Engine cylinder liners</i>	+	+						
<i>Pistons</i>	+	+						
<i>Worm gears</i>	+	+						+
<i>Aircraft skins</i>	+							+
<i>Bicycles frames</i>	+		+					+
<i>Electronics packaging</i>	+			+	+		+	
<i>Ground vehicles</i>	+							+
<i>Medical implant</i>	+					+		+
<i>Sea vehicles</i>	+		+			+		
<i>Space structures</i>	+		+	+			+	
<i>Transmission components</i>	+	+				+		
<i>Turbine engine components</i>	+	+						+



Figure 1.2: Applications of Al-based MMC's (Stojanovic and Ivanovi, 2015).

1.9 Fabrication techniques of Al-based MMC's

Metal matrix composites offer promising mechanical and physical properties for various applications, but their applicability has been limited. Processing MMC's using sophisticated fabrication techniques, result in a high cost of the end product and therefore, is one of the greatest barriers to expanding the applications of MMC's. By developing good and low-cost fabrication techniques one can improve the commercial applicability of MMC's. Generally processing of MMC's is divided into three main classes, (i) liquid-state, (ii) solid-state and (iii) gaseous-state processing. A brief discussion on all the three processing routes and their advantages are documented below with some examples (Surappa, 2014; Kaczmar et al. 2000; Miracle, 2005; Harrigan, 1998).

1.9.1 Liquid state fabrication

In this type of fabrication technique, the reinforcement is added when the metal matrix is in liquid state. This technique is capable of producing large scale products at a faster

rate and has been proven to be more beneficial for low melting temperature metals such as aluminium and magnesium. This technique can be further divided into four important categories like, stir-casting/dispersion process, squeeze casting/pressure infiltration, in-situ process, and spray process. Each of these fabrication techniques have their specific applications. No single technique can be considered to be universally applicable for all alloys, casting sizes, and final components. The present work involves casting of MMC's using stir casting technique, which is one of most widely used techniques for fabricating MMCs. Companies such as Duralcan use this technique to produce aluminium composites reinforced with particulates. Hence only stir casting technique along the different liquid state fabrication techniques is discussed herein. In case of stir casting the casting of MMC's is done at semisolid conditions which means the temperature is between liquidus and solidus. A simple schematic depicting the stir casting is shown in Figure. 1.3 where a mechanical stirrer is provided in middle of the furnace for creating agitation in semisolid slurry. Here the molten metal is agitated vigorously and allowed to cool down in semisolid state. The agitation is done by using a mechanical stirrer whose material is entirely different from those which are being cast. The advantage of continuous agitation is to prevent rise of viscosity of slurry and breaking of solidifying dendrites into spheroidal particles. During agitation, the reinforcement such as particulates and short fibers or whiskers are added into the semisolid metal.

The reinforcement which is in agitated condition doesn't agglomerate or flow on top of semisolid slurry, but in turn is trapped by the solid in this slurry and allows it to disperse uniformly. Here the stirring or agitation of semisolid slurry is very important as it breaks the agglomerates of particulates. Regardless of lack of wettability of ceramic particulates with metal matrix, this technique helps in entrapping them in semisolid slurry with uniform dispersion. The continuous agitation helps in bonding between both the constituents of MMC's by bringing them in direct contact. The direct and intimate contact helps in bonding and improving wettability which improves further with the increase in mixing time. Since the agitation causes decrease in viscosity, the advantage is that this composite mixture with low viscosity can be

directly cast into required shape. The other advantage of this technique is absence of shrinkage cavities in final product which is mainly because of processing at semisolid conditions where the slurry is nearly in solid state (Flemings, 1981; Levi et al. 1977).

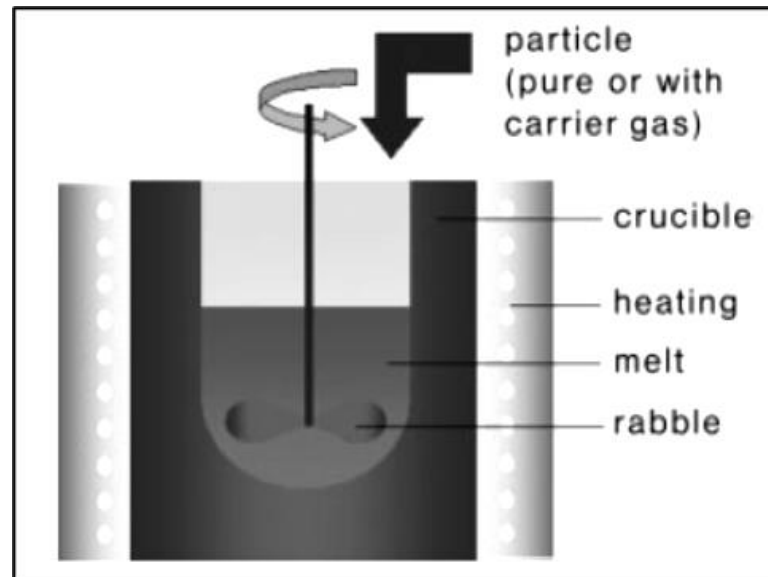


Figure 1.3: Schematic of stir casting technique (Kainer, 2006).

1.9.2 Solid state fabrication

This is another important fabrication technique in which a high-volume fraction of reinforcement can be incorporated into the metal matrix. In solid state fabrication, powder metallurgy is the most widely used processing method for fabrication of metal matrix composites. The reinforcements are mixed with the metal powders using different mixing techniques and consolidated either at room or elevated temperatures. If the powders are consolidated at room temperatures than additional processing method known as sintering is adopted. In addition to this, secondary processing techniques such as extrusion, rolling, equal channel angular extrusion, forging or multi-axial forging techniques are also used. However, such techniques are very expensive and mass production is not possible thereby restricting them to specific applications. Further, the tooling costs required for the powder metallurgical processing is very high which also limits its applications.

1.9.3. Gaseous state fabrication

This fabrication technique includes deposition of vapor on the substrate material with control over the composition of composite. Two different types of fabrication techniques are chemical vapor deposition (CVD) and physical vapor deposition (PVD) processes. Here control of various factors like gas mixing, oxygen contamination and vapor transport are very important for good coating of composite. However, in case of gaseous state fabrication techniques, availability of metal and compound target is quite difficult and deposition rates are slow. In case of thermal spray techniques, the parts with complex shapes are difficult to coat but the main issue is related to starting materials which are quite expensive.

Out of all processing techniques, the liquid state fabrication technique is more popular due to its inherent advantages over solid and gaseous state fabrication techniques. Firstly, the liquid metal is less expensive when compared to powders and secondly the handling of liquid metal is lot easier and more flexible when compared to that of powders. More importantly wide variety of shapes can be produced using liquid state processing technique which is not the case with solid and gaseous state fabrication techniques. But there are some concerns such as poor control of fabrication parameters and formation of undesirable interfacial products at the interface between matrix and reinforcement. The chemical reactions taking place at the interface can lead to formation of carbides and oxides which are highly brittle in nature. However, one needs to consider the economic viability of the liquid state fabrication technique with its potential for near-net casting.

1.10 Factors influencing the mechanical performance of composite materials

The mechanical performance of composite materials depend on (i) Interfacial bonding, (ii) Orientation, (iii) Material, and (iv) Wettability. A brief discussion on all these is herewith provided below.

1.10.1 Interfacial bonding

There are different types of bonding between reinforcement and metal matrices namely: chemical, mechanical and reaction. Generally, a metallic coating such as nickel or copper on the surface of fibers or particulates is applied by electroless technique. The thin layer formed on the surface of the reinforcement tends to form a good adhesion with the metal matrix thereby increasing the bond strength. On the other hand, reaction bonding occurs when the atoms of reinforcement diffuse into that of matrix and vice-versa. Mechanical bonding between the reinforcement and matrix is created by etching the surface of reinforcement in such a way that the increased surface roughness causes interlocking. When load is applied parallel to the interface then mechanical bonding plays an important role wherein load is efficiently transferred from matrix to reinforcements. But one should understand that the mechanical bond is alone insufficient for good interfacial bonding between reinforcement and matrix. However high surface roughness is fraught with the danger of formation of interfacial voids owing to incomplete penetration. Overall, chemical bond is known to be strongest bond and mechanical bond is known to be the weakest (Schoene and Scala ,1970; Vennett et al. 1970).

1.10.2 Orientation

The orientation of reinforcements plays an important role since the properties along the direction of reinforcements (especially for fibers) are significantly improved. Similarly, in the materials where the fibers are oriented in different directions, the properties such as strength will be high in the direction of fiber orientation. However, in case of particulates, the orientation does not play a significant role since the properties are same in all directions unlike in case of fiber reinforced composites. Strength of unidirectional composites is unmatched when compared to that of woven fabric and particulate composites (Campbell, 2010).

1.10.3 Material

The strength of MMC's mainly depends on the material of reinforcement. Though the material plays an important role, the application decides the type of reinforcement material. In certain industries such as aerospace where cost is not the constraining factor then high strength and high elastic modulus fibers based on carbon are used. For applications, where both cost as well as properties are important factors then in such cases glass and Aramid fibers are utilized. However, for automotive applications economical materials like ceramic particulates are utilized. Diamond and nanomaterials like graphene which possess higher thermal properties are used for heat management applications.

1.10.4 Wettability

This is one of the important criteria when metal matrix composites are produced by casting or pressure infiltration techniques. The degree of wettability is usually determined by the contact angle of a drop of molten metal on the surface of a solid. One should study the surface and interface energies for composite systems to understand wettability. Based upon the interface energy and contact angle adjustment, the angle limit for a wettable system is $< \pi/2$ while for a non-wettable system the angle limit is $> \pi/2$. One should understand that as the contact angle decreases the wettability of a molten metal with its solid base increases. The wetting of molten metal/drop, in this case, depends on kinetics, which means it depends on temperature and time. Further, if any alloying element is added to the metal the wettability is affected because the surface tension of the melt droplet changes. For example, in infiltration, if the wettability is good then one can observe the capillary effect of melt in between the fibers. However, if the wettability is not good then such an effect is not seen. In the case of particulate reinforced MMC's, poor wetting of particles can result in segregation of particles (Lloyd et al. 1989; Stephenson et al. 1993).

1.11 Heat treatment

The purpose of heat-treatment of Al alloys is to achieve the best possible mechanical properties for the desired industrial applications. A sequence of microstructural modifications enhances the mechanical properties based on thermal treatment factors, i.e., temperature and time (Ceschini et al. 2009; Wang and Davidson, 2001; Tan et al.1995)

1.11.1 Temper designations used in heat treatment

The temper designations used for as-cast alloys are F, O and T which stand for: as fabricated, annealed, and thermal treatment. Here the temper designation T is further subdivided into T4, T5, T6 and T7 (commonly used designations) which indicates artificial and natural aging conditions. A schematic of aforesaid temper designations is summarized in Figure. 1.4.

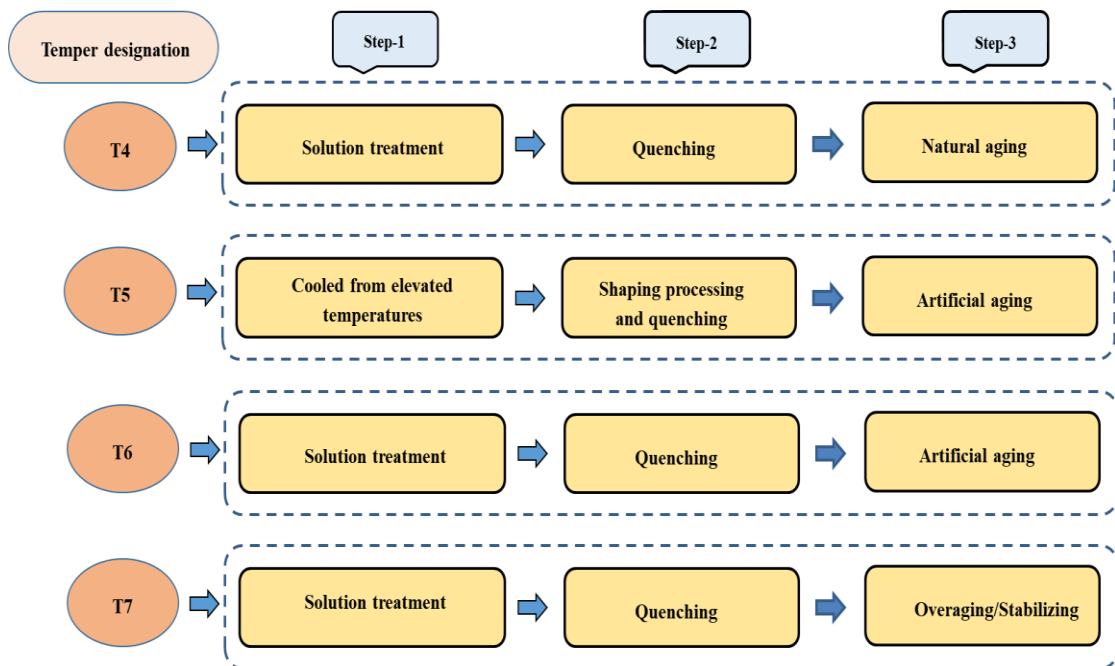


Figure 1.4: Schematic of commonly used temper designations in heat treatment.

1.12 Heat treatment of aluminum alloys (Precipitation hardening)

In addition to heat treatments such as stress annealing for removing residual stresses, the Al-Si-Mg alloy castings are subjected to different types of heat treatment processes, one of which is solution heat treatment that is carried out with and without quenching.

Heat treatment which is generally adopted for enhancement of mechanical properties starts with homogenization and precipitation hardening. The precipitation hardening process involves solutionizing followed by quenching and artificial aging (Shivkumar et al. 1989; ASTM handbook, 2002; Heat treating, 1991)

(i) Solutionizing: Solutionizing aims to get a homogeneous solid solution of the material. Here the alloy is heated to a pre-set temperature to dissolve all soluble alloying elements and is retained at that temperature for a sufficient time.

(ii) Quenching: The aim of quenching is to keep the alloying elements trapped in the solution and to achieve maximum super saturation of alloying elements.

(iii) Artificial aging: Artificial aging aims to reduce the time for precipitating the dissolved impurity or solute phase.

A schematic of precipitation hardening (Temperature versus Time diagram) is shown in Figure. 1.5.

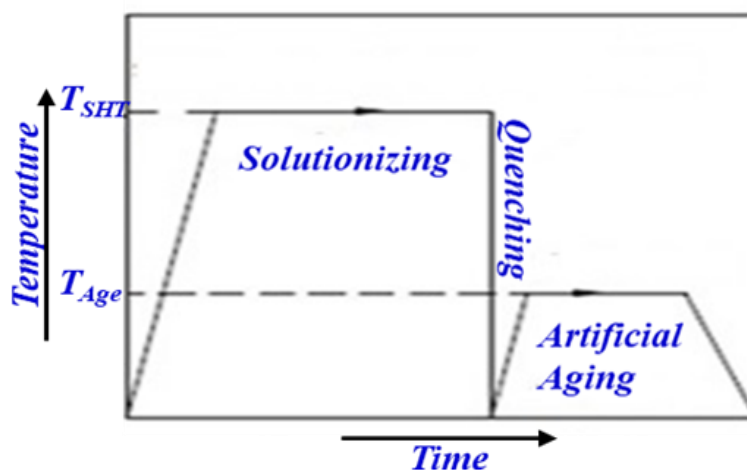


Figure 1.5: Schematic of precipitation hardening (Temperature vs Time diagram).

For Al-Si-Mg alloys, T6 temper conditions are preferred, which is documented by ASTM standards such as B917 and B91. According to these standards and as documented by several researchers, the solution treatment suggested varies from 450°C to 560°C for 4-12 hours and aging temperature ranges from 150°C to 250°C for 6-12 hours (ASTM handbook, 2002; Apelian et al. 1990; Colley et al. 2014; Colley et al. 2014). Different combinations of eutectic phases like Mg₂Si, Al₈Fe₂Si, and eutectic Si are formed with solid solutions.

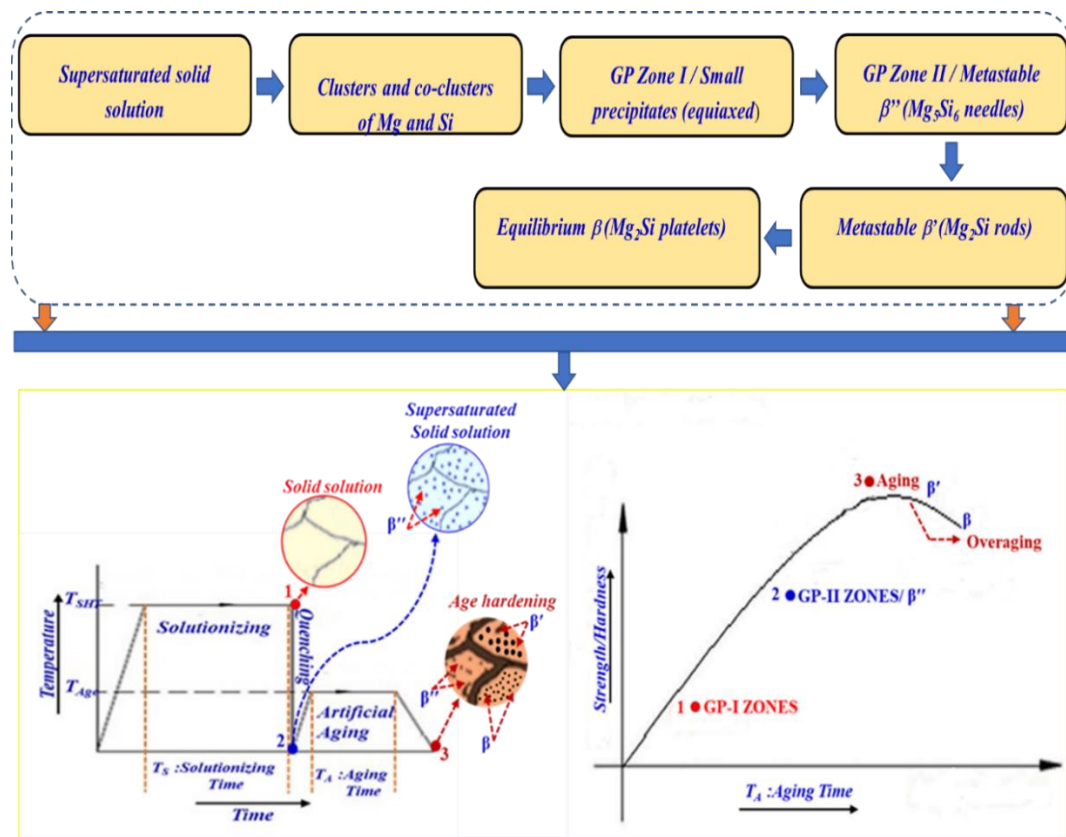


Figure 1.6: Precipitation sequence of Al-Si-Mg alloy.

Further addition of reinforcement like ceramic and carbon particulates changes the aging sequence, and also decreases the time required for aging. Overall, the aging sequence (Figure. 1.6) after the heat treatment process in Al-Si-Mg alloy is shown below (Chakrabarti and Laughlin, 2004; Hasting et al. 2009; Anderson et al. 1998; Pashley et al. 1967).

1.13 Effect of heat treatment on mechanical behaviour and strengthening mechanisms

Addition of reinforcement to the metal matrix can bring a number of changes in the microstructure of MMC's. Mechanical properties such as strength, modulus, fracture toughness and creep resistance are increased significantly when ceramic or organic reinforcements are added to the metal matrix. For example, when reinforcement is added to metal matrix, the difference in CTE can introduce the dislocations especially near the interface region. Apart from dislocations, other defects like vacancies are found to appear near the reinforcement/matrix region. Introduction of such defects are capable of affecting the chemical reactions as well as aging kinetics. Aging kinetics of a precipitation hardenable alloy such as A357 is highly influenced due to addition of reinforcements but the precipitation sequence remains the same. The aging kinetics is accelerated in the presence of reinforcement by virtue of enhancement in dislocation density. These dislocations act as heterogeneous nucleation sites for precipitates during natural aging treatment. But the hardness and strength enhancement greatly depend on the type of precipitates formed and their respective size. However, it is necessary to have controlled reactions at the interface to obtain strong bonding between matrix and reinforcement. A thick interaction region will have detrimental effect on the properties of composites. A strong and continuous interfacial bond will ensure transfer of applied load from matrix to the hard and strong reinforcements. Here, the interfacial bonding does depend significantly on wettability of reinforcement by the metal matrix. In case of MMC's produced by casting technique, the normal dendritic structure is entirely different when compared to unreinforced metals. The morphology of dendritic structure is completely controlled by fiber or particle dispersion due to which grain refinement is achieved. On the other hand, the secondary phases prefer to appear at the interface region since most of the chemical and mechanical interactions occur here. Overall, such high densities of defects will alter the various properties of MMC's which can be tailored based upon reinforcement size, morphology, and weight fraction.

1.14 Wear behaviour

Tribology is an interdisciplinary field which embraces the study of lubrication, friction, and wear of two different surfaces of a component which are in relative motion. So, when pure aluminium or its alloy comes in contact or slides with the hard surface such as that of steel then the former is expected to undergo progressive loss of its surface layers. The loss starts with the process of adherence of aluminium surface layer to iron surface followed by creation of interface with shear strength. When the relative motion of these two counterpart surfaces increases there will transfer of aluminium to steel surface. The wear debris is formed due to ploughing action by hard asperities of iron surface which continues with the increase in sliding. In some other cases, due to poor lubricating conditions, aluminium alloys are more vulnerable to seizure. However, it is very important to note that both friction and wear resistance are not intrinsic properties of material but are system dependent properties. Therefore, it is necessary to understand the response of materials and to tailor their properties to achieve desired resistance to friction and wear. In this regard, the properties should be controlled for specific component by changing the composition during processing stage itself.

Simple correlation between wear resistance and hardness can be obtained using Archard equation for dry sliding wear conditions. However, the obtained empirical data cannot be compared with generalized wear behavior due to wide difference in test conditions. Several research works have shown that the addition of ceramic reinforcements have resulted in considerable increase in wear resistance of MMC's. But in order to obtain better wear resistance the interface between the reinforcement/matrix should be strong such that reinforcements do not debond during wear test. It is generally well known that SiC particles exhibit better wear resistance compared to other particulates. Hence one of the objectives of the present work is to evaluate the tribological behavior of dual size SiC reinforced A357 composites.

CHAPTER 2

2. LITERATURE SURVEY

This chapter presents critical review of the published literature relevant to the present work. Literature review begins with prior work on Al-based MMC's. Next, a review of prior work on tribological properties of Al-based MMC's is presented. Finally, a review on dual particle reinforced composites is presented.

2.1 Mechanical properties of Al-based MMC's

The mechanical behaviour of materials plays a significant role in the development of new materials. There are different techniques to increase the mechanical properties which includes addition of reinforcements, heat treatment and secondary processing techniques. This section summarizes the research work that has been carried out by several researchers on single particle size (SPS) reinforced Al-based MMC's and also the influence of heat treatment on their mechanical properties.

Zulfia et al. (1999) studied the effect of SiC reinforced A357 composite fabricated by stir casting and hot isostatic processing technique. The SiC particulate chosen had an average particle size of 30 μm and about 15 vol% SiC was reinforced to A357 matrix. This work reported the yield (163 MPa) and nominal strength (367 MPa) of A357 alloy in as-cast condition. In contrast, the reported strength values for the A357/SiC composite were much lower. Further, the reported strength values of the A357/SiC composite obtained from the hot isostatic process (HIP) were also lower at 96 and 214 MPa compared with the base alloy A357 (121 and 274 MPa). The reduction in properties of reinforced composites were attributed to the formation of brittle phases and high levels of porosity.

Churyumov et al. (2019) studied the mechanical properties of Al-Si-Mg composite reinforced with SiC particles fabricated by stirring and pressure crystallization techniques. Different percentage (5, 10 and 15%) of SiC particles of 40 μm size were

added to the Al-Si-Mg matrix. The yield strength of Al-Si-Mg alloy and composites with different SiC content (5, 10 and 15%) were 295, 310, 325 and 330 MPa, respectively. The improvement in strength was attributed to the pressure crystallization process as it enables uniform dispersion of SiC particles when compared to that of cast composites. In addition to this the pressure crystallization process helped in better bonding between SiC particulate and Al-Si-Mg matrix.

Electromagnetic frequency effect on the mechanical behavior of A357 composite reinforced with SiC nanoparticles was investigated by Badizi et al. (2018). The nanocomposites were produced using electromagnetic stirrer fixed in resistance furnace with the entire set up in a chamber of vacuum at 750°C. With the increase in the frequency of electromagnetic stirring, grain size of both A357 alloy and the nanocomposite was found to decrease. The nanocomposites exhibited higher hardness (60 BHN) when compared to that of A357 alloy (55 BHN). The yield and ultimate tensile strength of A357 alloy are 79 and 119 MPa. A357/SiC nanocomposite showed higher strength of 120 and 188 MPa respectively for 60 Hz electromagnetic stirring. The homogenous dispersion of hard ceramic nanoparticles were attributed to be primarily responsible for the increase in the hardness and strength of nanocomposites.

Kandemir (2017) employed the ultrasonic cavitation method for processing A357/SiC composites and evaluated their microstructure and mechanical properties. The A357/SiC composite exhibited higher hardness (73 HV) and tensile strength (198 MPa) when compared to that of A357 alloy, which exhibited a hardness of 60 HV and tensile strength of 138 MPa. They attributed this increase in strength and hardness to reduction in grain size of composites, thereby assisting the Orowan mechanism. On the other hand, A357/SiC composite had little effect on load-bearing mechanism.

Tekmen and Cocen et al. (2003) studied the effect of heat treatment on Al-Si-Mg/SiC composite developed by compocasting technique followed by extrusion. All unreinforced and reinforced materials were solutionized at 530°C for about 2h followed by artificial aging at 175°C for about 48 hours. For Al-Si-Mg alloy and 20 wt% SiC reinforced composite the hardness obtained after peak aging time varied

with cold working plastic strain (4, 10, 25 and 50%). For strain rates of 4 and 10%, the peak aging time was 8 and 7 hours and hardness of alloy and composite were 106 and 120 HV, respectively. Increase in hardness was due to grain refinement and transformation of coherent and semi-coherent precipitates.

Li et al. (2018) studied the effect of heat treatment on Al-Si-Cu-Mg/SiC composite developed by electromagnetic stirring technique. The composite was solutionized at 520°C for about 6h and water quenched at room temperature followed by artificial aging at 175°C for about 6h. The microhardness and UTS of composite before heat treatment were 87 HV and 239 MPa respectively while after T6 heat treatment the hardness and strength increased to 102 HV and 274 MPa. Al₂Cu based needle like precipitates of 100 nm length formed after heat treatment were primary responsible for improvement in the mechanical properties.

Cocén et al. (1997) reported the age hardenability of Al-Si-Mg/SiC composite fabricated by compocasting technique. Composite samples were solutionized at 530°C, quenched in water and aged at two different temperatures of 150 and 175°C. The composite aged at 150°C showed a peak aging time of 180 minutes and hardness of 33 HB. When the same composite was aged at 175°C the peak aging time was 100 minutes, and the hardness was 16 HB. The decrease in hardness after 150°C aging temperature was attributed to low hardening efficiency and depletion of Mg content to form Mg₂Si precipitates. The work showed that the critical aging temperature was highly dependent on both the microstructure of the matrix and also the amount of Mg₂Si precipitates.

Bloyce and Summers (1991) employed the squeeze casting technique to process A357/SiC Al-based MMC's and carried out heat treatment at two solutionizing temperatures (525°C and 540°C), and two aging temperatures (170 and 160°C). From the studies on static and dynamic mechanical properties, they concluded that solutionizing at 540°C and aging at 160°C resulted in higher mechanical properties for both A357 alloy and the A357/SiC composites.

Liu et al. (2018) studied the precipitation kinetics of in-situ Al-Si-Mg composite reinforced with TiB_2 particles. A composite with 5 wt% percentage of TiB_2 was produced using salt reaction technique. This composite was solutionized at 540°C for about 8 hours followed by hot water quenching. Artificial aging was conducted at 170°C for time duration of about 7 hours followed by mechanical testing. Hardness of the alloy increased from 62 to 95 HB with T6 heat treatment. Similarly, the hardness of the composite increased from 72 to 105 HB with heat treatment. Tensile strength of the alloy increased from 98 to 155 MPa with T6 heat treatment. Similarly, the tensile strength of the composite increased from 114 to 212 MPa with heat treatment. Strengthening of aged composites was attributed to both modification of eutectic Si phase and also to better dispersion of TiB_2 particles.

Wang et al. (2014) studied the effect of T6 heat treatment and addition of Sr on mechanical properties of A356/ TiB_2 composites. The composites were heat treated wherein solutionizing was carried out at 540°C for about 12 hours followed by cold water quenching. The final step was artificial aging which was conducted at 155°C for about 10 hours. The YS and UTS of A356 alloy before heat treatment were 97.5 and 151.5 MPa respectively while that of composite were 109 and 164.5 MPa, respectively. After heat treatment the YS and UTS of A356 alloy increased to 208.1 and 263.1 MPa respectively while that of composite increased to 255.5 and 312.5 MPa, respectively. The formation of fine size Mg_2Si precipitates in the Al grains were primarily responsible for increase in strength after heat treatment.

Satish Kumar et al. (2016) investigated age hardening effects of Al-Si-Mg hybrid composites reinforced with ZrSiO_4 and Al_2O_3 particulates. The composite fabricated using casting technique was solutionized at 540°C for about 3h hours followed by cold water quenching. Then aging was done at 170°C for different time durations ranging from 0 to 480 minutes. Compared to zircon reinforced composites, the one reinforced with alumina showed high hardness of 118 HV for an aging duration of 360 minutes. The hardness increased with increase in aging time up to 360 minutes

thereafter it started to decrease. Formation of Mg_2Si precipitates in the matrix material was responsible for increase in hardness.

Deepak Kumar et al. (2015) studied the age hardening behavior of A356/TiB₂ composites fabricated by thixoforming. Solution treatment was conducted at 540°C for a time duration of 8 hours and quenching was done in cold water. Soon after quenching the samples were aged at 160°C for a time duration varying from 0 to 24 hours. The samples were air-cooled to room temperature after artificial aging and subjected to microstructure analysis. A356 alloy showed a coarse dendritic structure, while after the addition of TiB₂ and heat treatment, the structure was transformed into fine equi-axed structure. This study reported that the time taken for peak aging in case of A356 alloy was 12 hours while that in case of composites it was 8 hours. The peak aged samples were subjected to transmission electron microscopy studies which revealed the formation of Guinier–Preston (GP) II zones and Mg_2Si precipitates. The size of these precipitates were in the range of 10 to 20 nm with most of them located at the grain boundaries.

Samuel et al. (1993) studied the effects of heat treatment on SiC reinforced Al-Si-Mg composites. Solution treatment was carried out at 538°C for about 8 hours while the quenching was in warm water at 60°C. The artificial aging was at 155°C for 5 hours followed by air-cooling to room temperature. Microstructure showed formation of Al₄C₃, Al₂O₃ and MgAl₂O₄ spinels at the SiC and Al interface. Formation of Mg_2Si precipitates were also seen in the microstructure after T6 heat treatment.

Abdulwahab et al. (2017) in their work, studied the effect of heat treatment on Al-Si-Mg/melon ash composite developed by stir casting technique. Here, the heat treatment was carried out with solution treatment conducted at 540°C for about 1 hour followed by warm water quenching at 65°C. Aging was conducted at 180°C for about 2 hours and later air cooled to room temperature. The heat treatment process resulted in the formation of Mg_2Si precipitates along with Al₂Mg₃ intermetallic compound. On the other hand, plates corresponding to Al-Si-Mg were also seen in the aluminium matrix.

Menargues et al. (2015) reported heat treatment of semisolid processed Al-Si alloy. In this study, the alloy was subjected to T6 heat treatment with solution treatment less than 30 minutes as mentioned in standard procedures. Solution treatment of alloy was carried out at three different temperatures 520, 530 and 540°C with varying times ranging from 5 minutes to 5 hours. After solution treatment, the alloy was quenched in liquid media such as water which was kept at room temperature. Then artificial aging was conducted at 160, 170 and 180°C with the time duration ranging between 1 to 5 hours. Here aging was necessary to decompose the supersaturated solid solution and then in turn form fine precipitates. Microstructural analysis showed formation of π -AlFeSiMg, needle shaped β -AlFeSi intermediate phase and dark coloured Mg₂Si phases.

Shabestari et al. (2016) studied the effect of heat treatment on impact toughness of aluminium alloy A356. The alloy samples were solution treated for 540°C for about 6 hours followed by quenching in water. The artificial aging process was conducted at 155°C for a time duration of 4 hours and then air cooled. The time gap between solution treatment and artificial aging was less than 30 seconds which also involved quenching in water. The morphology of eutectic silicon was changed from plate to rod and then to spherical shape after heat treatment. The coarse α -Al dendrites were transformed to fine equi-axed grains with fine fibrous silicon particles after heat treatment.

2.2 Tribological properties of Al-based MMC's

Interaction of two sliding bodies changes when reinforcement is added to the one of them. The influence of these interactions can be seen on coefficient of friction and wear rate. This is because, when two different pure metals or alloys are subjected to sliding motion the coefficient of friction and wear rate would be very high and sometimes can lead to seizure of the surfaces. On the other hand, significant changes in microstructure of metal or alloy due to addition of reinforcement can result in different friction coefficient and wear behaviour. Numerous studies have been devoted to reduce the coefficient of friction and wear rate by adding alloying

elements, reinforcements, and microstructure modification in the surface region. This sub-section reviews the research carried out on understanding tribological behavior of single-particle size (SPS) reinforced Al composites. The review also includes effect of heat treatment of Al-based MMC's on its tribological properties.

Leonard et al. (1997) reported dry sliding wear of SiC reinforced A357 composite that was developed by casting technique. The 30 vol% SiC reinforced A357 composite was subjected to tri-pin -on-disc testing machine with grey cast iron having 180 HV₁₀ as the counterface. At a load of 6 N, the alloy exhibited high wear rate of 169.6×10^{-6} mm³/Nm while composite exhibited low wear rate of 3.1×10^{-6} mm³/Nm. At a load of 74 N, the composite exhibited high wear rate of 176.8×10^{-6} mm³/Nm while the A357 alloy exhibited lower wear rate of 89×10^{-6} mm³/Nm. At lower loads, the dominant wear mechanism was oxidation with some contribution from three body abrasion. At higher loads, adhesive wear was more predominant with detachment of large metallic sheets due to subsurface cracking which is why the composite exhibited higher wear rate.

Zulfia et al. (2017) reported the wear testing of Al-Si-Mg/SiC composite fabricated using stir casting technique. The test was conducted as per Ogoshi method with an applied load of 12.6 kg, sliding speed of 1.97 m/s and sliding distance of 400 m. The wear rate of composites was found to decrease with increase in SiC content from 2 to 15% volume percentage. Al-Si-Mg alloy showed 0.022 mm³/m wear rate while the composite with 15% SiC showed 0.004 mm³/m wear rate. Microstructure showed formation of MgO.SiO₂ and MgAl₂O₄ spinels at the SiC and Al interface which offered wear resistance to the composite. The spinels formed also ensured minimal SiC particle pull out during wear test, thereby avoiding severe wear.

Natarajan et al. (2006) studied the wear behavior of A356 reinforced SiC composites with sliding against grey cast iron. The composite with 25% weight percentage of SiC was produced by stir casting and later heat treated following T6 temper conditions. At 40 and 60 N loads the volume loss of cast iron was higher than that of A356/SiC composite for all cases of sliding velocities. Similarly, at sliding velocities of 2.5 and

3.7 m/s, the volume loss of cast iron was significantly higher than that of composite for all cases of load. On the other hand, the friction coefficient of A356/SiC composite at 2.5 and 3.73 m/s sliding velocities at varying load was found to be significantly higher (0.57-0.64) than that of cast iron (0.29-0.39). Based upon high coefficient of friction the authors recommended the composite for brake rotor applications.

Rahimipour et al. (2014) reported wear studies on A356/Al₂O₃ composite produced by compocasting. The cast composite was heat treated with solutionizing being carried out at 545°C for about 4 hours followed by aging at 155°C for about 6 hours. The weight loss of composite was found to increase with the increase in applied load from 5 to 30 N. For a load of 5 N the weight loss was 1.8 mg while at a load of 30 N the weight loss was 5.8 mg. Similarly, with the increase in sliding distance and at constant load of 10 N, the weight loss was found to increase. The worn surface observed for 10 N load tests was composed of deep continuous grooves and extensive plastic deformation. In case of higher specific load, the debris morphology was plate shaped and had sharp edges which imply that adhesive wear was predominant.

Cam et al. (2016) reported the wear properties of A356 in-situ composite reinforced with TiAl₃ fabricated using mechanical alloying and powder metallurgy techniques. Here, wear test was conducted at room temperature and under dry sliding conditions at load of 30 N and sliding speed of 1 m/s. The weight loss of composite increased with an increase in sliding distance from 400 to 2000 m. The wear-rate of composite reinforced with 8 wt% Ti was less than that of composite reinforced with 4 wt% Ti. This decrease in coefficient of friction was attributed to the higher amount of intermetallic phases which play a big role in increase in hardness. For different Ti contents the coefficient of friction was evaluated, and it was found that the coefficient of friction decreased with increase in Ti content from 4 to 8 wt.%. The composite with 4 wt.% Ti exhibited highest weight loss and also showed extensive plastic deformation when examined under electron microscope.

Sam et al. (2020) reported tribo-mechanical studies on LM25 composite reinforced with TiB₂, WC, and ZrO₂ produced by squeeze casting. The cast composite was solutionized at 520°C for about 8 hours, followed by aging at 165°C for 4, 6, and 8 hours. The wear tests were conducted as per Response Surface Methodology (RSM) model with applied load, sliding speed and distance ranging from 10–50N, 1–4 m/s and 500–2500 m respectively. Optimal results were obtained by solutionizing at 520°C for 8 h followed by quenching and aging at 165°C for 8 h. The worn surface observed for 50 N test load had deep grooves and extensive plastic deformation.

Radhika et al. (2020) studied the tribo-mechanical behavior of A359 composite reinforced with TiB₂, TiO₂, and TiC produced by modified stir casting. The cast composite was solutionized at 540°C for about 10 hours, followed by aging at 155°C for 10 hours. Linear reciprocating wear test was carried out with applied load and sliding distance ranging from 15–55 N and 500–2500 m, respectively. A359/TiB₂ composite exhibited the least weight loss when compared to A359/TiO₂ and A359/TiC composites. The worn surfaces of T6 treated A359 composites displayed mild plastic deformation compared to severe plastic deformation of untreated composites.

2.3 Dual particle size (DPS) composites

Some recent studies were carried out on reinforcing metal matrices with dual size (bimodal sized) particulates. The composites reinforced with dual size particles have shown better strengthening and wear resistant properties compared to single reinforcement composites. Out of two different sized particles, the larger size particles contribute towards improvement in hardness and wear resistance while the small size particles contribute towards improvement in strength. This section summarizes the research carried out on dual-particle size (DPS) reinforced Al-based composites. A review on mechanical and tribological properties of dual particle size Al-based MMC's is also herewith provided.

Kheirifard et al. (2018) in their work, used Ni-P coated Al₂O₃ and SiC particles of two different sizes namely 170 and 15 µm respectively to reinforce A356 alloy. The Al₂O₃

and SiC particles used were of 99.7% and 99.4% purity with irregular and angular morphology. The Ni-P coated particle reinforced composites were fabricated using stir casting technique and hot rolling. This work reported that compared to single reinforcement, the dual particle size reinforced composite exhibited high strength and hardness.

Sadeghi et al. (2018) studied the mechanical behavior of spark plasma sintered Al/Al₂O₃ bimodal composites. The Al₂O₃ particles chosen had average particle size of 20 nm (smaller particle size) and 10 μm (larger particle size) and different weight ratio combination (2:8, 4:6, 6:4) were used to reinforce Al. The hardness of composites increased with increase in ratio of nm to μm size particles when compared to that of unreinforced Al. Here, the addition of nanoparticles helped in inducing recrystallization which helps in grain refinement and increasing the hardness of composites. In addition to this, the particles especially the nanosize ones help in formation of new grains by particle size nucleation mechanism and also inhibit grain growth.

Wang et al. (2013) used pressure less infiltration process to prepare dual-particle size A356-SiC composites with different SiC sizes (14, 28, 50 and 85 μm). The size dispersal ratios were 50:14 and 85:28. They did not observe any particle damage due to the infiltration process. Further, good bonding was confirmed by the absence of pores. The bending strength of composites was found to increase with decrease in particle size. The thermal conductivity of composite decreased because of interfacial heat barrier and presence of Fe impurities.

Davila et al. (2007) reported the hardness of bimodal SiC reinforced Al composites developed by pressure infiltration process. SiC particles of average sizes 10 μm and 68 μm were used to reinforce Al in different ratios of 1:1, 3:1 and 1:3. The bimodal composites showed hardness of 34 HRC while unimodal composite showed a value of 40 HRC. Similarly, the microhardness of unimodal and bimodal composites were 2339 and 3360 kg/mm², respectively. The bimodal composites required higher stresses for plastic deformation, and this was considered as the primary reason for

their high hardness. This study concluded that work hardening in case of bimodal composites was quite higher than that of unimodal composites.

Dhandapani et al. (2016) studied the effect of dual particle size reinforcements (carbon nanotubes and B₄C particles) on density and microhardness of Al composites. The size of carbon nanotubes and B₄C particles were 50 - 80 nm and 150 μm respectively with both having purity close to ~99.5%. The composites were fabricated using powder metallurgy technique with sintering carried in the temperature range of 420 - 450°C. The hardness of single reinforcement composite (Al/B₄C) was 70 VHN while that of dual particle size composites was 78 VHN. However, with the increase in CNTs content from 1% to 2% the hardness decreased to 74 VHN. Even though the hardness decreased with increase in CNT content, it was still higher than that of single reinforcement composite (Al/B₄C).

Khosroshahi et al. (2015) studied the effect of dual particle size on mechanical properties of A356 composites. The dual size reinforcements Al₂O₃ (~170 μm) and SiC (~15 μm) were used to reinforce A356 alloy using semi-solid stir casting and rolling techniques. Dual particle size composites showed fine grain size of 49 μm compared to that of single reinforcement composite (SiC) and A356 alloy which exhibited a grain size of 59 μm each. The effect of grain size was seen on ultimate tensile strength and yield strength of all materials. For example, yield strength of A356 alloy, single and dual particle size composites was 148, 191 and 237 MPa, respectively. Similarly, ultimate tensile strength of A356 alloy, single and dual particle size composites was 215, 266 and 302 MPa, respectively. It can be seen that dual size particle composites had very good mechanical properties when compared to both the A356 alloy and single reinforcement composites due to grain growth restriction caused by dual size particles.

Dual sized particles are not only used to enhance the mechanical properties of many metal matrices, but they are used to tailor the thermal properties. Arpon et al. (2003) studied the thermal response of aluminium composites reinforced with dual size SiC particles. The composites were produced using infiltration technique with average

size of SiC particles being 16 and 170 μm respectively with 98.5% purity. The coefficient of thermal expansion of the composite decreased linearly with increase in the particle content. However, no simple relationship between bimodal particles and hysteresis was obtained for the composites.

Chu et al. (2009) studied the thermal conductivity of dual particle size SiC reinforced Al-12Si alloy developed by infiltration technique. Very high SiC particle content (56-65 vol%) were used to produce Al/SiC composites by employing powder injection molding followed by infiltration. SiC particles of average sizes 14 μm , 28 μm , 40 μm , and 70 μm with 99.5% purity were used to reinforce Al in different unimodal (28,40,70) and bimodal (70:28 μm and 40:14 μm) combination ratios which were subjected to laser flash method. The dual particle size reinforced composite showed better conduction properties when compared to single particle reinforced composites.

Apart from mechanical and thermal properties, the tribological properties of dual-particle size reinforced Al-based MMC's have also been studied. Bindumadhavan et al. (2001) studied the effect of dual-size SiC (47 and 120 μm) on impact energy and wear rate of Al-Si-Mg composites which were then compared with single-particle reinforced composites. The impact energy of dual particle size SiC composite (12.2 J) was found to be nearly double than that of single-particle reinforced composite (6.7 J). Further, the wear resistance of dual particle size composite was nearly 60% higher than that of the single-particle reinforced composite. The authors concluded that dual-sizing the composites improves both the wear resistance and also the impact energy significantly.

Sharma et al. (2018) showed through their experiments conducted on dual-size Al-Si-sillimanite (1-20 μm and 75-106 μm) composites that a ratio of 3:1 (between the smaller size particles and bigger particles), resulted in maximum nano-hardness and minimum wear rates.

Prabhu (2016) processed Fe based composites wherein Fe matrix was reinforced with the bimodal size dissimilar nature (SiC and SiO₂) particles through powder

metallurgy. The author showed that the addition of bimodal size particles improves the wear resistance of the composites significantly by comparing with single size particle reinforced composites. Further the author concluded that, the formation of a mechanically mixed layer as the main reason for the reduced wear rate in Fe matrix composites reinforced with SiC and SiO₂.

Maleque and Karim (2008) reported wear behavior of dual particle size SiC reinforced Al6061 composites developed through liquid metallurgy route. The particles of SiC had an average size of 20 and 80 µm and the combination of weight percentage of dual particle size SiC are 7:13 and 13:7. The tribology test was conducted using pin on disc tribotester with a counterface made of steel having a hardness value of 60 HRC. The composite with higher content of fine SiC particle size showed lowest cumulative wear of 22 mg while the one with highest coarse SiC content showed highest wear loss of 24 mg. However, the coefficient of friction for higher weight fraction of fine sized SiC particles was higher (0.57) than that of higher weight fraction of coarse sized SiC particles (0.56). The composite with highest content of fine SiC particle size showed grooving wear mechanism while the one with highest coarse SiC content exhibited ploughing wear mechanism.

Arora et al. (2015) studied the influence of dual particle size rutile on wear properties of LM13 aluminium alloy composites. The rutile particles with coarse size (in the range of 106-125 µm) and fine size (in the range of 50-75 µm) were reinforced to LM13 alloy using stir casting process. Sliding wear tests were conducted using pin on disc testing machine with EN32 (of 65 HRC) as counterface disc. Composites with fine size rutile particles exhibited lower wear rate (4.7×10^{-3} mm³/m) when compared to that of coarse rutile particle reinforced composites (8.4×10^{-3} mm³/m). Fine size particles help in increasing the hardness and refinement in morphology of eutectic silicon. The extent of hardness enhancement and silicon refinement by fine size particles was higher than that of coarse size particles. In both the cases, oxidative wear was the more predominant mechanism followed by plastic deformation.

Arora et al. (2015) also reported the wear behavior of stir cast processed LM13 alloy composite reinforced with rutile particles at high temperatures. The LM13 alloy was reinforced with rutile particles of different sizes, 50-75 μm and 106-125 μm and different weight percentages 10 and 15%. Dry sliding wear tests were conducted on pin on disc machine using sliding distance of 3000 m, sliding speed of 1.6 m/s and two different loads. The wear rate was found to increase slightly with temperature up to 150°C. But at higher temperatures above 200°C there was abrupt increase in wear rate. However, at the higher load of 5 Kg the wear rate was found to decrease above temperatures of 200°C. Formation of mechanically mixed layer was attributed to be the main reason as to why the wear rate decreased at this temperature. Further, the fine size particle reinforced composites showed minimal wear loss when compared to that of coarse particle size reinforced composite.

In another work Singh et al. (2015) studied the wear behavior of Al reinforced with SiC and Al₂O₃. The wear test was conducted using pin on disc machine at constant load of 29.41 N, sliding speed of 239 rpm and sliding diameter of 80 mm. Design of experiments were conducted using Taguchi L9 array to study the significant parameters responsible for the wear of the composites. The authors found that particle size played a prominent role on the wear rate of composites. The other significant parameters were hybrid solute proportion and vacuum pressure. Further, it was found that when compared to triple particle reinforced composite the dual particle reinforced composite displayed better wear resistance.

Sharma et al. (2015) in their work studied the influence of dual size garnet on wear properties of Al-Si alloy fabricated using stir casting route. The particle sizes of garnet used were 50-75 μm and 106-125 μm respectively and about 10-15 weight percentage of garnet were reinforced to Al-Si matrix. The study on the effect of reinforcement revealed that the highest content of fine particle size reinforced composite showed lower wear rates than that of composite with higher weight fraction of coarse particle size. For two different weight percentages of 10 and 15% the wear rate of maximum fine particle size composites showed about 7 and 5% better wear

resistance compared to that of coarse particle size composites. Further at higher loads, deep and continuous ploughing groves were found indicating abrasion of composites.

Kumar et al. (2012) reported the effect of dual size zircon sand on wear properties of LM13 aluminium alloy composites developed using stir casting technique. The average particle size of zircon sand chosen was 20-32 μm (fine) and 106-125 μm (coarse). Further, different weight percentage combinations of these particles utilized were 3:12 and 12:3. At a load of 5 kg, the wear rate of composite with higher fine size particle content showed lower wear rate of $7.1 \times 10^{-3} \text{ mm}^3/\text{m}$ while the composite with higher coarse size particle showed higher wear rate of $9.6 \times 10^{-3} \text{ mm}^3/\text{m}$. Wear rate of both dual size composites was found to be considerably lower than that of single particle composite whose wear rate was $12.7 \times 10^{-3} \text{ mm}^3/\text{m}$. Both the dual particle size composites showed crack propagation and wear loss of material by delamination at 5 kg load.

In another work Kumar et al. (2013) reported the high temperature wear behavior of LM13 reinforced with zircon sand and the composite was fabricated using stir casting technique. Two different sizes of zircon sand used were 20-32 μm and 106-125 μm in different weight percent combinations of 3:12 and 12:3. The composite with higher weight fraction of fine particle size showed highest wear rate at 1 kg load and up to a temperature of 475 K followed by composites with higher weight fraction of coarse particle size. But at a load of 5 Kg, the composite with higher weight fraction of coarse particles showed minimal wear rate when compared to that of composite with higher weight fraction of fine particles. Both the composites showed delamination and abrasive wear mechanisms at temperatures below 100°C while oxidative wear was predominant wear mechanism for temperatures above 150°C .

Kumar et al. (2013) also reported the effect of dual reinforcement zircon and SiC on tribological behavior of LM13 aluminium alloy. Dry sliding wear test was conducted at different temperatures ranging from 50 to 300°C using pin on disc test machine. The counterface used was hardened disc made up of EN32 steel with the hardness of 65 HRC. For a temperature range of 50 to 200°C the wear rate of dual and single

reinforcement composites was found to decrease. This was attributed to the fact that at these temperatures the matrix material expands due to which the particles are held very tightly. With good interface bonding by mechanical interlocking, the wear resistance was minimal at these temperatures. Here dual particle reinforced composite showed better wear resistance compared to that of single particle reinforced composite because SiC refines silicon while zircon act as nucleation site for silicon particles.

Table 2.1 gives various combinations of dual particle size reinforcements used in literature for making MMC's to achieve better properties. In many cases, the reinforcement is the same, but the average particle size will be different while in some different types of reinforcements with different particle sizes were chosen to reinforce MMC's.

Table 2.1: Dual particle size combinations used in different studies

Reference	First particle type		Second particle type	
	Material	Size	Material	Size
Kheirifard et al. (2018)	Al ₂ O ₃	170 μm	SiC	15 μm
Sadeghi et al. (2018)	α-Al ₂ O ₃	20 nm	α-Al ₂ O ₃	10 μm
Montoya et al. (2007)	SiC	10 μm	SiC	68 μm
Dhandapani et al. (2016)	CNTs	50-80 nm	B ₄ C	150 μm
Khosroshahi et al. (2015)	Al ₂ O ₃	170 μm	SiC	15 μm
Arpon et al et al. (2003)	SiC	16 μm	SiC	170 μm
Bindumadhavan et al. (2001)	SiC	47 μm	SiC	120 μm
Sandeep et al. (2018)	Al ₂ SiO ₅	1-20 μm	Al ₂ SiO ₅	75-106 μm
Maleque et al. (2008)	SiC	20 μm	SiC	80 μm
Rama Arora et al. (2015)	Rutile	50-75 μm	Rutile	106-125 μm
Anju Sharma et al. (2015)	Garnet	50-75 μm	Garnet	106-125 μm
Suresh Kumar et al. (2012)	ZrSiO ₄	50-75 μm	Zircon	106-125 μm
Suresh Kumar et al. (2013)	ZrSiO ₄	3.75 μm	SiC	11.25 μm
Prabhu et al. (2017)	Nano clay	15-20 nm	CaSiO ₃	75-150 μm
Mizuuchi et al. (2014)	Diamond	34.8 μm	Diamond	310 μm
Wang et al. (2016)	SiC	0.2 μm	SiC	10 μm
Zhang et al. (2015)	SiC	40 nm	SiC	15 μm

2.4 Summary of literature review

A comprehensive literature survey on the development and processing of Al-based metal matrix composites was conducted. From this review, it can be seen that the emphasis has been to replace cast iron, which is a traditional material used for aerospace and automobile applications by MMC's. Further, it is reasonable to draw conclusions that the dual-particle reinforced composites exhibit better properties than the single particle reinforced composites. However, a question arises as to what is the optimal ratio between the two sizes of particulates that should be used to obtain optimum combination of mechanical and wear properties.

From the literature review, it is found that there are certain areas which have not yet been addressed and they are:

- The effect of the addition of dual particle size SiC on mechanical and tribological properties of A357 alloy.
- The effect of heat treatment on the mechanical and tribological properties of dual particle sized SiC reinforced A357 alloy.

2.5 Objectives of present research

A systematic review of literature revealed no studies reported on the effect of dual particle size SiC reinforcements on the mechanical and tribological properties of A357 alloy. Further, no work was also reported on heat treatment of dual particle size reinforced A357 alloy. These gaps in literature are the motivation for taking up research on A357-SiC dual-size composites. The objectives of the study were formulated as follows:

1. Processing of dual particle size (DPS) SiC reinforced A357 composites using permanent mould casting technique.
2. Microstructural characterization of A357 alloy and its dual particle size composites
3. Evaluation of the physical, mechanical and tribological properties of the developed DPS composites.
4. Heat treatment of developed composites at varying solutionizing and aging temperatures.
5. Study the effects of heat treatment on the physical , mechanical and tribological properties of the developed DPS composites.
6. Correlation of the microstructure of the heat-treated composites with their mechanical and tribological properties.

2.6 Organization of the thesis

A brief skeletal structure of the thesis along with summary of the different chapters are as follows:

Chapter 1 begins with a brief introduction on the background of composite materials, and the available matrix and reinforcement materials. Further, the classification of composites based on matrix and reinforcement materials is presented. Since the present research is focused on MMC's, their classification is elaborated in detail. The particulates used in MMC's are also discussed in detail. In addition, brief background is provided on cast aluminium alloys, and in particular on A357 alloy. Different techniques for fabrication of Aluminium-based MMC's are discussed. Finally, the heat treatment procedures for MMC's are also discussed in detail.

Chapter 2 presents a critical review of the published literature relevant to the present study. The literature review begins with prior work on aluminum-based MMC's. Next, a review of prior work on tribological properties of Al-based MMC's is presented. Finally, a review on dual particle reinforced composites is presented.

Chapter 3 provides details on the equipment used for processing and characterization of A357 alloy and the developed DPS composites. Initially, the equipment and materials used for developing the DPS composites using the stir casting route are discussed. Next, the details of the heat treatment study carried out in this work is documented. Finally, the various techniques and equipment used for microstructural characterization, evaluation of mechanical and wear properties of both A357 alloy, and the developed DPS composites are discussed in detail.

Chapter 4 presents the results of various characterization studies and tests carried out on the A357 alloy and the developed DPS composites. Influence of different weight fractions (3% coarse + 3% fine, 4% coarse + 2% fine, and 2% coarse + 4% fine) of

reinforcements on the mechanical and wear properties of A357 composites is discussed in detail herein.

Chapter 5 documents the effect of solutionizing temperature on the microstructure, mechanical and wear properties of A357 alloy and the developed DPS composites. Results also include wear debris and worn surface analysis.

Chapter 6 presents the effect of aging temperature on the microstructure, mechanical and wear properties of A357 alloy and the developed DPS composites. Results also include wear debris and worn surface analysis.

Chapter 7 presents the overall conclusions drawn from the results of various characterization studies and tests conducted on A357 alloy and the developed DPS composites. This chapter also lists the various directions identified for future research.

CHAPTER 3

3. EXPERIMENTAL DETAILS AND METHODOLOGY

This chapter provides details on the equipment used for processing and characterization of A357 alloy and the developed DPS composites. Initially, the equipment and materials used for developing the DPS composites using the stir casting route are discussed. Next, the details of the heat treatment study carried out in this work is documented. Finally, the various techniques and equipment used for microstructural characterization, evaluation of mechanical and wear properties of both A357 alloy and the developed DPS composites are discussed in detail. The overall work carried out in this thesis is depicted as a flow chart in Figure. 3.1.

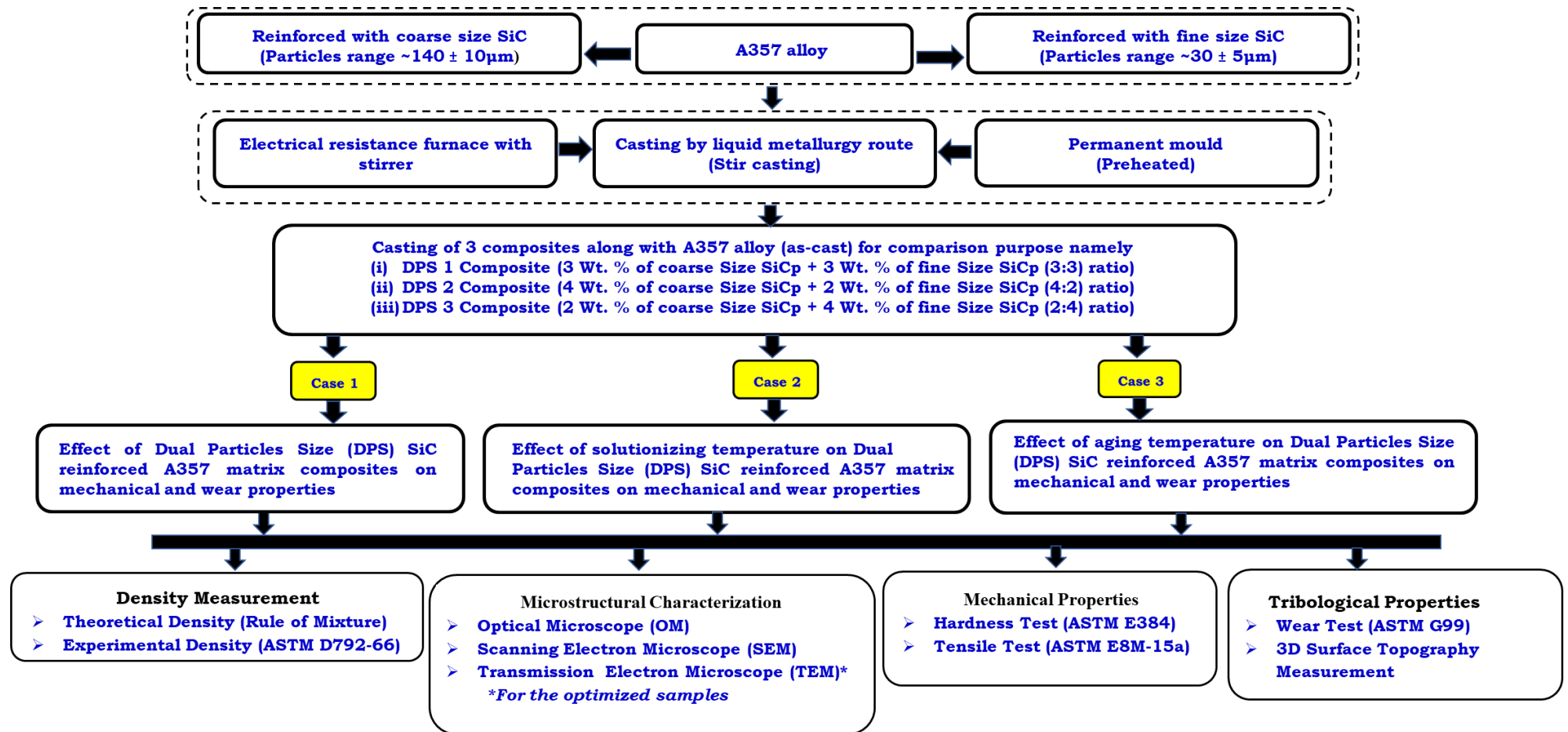


Figure 3.1: Flowchart of the work (Processing, characterization, and testing) carried out in this research.

3.1 Material selection

In order to develop dual particle size reinforced A357 composites, the materials A357 alloy and SiC particles (of two different sizes) were chosen as matrix and reinforcements, respectively. The alloy was procured from Fenfee Metallurgicals, Bengaluru, in the form of ingots (Figure. 3.2). The chemical composition of the procured alloy was carried out as per the ASTM E1251-07 standard using Optical Emission Spectrometer (Model: DV6 Baird, USA). The chemical composition and physical properties were tested at Raghavendra Spectro Metallurgical Laboratory, Bengaluru, and the results are presented in Tables. 3.1. and 3.2.



Figure 3.2: Aluminium A357 ingots.

Table 3.1: Chemical composition of A357

Elements	Si	Mg	Fe	Cu	Mn	Ti	Zinc	Others	Al
Weight %	7.398	0.540	0.086	0.017	0.024	0.177	0.003	0.073	Balance

Table 3.2: Physical properties of A357 (Al-7.4Si-0.55Mg) (Matweb.com, 2020)

Property	Density	Melting point	Shear modulus	Elastic Modulus	Poisson's ratio
Value	2.7 g/cc	557 - 613 °C	26.8 GPa	72.4 GPa	0.33

The SiC powder samples of two different particle sizes ($140 \pm 10 \mu\text{m}$ and $30 \pm 5 \mu\text{m}$) were procured from Snam Abrasives Private Limited, Hosur. The morphology of SiC particles along with EDS analysis are shown in Figures. 3.3 (a), (b), (c) and (d). The chemical composition and physical properties of SiC particles are presented in Tables. 3.3 and 3.4, respectively.

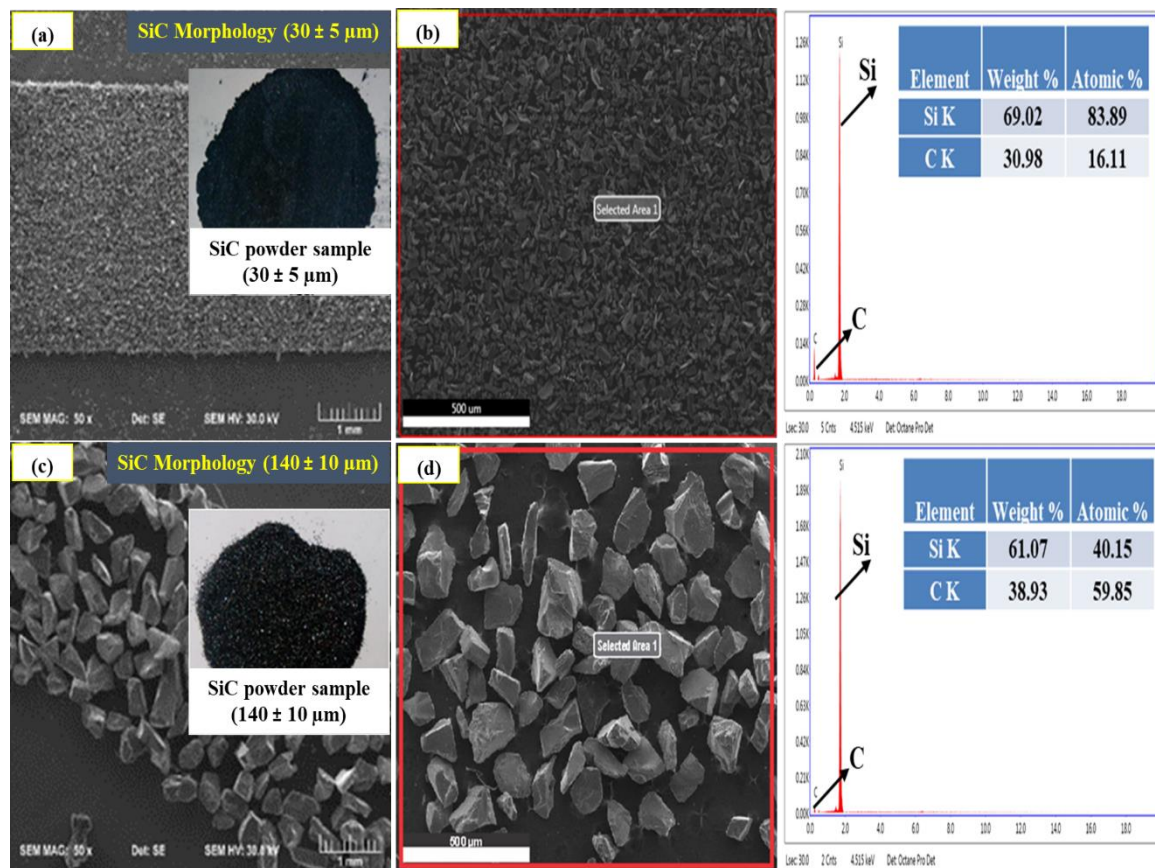


Figure 3.3: Morphology of SiC particles. Where (a) SiC powder sample (fine size), (b) Morphology of fine size SiC particles with EDS analysis, (c) SiC powder sample (coarse size), and (d) Morphology of coarse size SiC particles with EDS analysis.

Table 3.3: Chemical composition of SiC particles.

Element	Al	SiO ₂	CaO	MgO	Si	C	Fe	SiC
Weight %	0.24	0.560	0.040	0.052	0.62	0.24	0.15	Balance

Table 3.4: Physical properties of SiC particles (Matweb.com,2020)

Property	Density	Melting point	Shear modulus	Elastic modulus	Poisson's ratio
Value	3.21 g/cc	2200-2700°C	180 GPa	410 GPa	0.14

3.2 Processing set up

Melt-stirring assisted permanent mold die casting technique was adopted to fabricate the A357 alloy composites reinforced with dual particle size SiC.

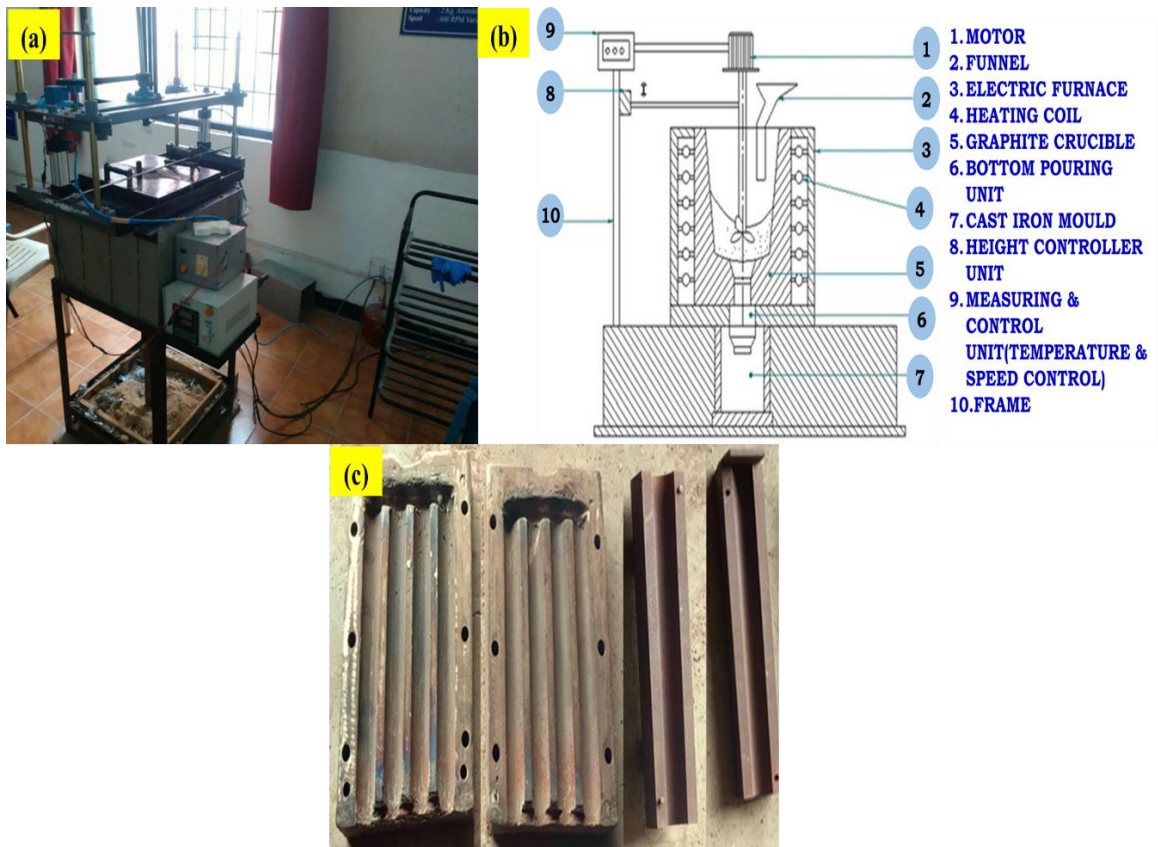


Figure 3.4: Details of fabrication of A357-DPS composites. Where (a) Stir casting set up (bottom pouring technique), (b) Line diagram of stir casting setup, and (c) Cast iron permanent mould.

To this end, a resistance-heated furnace with power rating of 230 V, 2 kW power and maximum temperature limit of 1000°C was used. The stir casting set up, its line

diagram and cast-iron permanent mould used for this purpose are shown in Figures. 3.4 (a), (b), and (c) respectively.

3.2.1: Composite fabrication

The process flowchart for fabrication of A357 composites reinforced with dual size SiC particles and the images of cast samples are presented in Figures. 3.5 and 3.6. respectively. Process parameters used for stir casting of composites are presented in Table. 3.5. The A357 alloy was melted in a graphite crucible and superheated to 800°C in a resistance furnace. The molten alloy was degassed using Hexachloroethane tablets. Pre-weighed mixtures of SiC powders (of suitable ratio) were preheated to 1100°C for 2h to remove any moisture, residue, and loose scales. Stirring was done at 550 - 600 rpm using a chromium steel stirrer whose blades were coated with zirconium oxide. The weight of SiC particles was kept constant at 6 wt. %, and the particles were introduced to the melt vortex at about 15 to 20 g/min using a funnel.

Further, stirring was continued for about 15 minutes to minimize segregation of SiC particles. Thereafter, the molten composite was poured into a pre-heated cast iron mold, maintaining a pouring temperature of 730°C. Cooling of the mold was carried out at ambient temperature. Three different composites with varying SiC percentages, viz., DPS1 (3% Coarse/Large SiC+ 3% Fine/Small SiC), DPS2 (4% Coarse/Large SiC+ 2% Fine/Small SiC) and DPS3 (2% Coarse/Large SiC+ 4% Fine/Small SiC) were prepared. In this thesis, the particles with $140 \pm 10 \mu\text{m}$ will be referred as to either large or coarse interchangeably. Similarly, the particles with size $30 \pm 5 \mu\text{m}$ will be referred to as small or fine interchangeably. A357 alloy without any SiC reinforcement was also cast for comparison purposes. The as-cast A357 alloy and the developed A357-SiC composites are designated as documented in Table. 3.6.

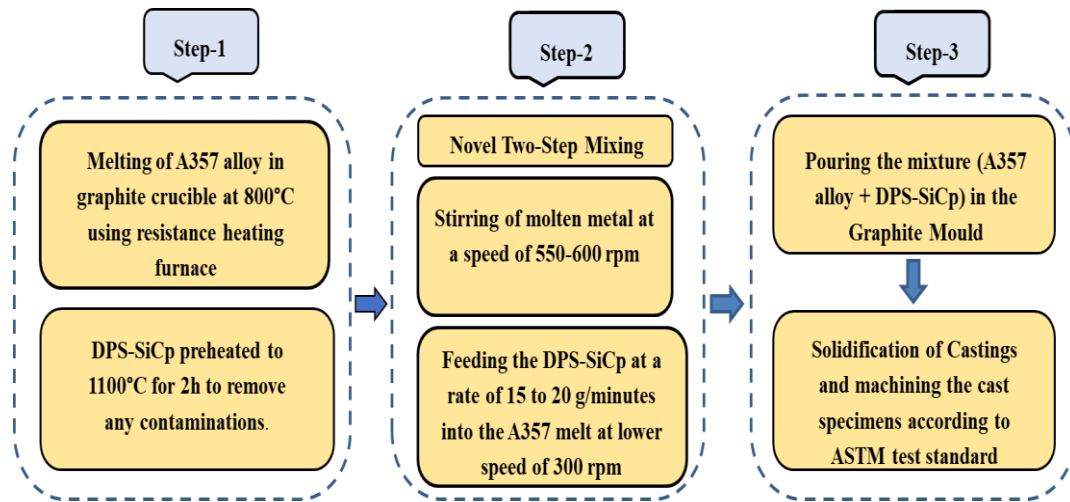


Figure 3.5: Process flowchart for fabrication of A357 composite reinforced with dual size SiC particles.

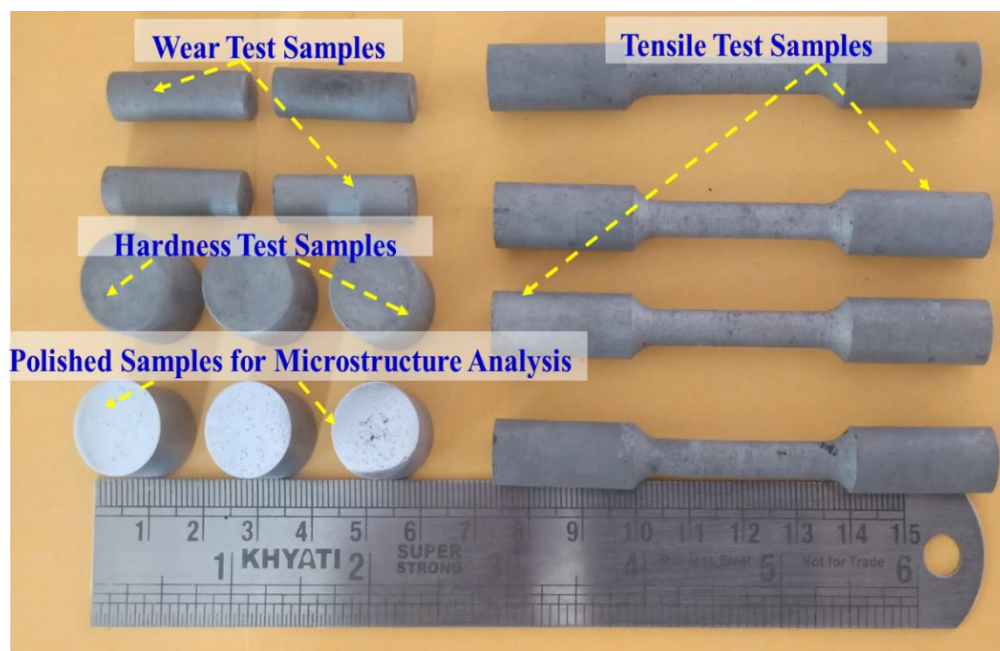


Figure 3.6: Images of cast sample.

Table 3.5: Process parameters used for stir casting of composites

Pouring temperature	Stirring duration	Stirring Speed	Stirrer position	Impeller
730°C	~15 min	550-600 rpm	~2/3" depth from the bottom of crucible	Zirconium coated chromium steel, 3 blade fan type

Table 3.6: Reinforcement combination of A357 alloy and its DPS Composites

S/No	Composition of composite base alloy (%)	Amount of reinforcement Wt. %	Coarse/Large size SiC particle ($140 \pm 10\mu\text{m}$)	Fine/Small size SiC particle ($30 \pm 5\mu\text{m}$)	Designation
1	100	0	0	0	A357 alloy
2	94	6	3	3	DPS1 composite
3	94	6	4	2	DPS2 composite
4	94	6	2	4	DPS3 composite

3.3 Heat treatment

Cast A357 alloy and the developed DPS composites were subjected to T6 heat treatment using a muffle furnace (8''x 8''x 12''/ 900°C) with a temperature controller (Figure. 3.7.). To this end, T6 temper treatment was chosen which consists of solutionizing, quenching, and artificial aging. The heat treatment process was carried out varying both solutionizing and aging temperatures. The steps involved in the heat treatment study carried out in this work are as given below:



Figure 3.7: Muffle furnace with a temperature controller.

(i) CASE 1: (Varying solutionizing temperatures at constant aging temperature)

One set of samples were solutionized at different solutionizing temperatures (500°C , 520°C , and 540°C) for 9 hours followed by water quenching and aging at 150°C for 6 hours. These samples are designated as:

- a) **500-9H-150**: Solution treatment at 500°C for 9 hours-- Quenching in water -- Aging at 150°C for 6 hours.
- b) **520-9H-150**: Solution treatment at 520°C for 9 hours -- Quenching in water -- Aging at 150°C for 6 hours.
- c) **540-9H-150**: Solution treatment at 540°C for 9 hours -- Quenching in water -- Aging at 150°C for 6 hours.

The temperature-time cycles for case 1 heat treatment study are shown in Figure. 3.8.

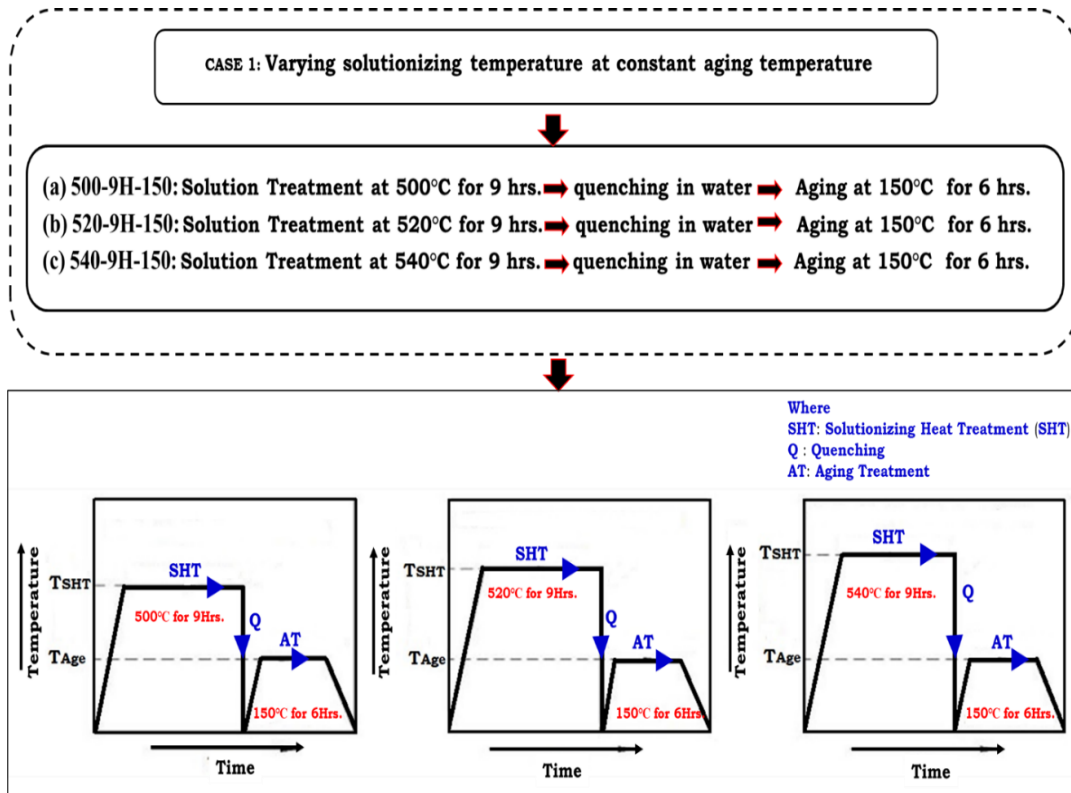


Figure 3.8: Precipitation heat treatment (T6-Cycle) for varying solutionizing temperature at constant aging temperature.

The designation of A357 alloy and the developed DPS composites for the case 1 heat treatment study (Varying solutionizing temperature at constant aging temperature) are given in Table. 3.7.

Table 3.7: Designation of A357 alloy and the developed DPS composites heat-treated by varying solutionizing temperature at constant aging temperature

Alloy/Composite	Heat treatment	Coarse/Large: Fine/Small (wt. %)	Designation
As-Cast A357 alloy	500-9H-150	Nil	A357-9H-500°C
As-Cast A357 alloy	520-9H-150		A357-9H-520°C
As-Cast A357 alloy	540-9H-150		A357-9H-540°C
DPS 1 Composite	500-9H-150	3:3	DPS1-9H-500°C
DPS 1 Composite	520-9H-150		DPS1-9H-520°C
DPS 1 Composite	540-9H-150		DPS1-9H-540°C
DPS 2 Composite	500-9H-150	4:2	DPS2-9H-500°C
DPS 2 Composite	520-9H-150		DPS2-9H-520°C
DPS 2 Composite	540-9H-150		DPS2-9H-540°C
DPS 3 Composite	500-9H-150	2:4	DPS3-9H-500°C
DPS 3 Composite	520-9H-150		DPS3-9H-520°C
DPS 3 Composite	540-9H-150		DPS3-9H-540°C

(ii) CASE 2: (Constant solutionizing temperature and varying aging temperatures)

The second set of samples were solution treated at 540°C, water quenched and aged at different aging temperatures(160, 180 and 200°C) for 6 hours. These samples are designated as:

- a) **540-160-6H**: Solution treatment at 540°C for 9 hours -- Quenching in water -- Aging
at 160°C for 6 hours.
- b) **540-180-6H** : Solution treatment at 540°C for 9 hours -- Quenching in water -- Aging
at 180°C for 6 hours.
- c) **540-200-6H** : Solution treatment at 540°C for 9 hours -- Quenching in water -- Aging
at 200°C for 6 hours.

The temperature-time cycles for case 2 heat treatment study are shown in Figure. 3.9.

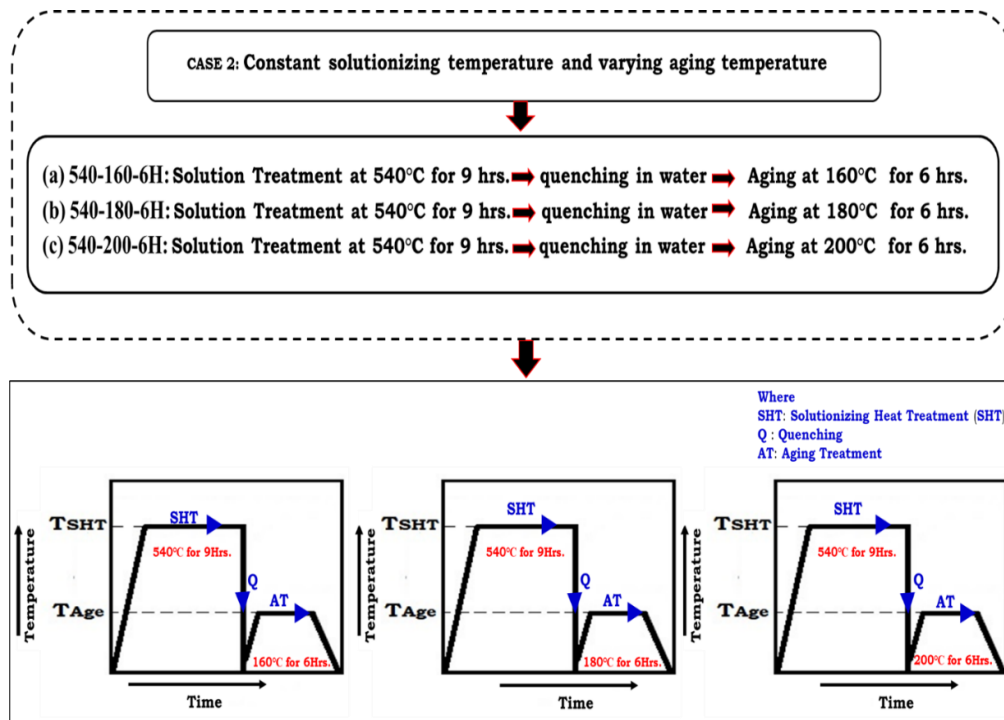


Figure 3.9: Precipitation heat treatment (T6-Cycle) for varying aging temperature at constant solutionizing temperature.

The designation of A357 alloy and the developed DPS composites for the heat treatment study of case 2 (Varying aging temperatures at constant solutionizing temperature) are given in Table. 3.8.

Table 3.8: Designation of A357 alloy and the developed DPS composites heat-treated by varying aging temperature at constant solutionizing temperature

Alloy/Composite	Heat Treatment	Coarse/Large : Fine/Small (wt. %)	Designation
As-Cast A357 alloy	540-160-6H		A357-160°C-6H
As-Cast A357 alloy	540-180-6H	Nil	A357-180°C-6H
As-Cast A357 alloy	540-200-6H		A357-200°C-6H
DPS 1 Composite	540-160-6H		DPS1-160°C-6H
DPS 1 Composite	540-180-6H	3:3	DPS1-180°C-6H
DPS 1 Composite	540-200-6H		DPS1-200°C-6H
DPS 2 Composite	540-160-6H		DPS2-160°C-6H
DPS 2 Composite	540-180-6H	4:2	DPS2-180°C-6H
DPS 2 Composite	540-200-6H		DPS2-200°C-6H
DPS 3 Composite	540-160-6H		DPS3-160°C-6H
DPS 3 Composite	540-180-6H	2:4	DPS3-180°C-6H
DPS 3 Composite	540-200-6H		DPS3-200°C-6H

3.4 Density measurement

Density (ρ_{exp}) of the A357 alloy and the developed DPS composites were measured experimentally as per ASTM D792-66 standard. Further, theoretical density (ρ_{th}) was also calculated using the rule of mixtures. The experimental and theoretical densities were calculated using the equations given below (Prasad et al. 2014; Ajith kumar et al. 2014; Aykut Canakci et al. 2014).

$$\text{Experimental density } (\rho_{\text{ex}}) = \frac{\text{Weight of sample in air } (W_a)}{\text{Weight of sample in air } (W_a) - \text{Weight of sample in water } (W_w)}$$

$$\text{Theoretical density } (\rho_{\text{th}}) = W_m \rho_m + W_r \rho_r$$

Where, W_m = Weight fraction of matrix material; ρ_m = Density of matrix material;

W_r = Weight fraction of reinforcements; ρ_r = Density of reinforcements.

3.5 Sample preparation for metallographic studies

Using metallurgical procedures as per ASTM E3-17 standards, the A357 and the developed composites were polished and then etched with Keller's reagent. Samples for microstructural analysis were prepared in form of cylinder-shaped pieces ($\text{\O} 20 \text{ mm X } 15 \text{ mm}$). Samples were then properly ground using emery papers. The final step includes polishing using a diamond paste of $0.25 \text{ }\mu\text{m}$ size along with an alcohol-based lubricant for a duration of 0.5 to 3 minutes at a rotational speed of 150 rpm in a double-disc polishing machine. This step is employed to attain flat and mirror finish surfaces. Next, the samples were etched with Keller's reagent. The highly polished surfaces were observed under an optical microscope (Model: Nikon LV150).



Figure 3.10: Steps involved in sample preparation for metallographic studies.

3.6 Microstructural characterization

Microstructure of A357 alloy and the developed DPS composites after stir casting, heat treatment and wear testing were studied using:

- Optical Microscope (OM)
- Scanning Electron Microscope (SEM)
- Transmission Electron Microscope (TEM)

An optical microscope (Model: Nikon LV150) (Figure. 3.11) was used to check dispersal of SiC particles within the A357 matrix. The dispersion and bonding of SiC particles with the A357 matrix, fracture surfaces after tensile testing and worn surface morphology after wear testing were studied using scanning electron microscopy (SEM) with an EDS attachment (Model: TESCAN Vega 3 LMU) (Figure. 3.12). The samples were sputtered with gold prior to SEM examination to avoid charging effect. A transmission electron microscopy examination was carried out using JEOL JEM 2100 High-Resolution Transmission Electron Microscope (HRTEM) to study the precipitates and dislocations. To this end, samples of 3 mm diameter and 10 μm thick were prepared using ion beam milling (Model: 691, Gatan) (Figure. 3.13).

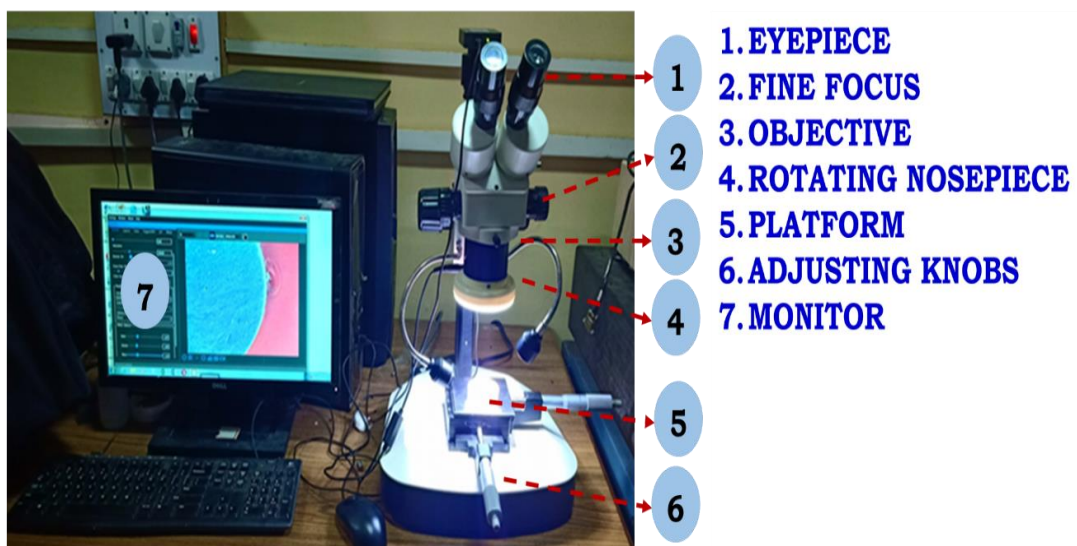


Figure 3.11: Optical microscope.

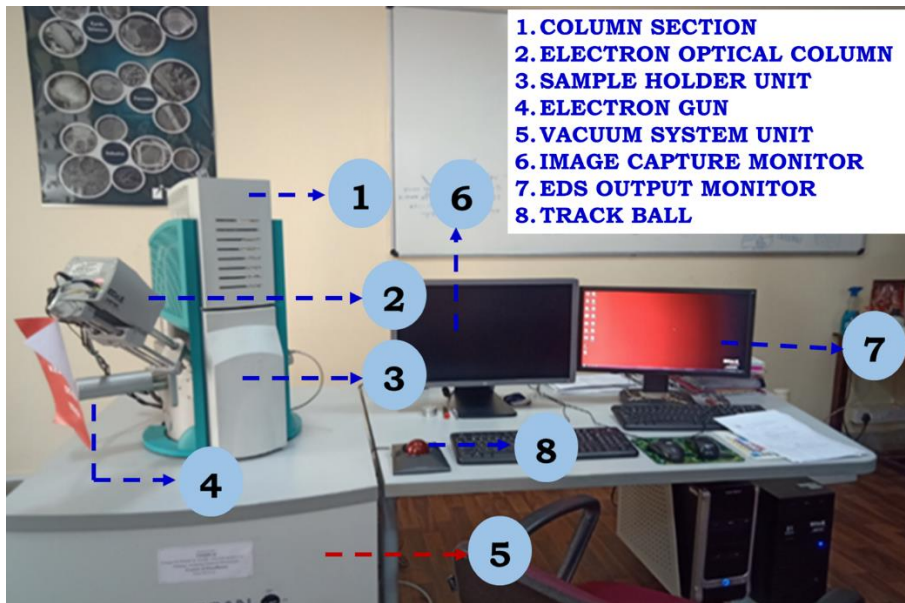


Figure 3.12: Scanning electron microscope (Courtesy: BMSCE).

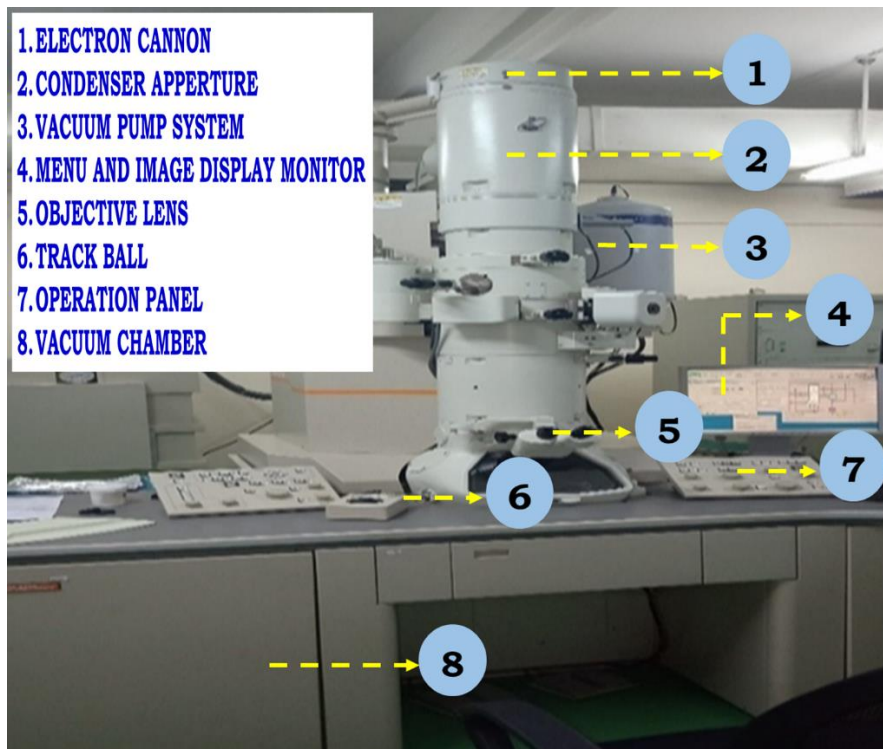


Figure 3.13: Transmission electron microscope (Courtesy: PSGCT).

3.7 Evaluation of mechanical properties

The mechanical behaviour of the A357 alloy and the developed DPS composite were analyzed by

- Hardness test
- Tensile test

3.7.1 Hardness testing

The hardness test was carried out using a micro cum macro-vickers hardness testing machine (Model: VH1150) as per ASTM E384 standard. A Vickers hardness tester having a standard rectangular pyramid diamond indenter ($136^\circ \pm 0.5^\circ$) was used to apply a load of 5 kgf for about 10 seconds. Five readings were taken on the surface and average of the same is reported. Photograph of hardness tester along with schematic of sample used for hardness testing is shown in Figures. 3.14 (a) and (b).

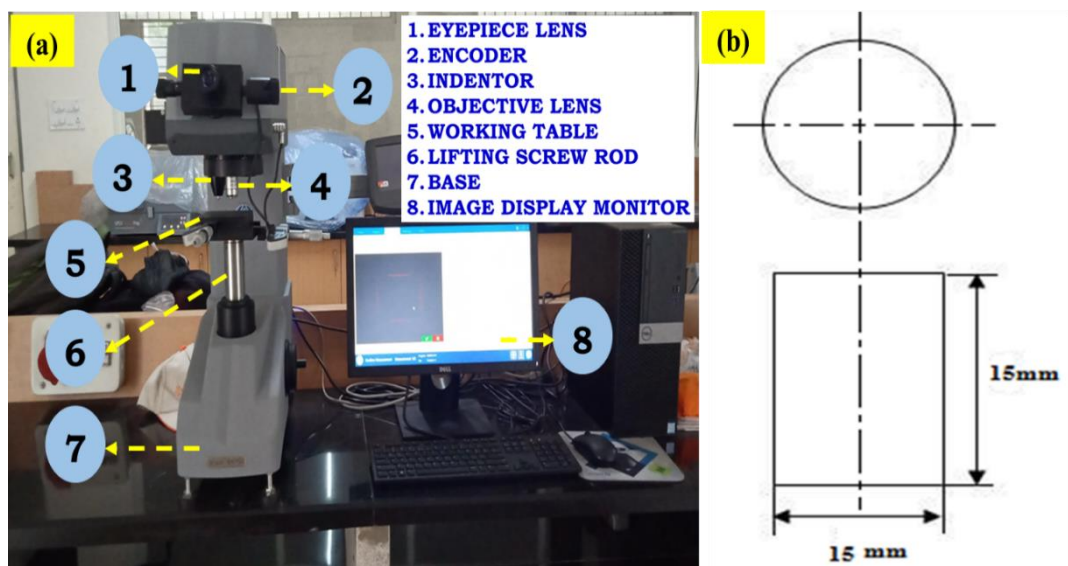


Figure 3.14: (a) Vickers hardness tester, and (b) Schematic of specimen used for hardness testing.

3.7.2 Tensile testing

Tensile testing was conducted as per ASTM E8M-15a standard. These tests were carried out at room temperature using a universal testing machine (Model: TUE-C-400) at a strain rate of 0.2 mm/s. After the test, strength and ductility values reported here in are based on an average of five measurements. Photograph of UTM used for testing and the dimensions are shown in Figures. 3.15 (a) and (b).

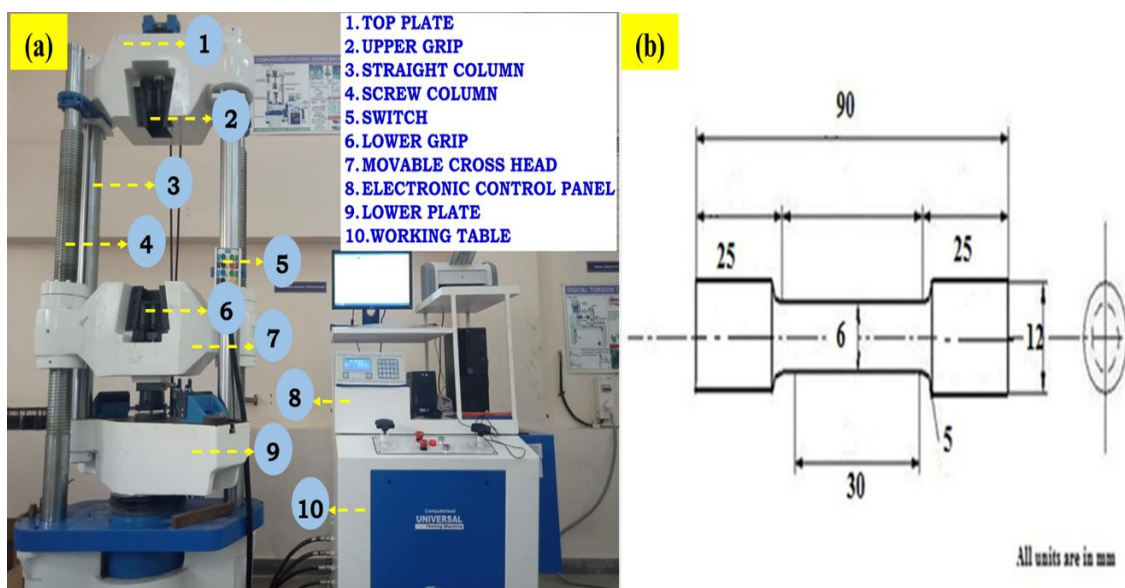


Figure 3.15: (a) Universal testing machine, and (b) Schematic of specimen used for tensile testing.

3.8 Wear testing

Wear testing was conducted test using pin-on-disc machine (Make: TR-20LE, Ducom) as per ASTM-G99 standard. Here, the applied load was varied from 10 N to 30 N in steps of 5 N at a fixed sliding velocity of 2.5 m/sec and sliding distance of 1500 m. The dimensions of the specimen for wear testing were \varnothing 8 mm x 25 mm. The specimens were ground to obtain a surface finish of $0.2 \pm 0.05 \mu\text{m}$ (R_a). The counterface disc used is made up of EN-32 steel having 160 mm diameter and 8 mm thickness with a hardness value of HRC65. The composition of counterface disc is given in Table. 3.9. The test was conducted at ambient room temperature (26°C) and

relative humidity condition of 35 - 40% RH, respectively. For each parameter, an average of 3 test results are reported herein for A357 alloy and the developed DPS composites. Photograph of pin-on-disc tribometer along with sample dimensions are shown in Figures. 3.16 (a) and (b).

Table 3.9: Chemical composition of EN-32 steel disc

Element	C	Si	Mn	S	P	Ni	Cr	Mo	Fe
Wt. %	0.14	0.18	0.52	0.015	0.019	0.13	0.05	0.06	Balance

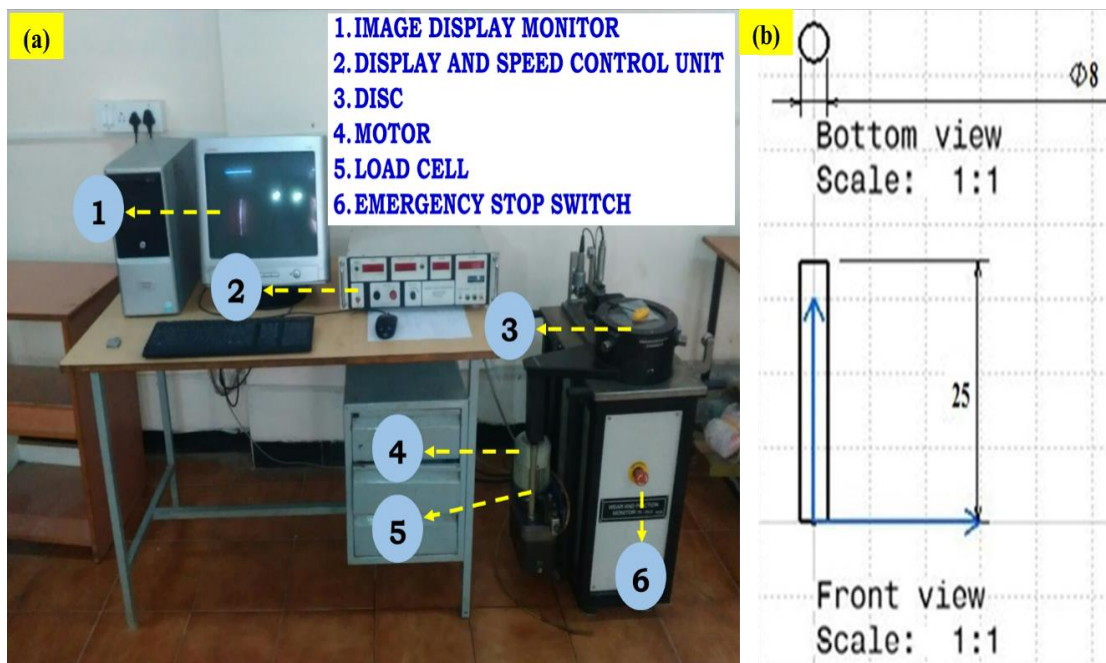


Figure 3.16: (a) Pin-on-disc tribometer and (b) Schematic of wear test specimen.

3.8.1 Three-dimensional surface topography measurement

Three-dimensional surface topography was measured using a non-contact 3D-optical-profiler (Model: Veeco-Wyko-NT1100) (Figure. 3.17). Surface profile distribution of A357 alloy and the developed DPS composites (as-cast and heat-treated) after wear testing were studied in terms of average surface roughness (R_a in μm).

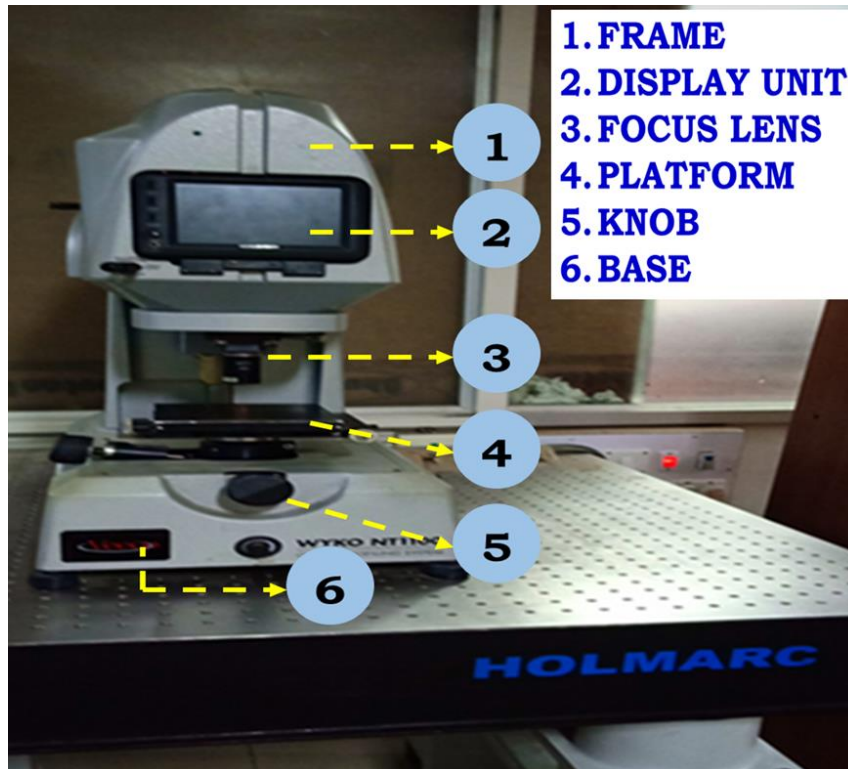


Figure 3.17: 3D - Optical- profiler (Courtesy: IISC).

CHAPTER-4

RESULTS AND DISCUSSION

Effect of dual particle size (DPS) SiC reinforcements on microstructure, physical, mechanical and wear properties of A357 composites

This chapter presents the results of various characterization studies and tests carried out on the A357 alloy and the developed DPS composites. Influence of different weight fractions of SiC reinforcements (3% coarse + 3% fine, 4% coarse + 2% fine, and 2% coarse + 4% fine) on the microstructure, mechanical, and wear properties of A357 composites is discussed in detail.

4.1 Density of A357 alloy and the developed DPS composites

Table 4.1: Theoretical and experimental densities of A357 alloy and the developed DPS composites

S/No	Alloy/Composite	Designation	Theoretical Density (ρ_{th}) (gm/cc)	Experimental density (ρ_{exp}) (gm/cc)
1	As-Cast A357 alloy	A357 alloy	2.7000	2.6831
2	DPS 1 Composite	DPS 1 Composite	2.7306	2.7113
3	DPS 2 Composite	DPS 2 Composite	2.7306	2.7121
4	DPS 3 Composite	DPS 3 Composite	2.7306	2.7109

Theoretical and experimental densities of both A357 alloy and the developed DPS composites are presented in Table. 4.1. The experimental density of unreinforced A357 alloy is found to be lower than that of its theoretical value. Similarly, the experimental densities of DPS composites were found to be lower than that of their theoretical values. Difference between the theoretical and experimental values can be related to presence of defects arising from their processing. Any error in processing

conditions can result in the formation of defects which tend to lower the value of experimental density. One such processing defect are micro-pores which may possibly occur due to atmospheric air entrapment in the molten metal. The air could have been entrapped in the material during melting and long holding times or during pouring of molten A357 alloy or composites. In the case of composites, during addition of SiC particles and mixing, the air can easily go into the molten metal (Kandpal et al. 2017). Another reason could be hydrogen evolution and shrinkage due to alloy solidification (Prasad et al. 2014). Due to these reasons, the experimental density is generally lower than that of its theoretical counterpart.

4.2 Microstructural analysis of A357 alloy

Figures. 4.1 (a) and (b) show optical micrographs of as cast A357 alloy at lower (100X) and higher (500X) magnifications, respectively. Figure. 4.1 (c) shows scanning electron micrograph of as cast A357 alloy at higher magnification (1000X). Figure. 4.1 (d) shows scanning electron micrograph of as cast A357 alloy with EDAX analysis. The presence of alloying elements in A357 alloy i.e., Si and Mg were confirmed from the EDAX analysis (Figure. 4.1 (d)). The micrographs (Figures. 4.1 (b) and (c)) reveal two phases: primary α -Al phase, and eutectic phase silicon. The solid solubility of Si in Al is 1.65 wt% at 577°C. The solid solution of Al and Si forms the α -Al grains with dendritic grain structure. Solidification of Al alloy starts with the formation of primary α -Al phase. The dendritic structure formation is decided by: the type of nucleation, the cooling rates and the range of undercooling temperature. In the present case, solidification is a slow process. Nucleation preferably starts heterogeneously at Ti nucleants, the mold wall and SiC particles. When the alloy solidifies, it forms the α -Al grain primary dendrites. The growth of primary dendrites is retarded by the increase of temperature in the solidification front due to the loss of heat by cooling, the presence of the second phase particles and the solidification front of the neighbor growing grain primary dendrites. At the same time, the undercooling is relatively high in the liquid surrounding the sides of the dendrites. This results in the formation of solid branches in the primary dendrites called the secondary

dendrites. Hence, the solidification of the composites is driven by the formation of primary and secondary dendritic arms in the liquid.

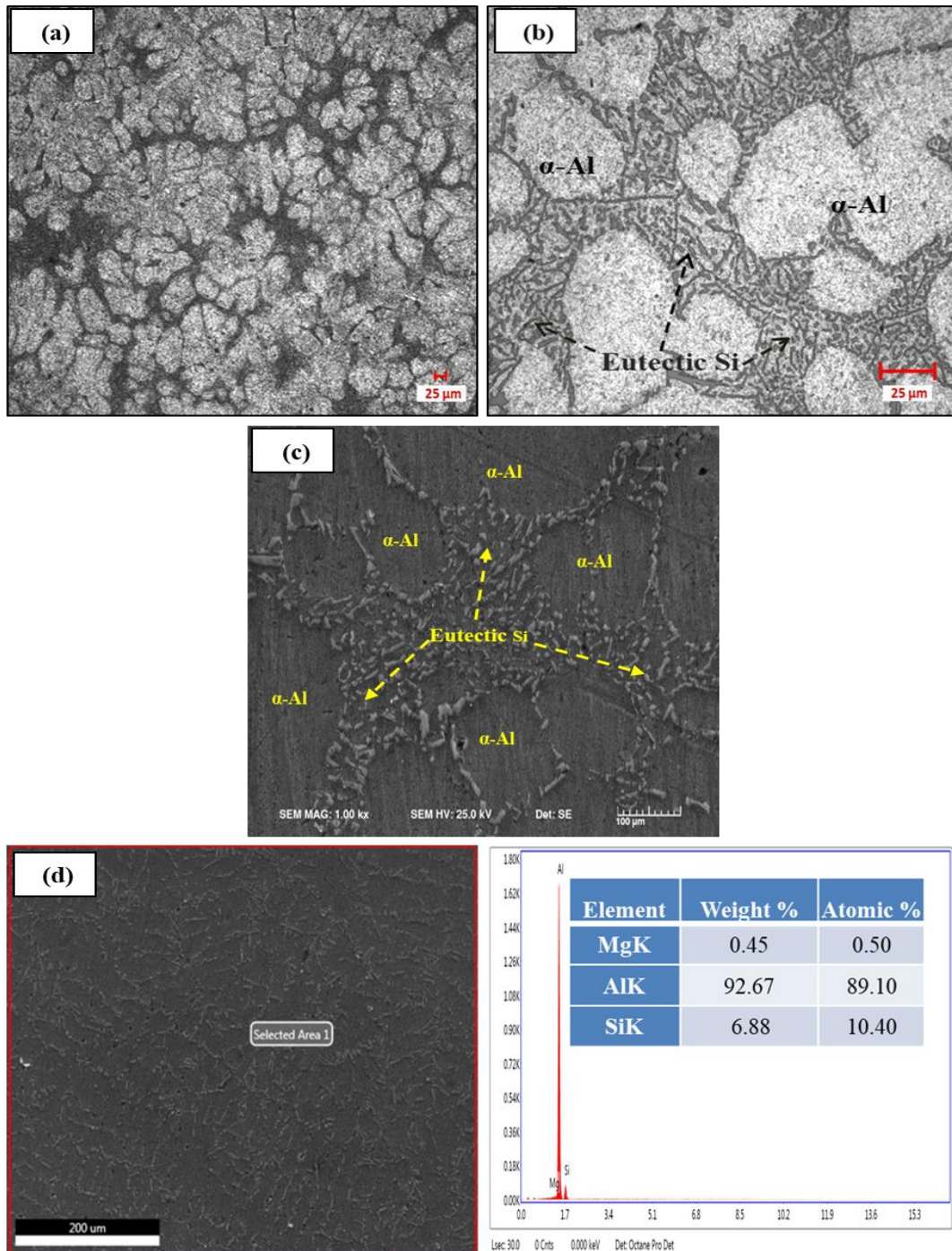


Figure 4.1: Micrographs of (a) A357 alloy showing dendritic structure, (b) A357 alloy showing inter dendritic region, (c) SEM image of A357 alloy at higher magnification, and (d) EDAX spectra taken on A357 alloy.

4. 3 Microstructural analysis of the developed DPS composites

Figures. 4.2 (a), (b), (c), and (d) show optical micrographs of the developed DPS composites. In these figures number 1 represents coarse SiC particles, 2 represents fine SiC particles and 3 shows clustering of fine SiC particles. The optical micrograph of Figure. 4.2 (a) shows fairly uniform dispersion of both sizes of SiC particles in the DPS1 composite. The distribution of SiC particles is homogenous in the composite. The SiC particles pin the grain boundary and restrict the grain growth in the present case in addition to acting as the nucleating sites during solidification. The absence of clustering zone in the microstructure implies that the particle distribution is uniform in the composite. The presence of dendrites mask the grain boundary in the composites. Figure. 4.2 (b) shows optical micrograph of DPS2 composite consisting of 4 wt. % of coarse SiC particles and 2 wt. % of fine SiC particles. The microstructure is dominated by large SiC particles with very few fine particles around them. The finer particles are pushed at a faster rate during stirring and they are distributed between the larger particles. The interface between the particle and matrix appear to be clean and smooth. This smooth interface provides better mechanical and tribological properties as the transfer of load occurs through the interface (Shen et al. 2013; Stachowiak and Batchelor , 2001; Zum Ghar ,1987). Figure. 4.2 (c) shows the optical micrograph of DSP3 composite which consists of 4 wt. % fine SiC particles and 2 wt. % of coarse SiC particles. Although both particles are distributed uniformly the finer particles have agglomerated and formed a network arrangement. This is mainly due to pushing of finer SiC particles by solid-liquid interface during solidification. Overall, the DPS composites show a fairly uniform distribution of dual size SiC particles in the matrix. Uniform distribution of particles is desired for achieving better wear and mechanical properties. Figure. 4.2 (d) shows optical micrograph of DPS2 composite at higher magnification which reveals good interfacial bonding of SiC particles with A357 matrix.

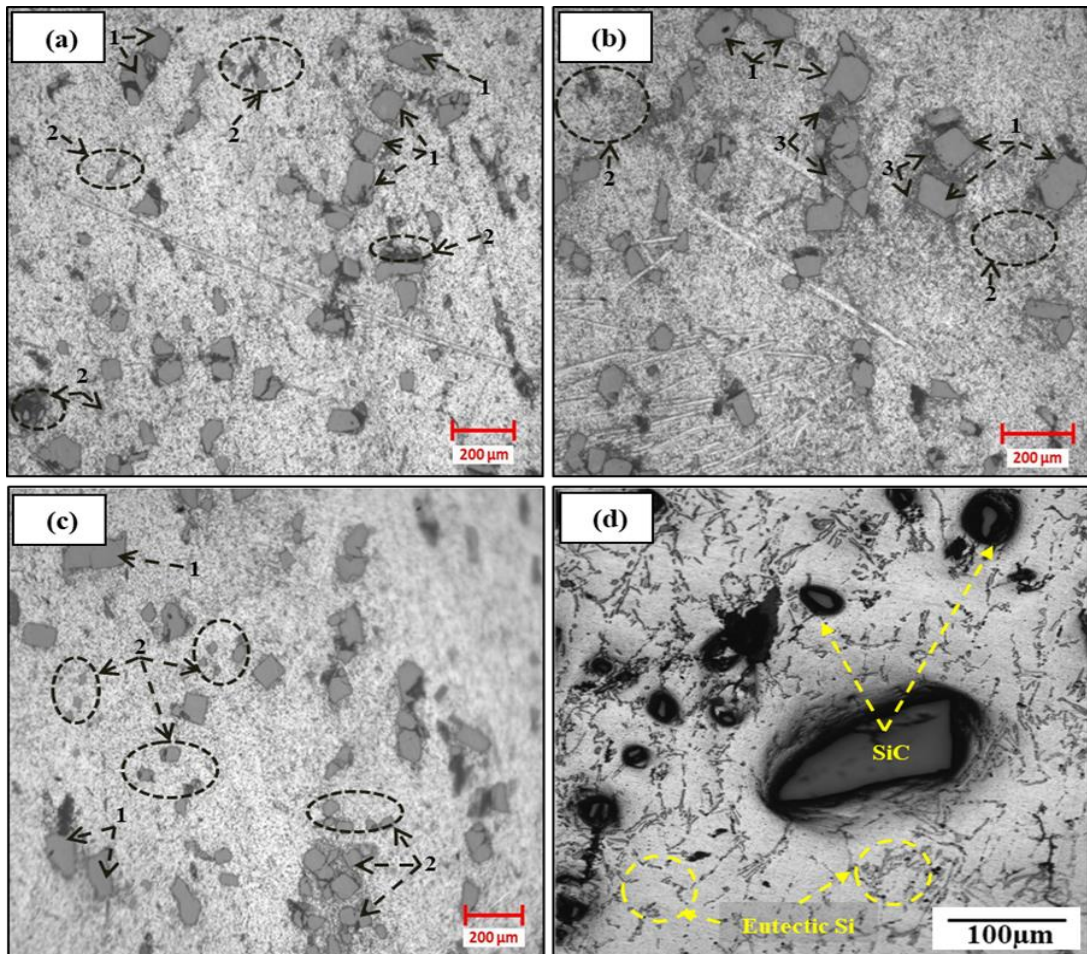


Figure 4.2: Optical micrographs of (a) DPS1 composite, (b) DPS2 composite, (c) DPS3 composite and (d) DPS2 composite at higher magnification.

Figure. 4.3 shows EDAX of DPS1 composite (at a higher magnification) exactly on SiC particle to confirm that these are SiC particles and not eutectic silicon. The purpose behind taking EDAX on SiC particle is that in many cases the presence of reinforcements can cause refinement of eutectic silicon along with the microstructure (Suresh Kumar et al. 2013). It was necessary to do EDAX to confirm that the particles seen in SEM micrographs are SiC particles.

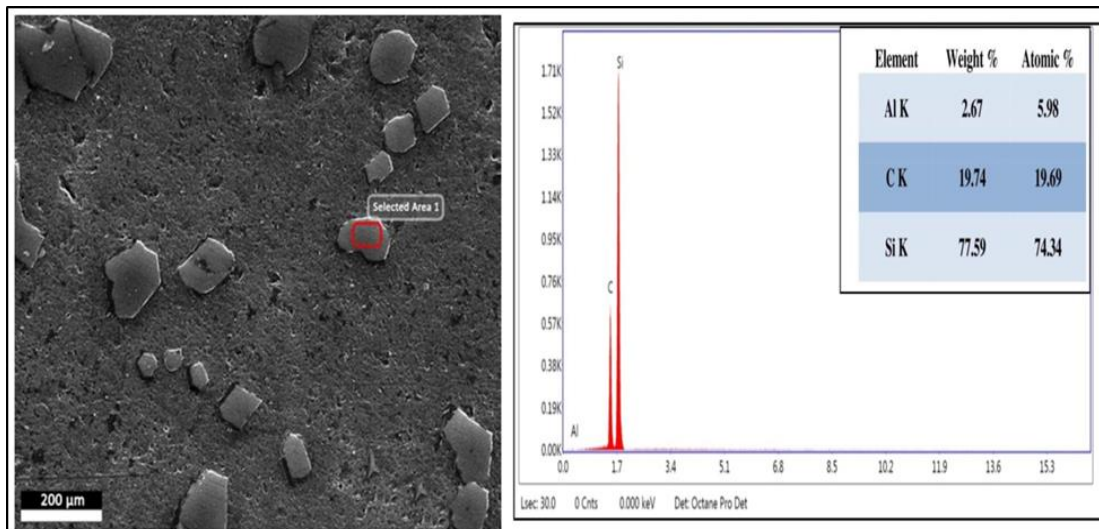


Figure 4.3: EDAX spectra taken on DPS1 composite confirming the presence of SiC.

4.4 Hardness results

Figure. 4.4 shows the variation of the hardness of A357 alloy and the developed DPS composites. Compared to the as-cast alloy, the DPS1, DPS2, and DPS3 composites showed an increment of 9.42%, 15.13% and 5.83% increment in hardness, respectively. Among the DPS composites, the DPS2 composite with 4 wt. % of coarse SiC particles and 2 wt. % of fine SiC particles exhibits slightly higher hardness. This may be due to the higher amount of large size SiC uniformly dispersed in the matrix compared to smaller size SiC particles as showed in Figure. 4.2 (b). The higher amount of coarser particles in composites shields the finer particles. Further, coarser particles help to carry a more significant portion of the applied load compared to the finer particles (Bindumadhavan et al. 2001).

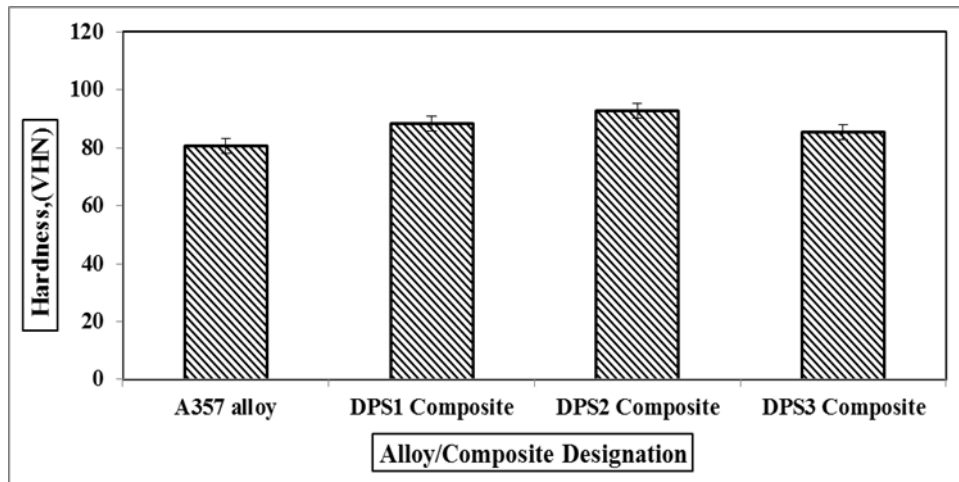


Figure 4.4: Hardness test results of A357 alloy and the developed DPS composites.

Compared to the coarse size particles, the fine size particles are more prone to particle clustering (Kumar et al. 2014). Hence, the dispersion of small size particles is very difficult. The improvement in hardness values of the DPS composites are attributed to the following factors. (1) dispersion of hard ceramic particles (SiC) in a soft ductile matrix leading to hardening of the matrix, (2) particle strengthening of the composites through dislocation density strengthening and plastic strain constraint effects and (3) grain refinement of the matrix by SiC particles and primary Si particle refinement (Kumar et al. 2014; Deng et al. 2012; Deng et al. 2010; Sanaty and Rohatgi, 2012; Naveen et al. 2016; Suresh et al. 2003). Similar trends were reported by several researchers (Kumar et al. 2014; Viswanatha et al. 2013; Ramprabhu, 2016).

4.5 Tensile strength

Figure 4.5 shows the strength values of A357 alloy and the developed DPS composites. It can be observed from Figure 4.5 that, the addition of dual particle size SiC has enhanced the tensile strength (UTS and YS) of all composites. The percent increase in the tensile strength of DPS1, DPS2, and DPS3 composites is 40.98%, 37.61%, and 45.30% respectively when compared to the as-cast A357 alloy. Similarly, the percent increase of the yield strength of DPS1, DPS2, and DPS3 composites is 67.64%, 53.48%, and 76.33% respectively when compared to the as-

cast A357 alloy. Among the DPS composites ,the DPS3 composite with 2 wt. % of large SiC particles and 4 wt. % of fine SiC particles shows slightly higher tensile and yield strength. This may be due to the higher amount of fine size particles distributed fairly uniformly in the matrix compared to coarse size SiC particles. Similar trends were reported by several researchers (Suresh et al .2003; Viswanatha et al. 2013; Ramprabhu , 2016).

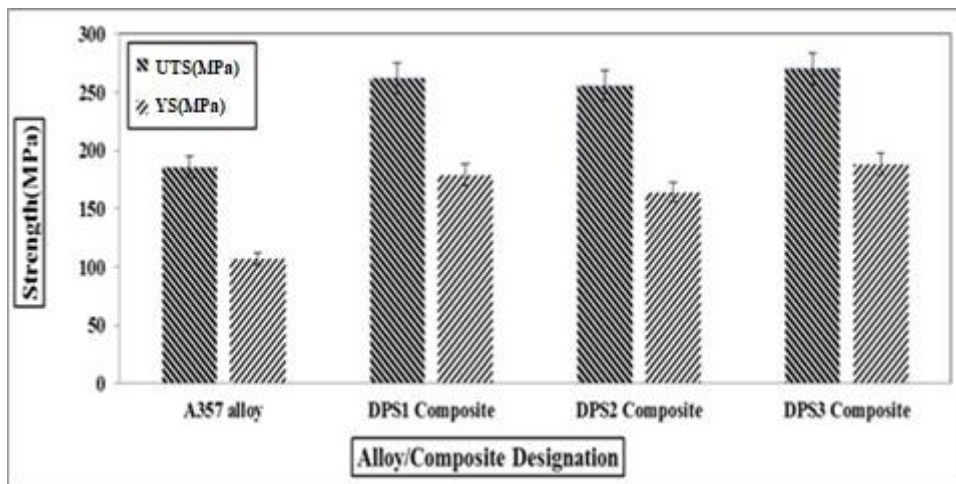


Figure 4.5: Tensile strength of A357 alloy and the developed DPS composites.

The addition of SiC particles helps to refine the primary Si in the Al-Si alloy by grain refinement through the nucleation site and particle grain pinning effects. The refinement of primary Si leads to the short fibrous shape Si in the composites, as seen in Figures. 4.2 (a), (b), (c) and (d). The refinement of Si particles improves the tensile properties by restoring the ductility. Also, the fine Si particles improve the strength by acting as a second phase. The SiC particles improve the tensile properties by three dominant processes: (1) grain refinement and primary Si particle refinement, (2) load transfer effect and (3) dislocation strengthening and plastic strain constraint effects (Sanaty and Rohatgi, 2012; Naveen et al. 2016). The thermal expansion and elastic modulus mismatch between the matrix and the particles generates dislocations around the particles and increases the dislocation density. The increase in dislocation density enhances the strength of the composites, called dislocation strengthening. Also, the

strain in the matrix is localized due to the non-deforming SiC particles during deformation. This causes strengthening through local plastic constraint (Dieter, 1986). The hard and stiff SiC particles act as load bearing elements in the composites and enhance the strength. As explained earlier, the SiC particles enhance the grain refinement through the nucleation site and grain boundary pinning effects. The Hall-Pitch relation explains the strength improvement though the decrease of matrix grain size (Dieter, 1986).

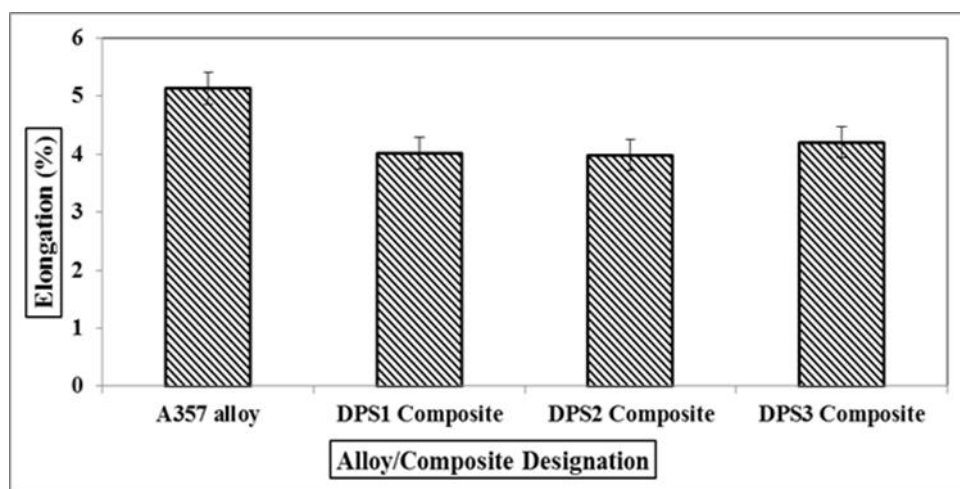


Figure 4.6: Percent elongation (%) of A357 alloy and the developed DPS composites.

The % elongation of A357 alloy and the developed composites are shown in Figure. 4.6. The reduction in ductility for DPS1, DPS2 and DPS3 composites is about 21.83%, 22.41% and 18.12% when compared to that of A357 alloy. These results indicate that the inclusion of dual size SiC particles in A357 matrix has resulted in a significant loss of ductility. The presence of hard SiC particles will act as barrier to the dislocation motion during tensile loading. These results are in good agreement with those reported in literature (Ahmed et al. 2011).

4.6 Tensile fracture surface analysis

Figures. 4.7 (a), (b), (c) and (d) show fractographs of as cast A357 alloy and the developed DPS composites after the tensile test. In these figures, number 1 represents α -Al grains, 2 represents voids and micro cracks and 3 represents small dimples. The A357 alloy exhibits a typical intercrystalline fracture as shown in Figure. 4.7 (a). The fracture is mainly due to the presence of dendritic shrinkage porosity. The crack nucleation takes place at these dendritic shrinkage porosity regions and propagates along these dendrites causing failure of A357 alloys. However, the porosity in the casting is also influenced by the formation of dendritic structures. On the other hand, all the A357 composites showed brittle failure along with quasi-cleavage feature, as shown in Figures. 4.7 (b), (c) and (d). The quasi-cleavage feature is generally seen in materials with lower elongation values. This can be due to breaking of Al-Si eutectic particles or large SiC particles. It is well known that the particle size and shape have huge influence on the tensile properties. The large and elongated Al-Si eutectic particles (Figures. 4.1 (b) and (c)) present in the A357 alloy are more prone to cracking. So, in case of A357 alloy the inter-dendritic cracking and cracking of silicon particles dominates the fracture process. While in case of composites the dislocations pile-up at the vicinity of SiC particles giving rise to stress fields which in turn cause the local fluctuations leading to cracking of SiC particles. It is important to note that the good bonding between A357 matrix and SiC particles has resulted in breaking of SiC particles during tensile loading rather than particle debonding. In case of tensile loading, the interfacial bonding between the SiC particles and A357 matrix plays an important role. If the interfacial bonding is good, then it tries to retain the SiC particles in the matrix during loading conditions. But, as the load increases, due to high interfacial bonding the SiC particles get fractured rather than debonding. Hence in case of composites, the nature of fracture is brittle and quasi cleavage feature mode (Chen et al.2014; Jiang et al. 2014).

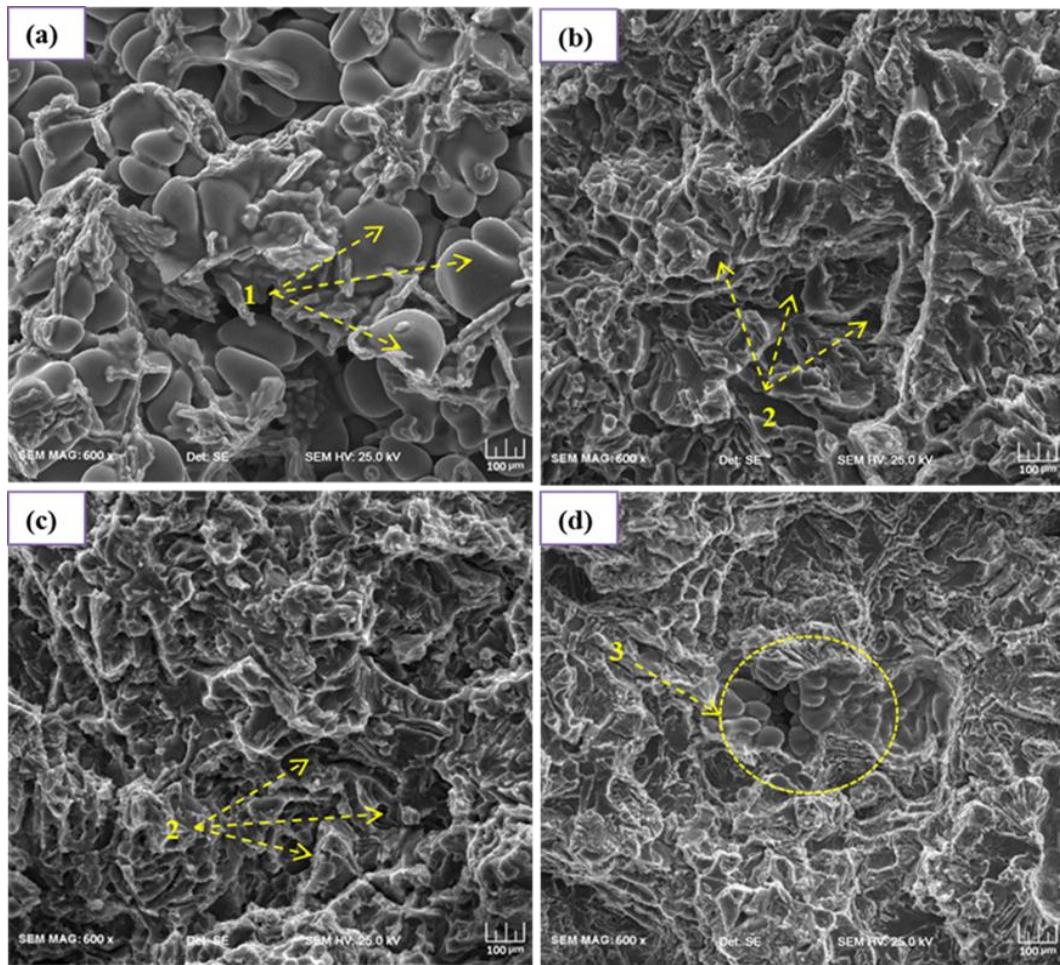


Figure 4.7: Fractographs of (a) A357 alloy, (b) DPS1 composite, (c) DPS2 composite, and (d) DPS3 composite.

4.7 Graphical interpretation of wear rate

The graphical interpretation of wear rate for A357 alloy and DPS2 composite is shown in Figures. 4.8 (a), (b), (b) and (d) for different loads. It can be observed that for A357 alloy, the wear rate is increasing linearly for both 10 and 30 N loads. However, in the case of 30 N applied load, there is rapid increase in wear rate of A357 alloy as shown in Figure. 4.8 (b). The degree of fluctuation is quite high in this case particularly at 350 s for 10 N and 270 s for 30 N loads indicating seizure phenomena taking place. In case of DPS2 composite, the wear rate is not as high as that of A357 alloy as seen in Figures. 4.8 (c) and (d) for 10 N and 30 N, respectively.

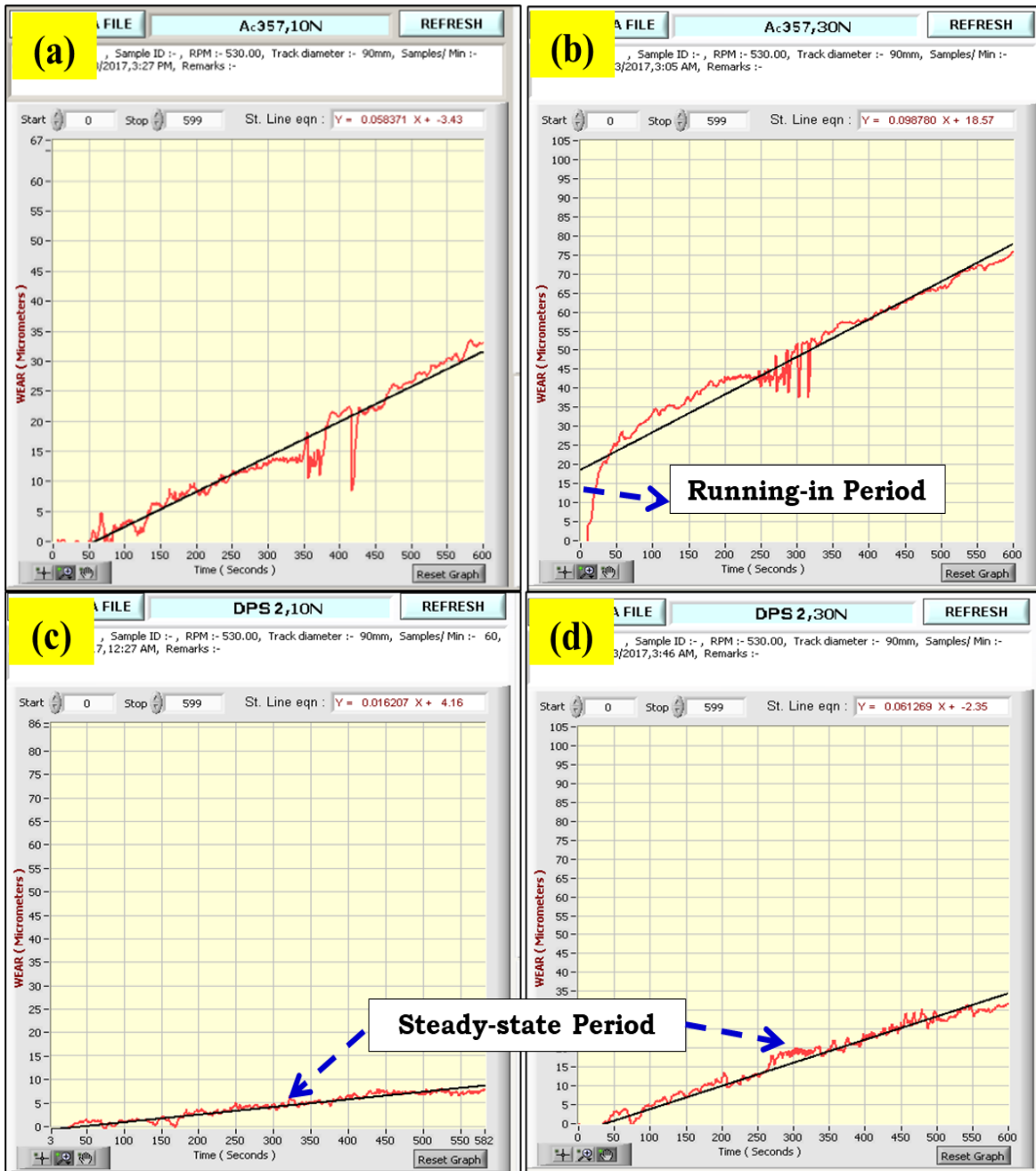


Figure 4.8: Graphical interpretation of wear rate for A357 alloy and DPS2 composite (a) A357 alloy at 10N, (b) A357 alloy at 30N, (c) DPS2 composite at 10N, and (d) DPS2 composite at 30N.

The degree of fluctuation is smaller for DPS2 composite when compared to that of A357 alloy indicating high seizure resistance. This is the reason why a steady state

regime without any notable fluctuations is observed in the A357 alloy which can be attributed to prohibition of direct contact between the two mating surfaces by the presence of dual particle size SiC in this composite. In addition to this, the strain hardening effect due to the presence of SiC particles also contributes to lower wear rate values for composites at both lower and higher loads when compared to A357 alloy under similar conditions (Guo and Chi , 2002; Show and Mondal, 2014; Rao and Das, 2010).

4.8 Wear behaviour

Figure. 4.9 shows the effect of applied load on the wear resistance of A357 alloy and the developed DPS composites at loads varying from 10N of 30N, sliding velocity of 2.5 m/sec and a sliding distance of 1500 m. From the figure, it can be observed that DPS composites have higher wear resistance than that of as cast alloy at all load conditions. In particular, DPS2 composite has the least wear rate among all DPS composites considered. From the above figure, it is also observed that up to a load of 20 N, the wear rate increases. With increase in load from 20 to 25 N, the wear rate stabilizes. Any further increase in load beyond 25 N, increases wear rate rapidly and enters into the severe wear regime. This trend is similar for all the DPS composites and A357 alloy.

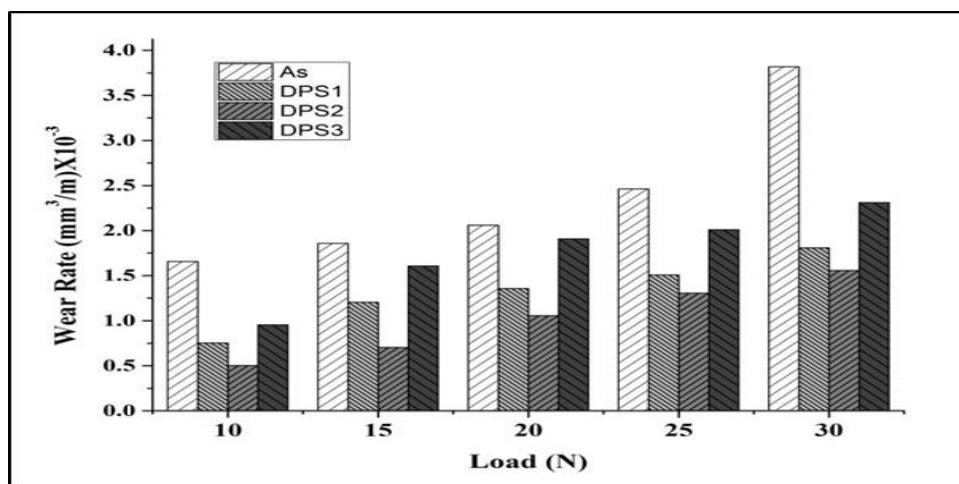


Figure 4.9: Effect of load on wear rate (mm³/m) of A357 alloy and the developed DPS composites.

The A357 alloy displayed highest wear rate for all load conditions which is mainly due to direct metal to metal contact. The increase of wear loss with an increase of load is attributed to several factors such as: (1) higher sub surface deformation and consequent delamination wear, (2) easier removal of load bearing particles, (3) increase of friction due to the higher contact couple surface asperities interlocking, (4) material softening and the matrix oxidation through the friction induced temperature rise and (5) faster generation and removal of tribolayer. With an increase of load, more factors act alongside resulting in high acceleration of wear rate above the critical load (Ramprabhu , 2016; Deuis et al. 1997; Ramprabhu et al. 2014).

4.9 Worn surface analysis

Figure. 4.10 shows the SEM micrographs of wear surface morphology of A357 alloy and the developed DPS composites at a varying load of 10N and 30N, sliding velocity of 2.5 m/sec and sliding distance of 1500 m. In these figures, number 1 represents groove lines, 2 represents delaminated wear sheets and particle pull-out regions and 3 represents sliding direction. One of the common features observed in the DPS composites is the formation of grooves and ridges running parallel to the sliding direction. The wear surface morphology of the as cast alloy at 10 N and 30 N are as shown in Figures. 4.10 (a) and (b). The micrographs showed extensive ploughed surface with abrasive grooves which appear deeper and broader. These cavities are formed by delamination wear. With the progress of sliding, these cracks propagate towards the surface along the sliding direction. During the propagation, they branch out and rejoin to cover a large area. Once they reach the surface, they are plowed out as delaminated wear sheets. This observation supports that the delamination wear is more dominant than abrasive wear in the A357 alloy. Further, with the increase in load, the worn surface has wider grooves and larger cavities indicating substantial amount of surface material removal. Increase in load applied above 25 N has caused an abrupt rise in the wear rate of A357 alloy thereby indicating large scale plastic deformation. As the load increases, the hard asperities of counter face penetrate deeper in the soft surface of the alloy. Increasing load results in plastic deformation at

the subsurface level resulting in the formation of micro-cracks. These cracks start to coalesce over a period of time during the sliding test in the subsurface region and get detached from the surface. Overall, in case of A357 alloy, worn surface exhibits microgrooves and presence of large cavities in the sliding direction indicating severe plastic deformation of the alloy. These features clearly indicate that the main wear mechanism is delamination wear along with contribution from oxidative wear (Rao and Das 2010).

Figures. 4.10 (c) and (d) show the SEM micrographs of wear surface morphology of DPS1 composite at 10N and 30N, respectively. The worn surface is comparatively smooth with shallow ploughing strips. Very small, damaged spots in the form of craters can be seen in the figure when compared to that of A357 alloy. However, DPS2 composite which possesses the least wear rate exhibits the least extent of grooving, as seen in Figures. 4.10 (e) and (f) at loads of 10 and 30N, respectively. The shallow and thin abrasive grooves running parallel to the sliding direction are mainly seen in the DPS2 composite which are indicative of abrasive wear. This is mainly due to the presence of uniformly dispersed dual size SiC particles which act as load bearing elements. Especially, DPS2 composite has a higher weight percentage of large size SiC particles which carry greater portion of the load. Further, these large size particles are also very effective in reducing the load on the A357 matrix and thereby save the fine size SiC particles from detachment (Bindumadhavan et al. 2001). In addition to this, the strengthening effect of SiC particles enhances the load bearing capacity of the composites by virtue of its high hardness. Further, good interfacial bonding between the SiC particles and the A357 matrix plays a crucial role in load transfer during sliding test. During sliding test when the load is applied on the A357 alloy the entire load is initially borne by the matrix. However, in case of composites the load is transferred from the matrix to SiC particles which in turn leads to low wear rate. (Bindumadhavan et al. 2001; Dwivedi et al. 2004).

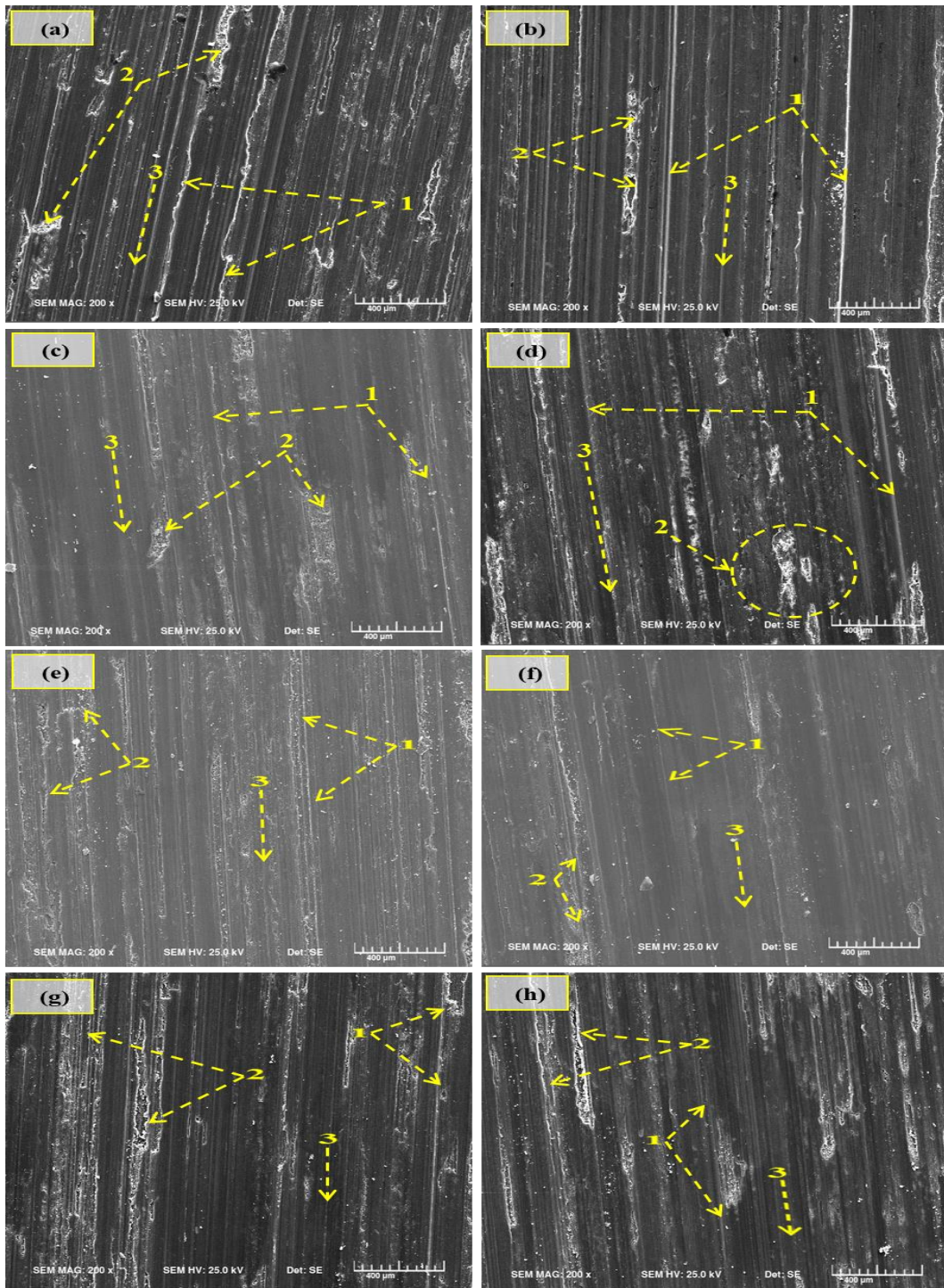


Figure 4.10: Wear tracks of (a) and (b) A357 alloy, (c) and (d) DPS1 composite, (e) and (f) DPS2 composite, and (g) and (h) DPS3 composite at loads of 10N and 30N, respectively.

Figures. 4.10 (g) and (h) show the SEM images of wear surface morphology of DPS3 composite at 10 and 30N loads, respectively. Irregular, larger, and deeper cavities are seen on the surface of the DPS3 composite. This is due to the DPS3 composite having higher weight percentage of fine SiC particles when compared to DPS1. Therefore, the chances of debonding of fine SiC particles from the matrix at higher loads is very high. The width and depth of the grooves increased with the increase in load from 10 to 30 N which is evident from worn surfaces shown in Figures. 4.10 (g) and (h). Biswas and Bai, (1981) have reported that the grooves on the matrix alloy are coarser and smoother in the case of composites. It is observed that with an increase in load, the extent of grooving also increases. This can be attributed to the fact that upon increased load there is an increase in wear rate and also the material gets plastically deformed.

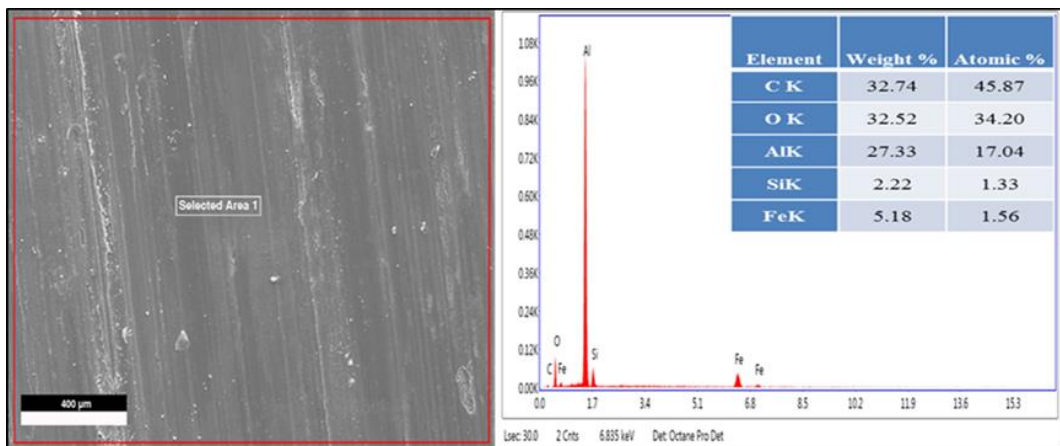


Figure 4.11: EDAX analysis of selected area on worn surface of DPS2 composite at a load of 30N.

EDAX analysis of DPS2 composite shown in Figure. 4.11 confirms the presence of Al, Si, C, Fe and O. The presence of Fe clearly indicates the transfer of Fe from the disc (EN32) to the worn surface, confirming the formation of mechanically-mixed-layer (MML) on the worn surface of the composite which provides protection to the matrix material. This oxide layer along with material from the pin surface creates a mechanically mixed layer which further protects the pin surface from any further wear. Thus, the formation of such layers efficiently reduces the wear rate in these composites (Rao and Das , 2011; Rao and Das , 2011).

4.10 Three-dimensional surface topographies of worn surfaces

Three-dimensional surface topographies of the worn surfaces of A357 alloy and the developed DPS composites were analyzed at a load of 30 N, sliding velocity of 2.5 m/sec and sliding distance of 1500 meters.

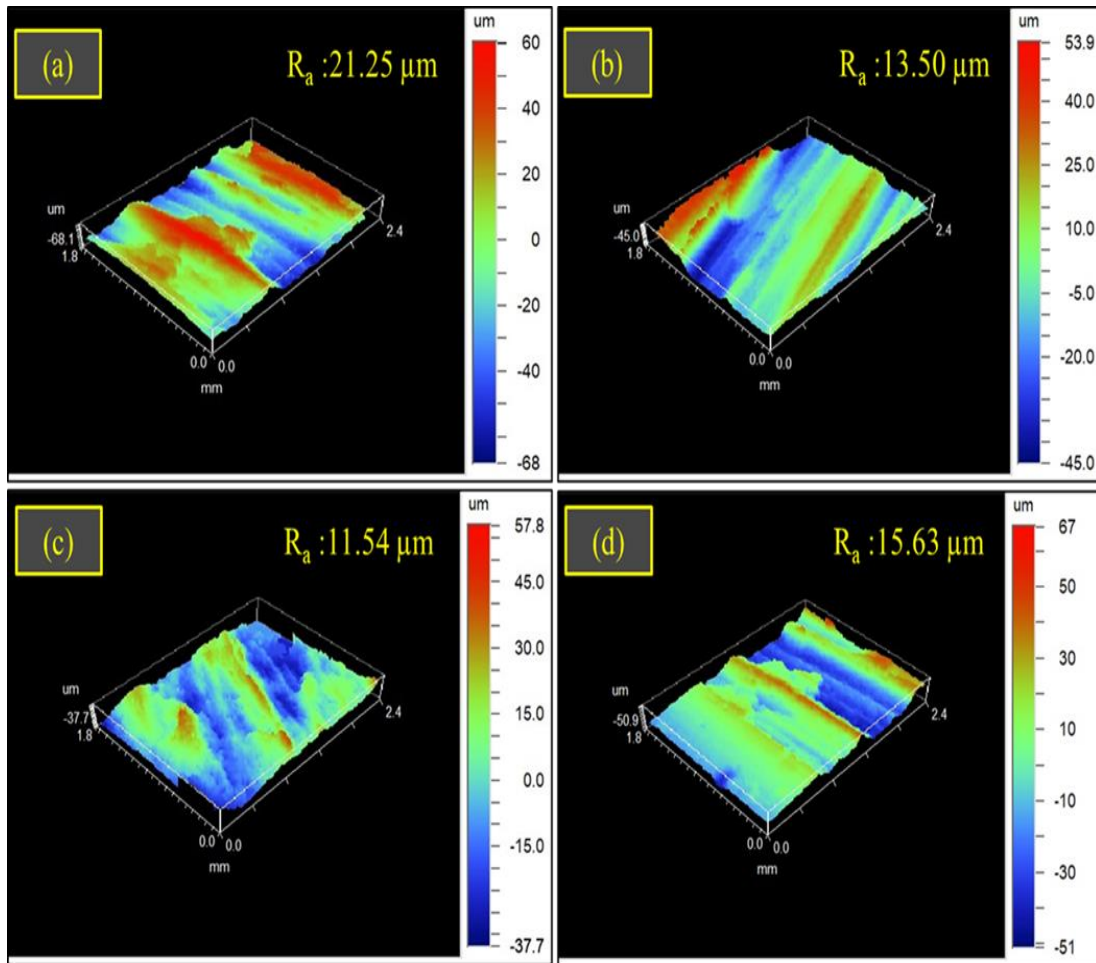


Figure 4.12: Three-dimensional surface topographies of worn surfaces of (a) A357 alloy, (b) DPS1 composite, (c) DPS2 composite, and (d) DPS3 composite at a loads of 30N.

Figure. 4.12 (a) shows the surface topography of A357 alloy which consists of large deformation grooves. Due to soft nature of A357 alloy, the asperities of the counterface were able to dig deeper. Therefore, the surface depth of the grooves is quite large. Further, due to the continuous contact between A357 alloy and the

countersurface, the surface roughness was found to be higher for A357 alloy. On the other hand, the surface roughness values of DPS composites were 13.50 μm , 11.54 μm and 15.63 μm respectively for DPS1, DPS2 and DPS3 composites as shown in Figures. 4.12 (b), (c) and (d). Unlike A357 alloy, the surface roughness of DPS composites was on the lower side, which can be attributed to: (1) minimized contact area between the composite surface and countersurface, and (2) presence of load-bearing material (SiC particles). The observations from SEM analysis are well supported by the surface topography analysis wherein deeper and large deformation grooves are seen in A357 alloy. While in composites, the depth of the grooves and their numbers are comparatively less.

4.11 Wear debris analysis

Figure. 4.13 shows the SEM images of wear debris analysis of A357 alloy and the developed DPS composites taken at 10 N and 30 N. In these images, number 1 represents scale like debris, 2 represents grooved structured debris, 3 represents curvy pattern debris and 4 represents micro-cracks. It can be observed that in case of A357 alloy, wear debris consists of microchips and delamination flakes as shown in Figures. 4.13 (a) and (b). The wear debris taken at 30 N load displayed that the size of laminates produced is more than 500 μm in size while that taken at 10 N load is around 200 μm in size. Due to continuous sliding, the debris generated showed a layered structure which is quite evident from the SEM micrographs. The increase in load results in severe plastic deformation of alloy surface which in turn nucleates the crack in the subsurface level. From the SEM micrograph shown in Figure. 4.13 (b), it is evident that wear debris of alloy shows presence of numerous cracks on surface adjacent to that of subsurface. These cracks are formed due to accumulation of dislocations due to severe plastic deformation taking place on the surface. In addition to this, the presence of deep micro-grooves on the wear debris clearly explains the material removal due to delamination (Sharma et al. 2012). These features indicate delamination wear mechanism in oxidative wear conditions.

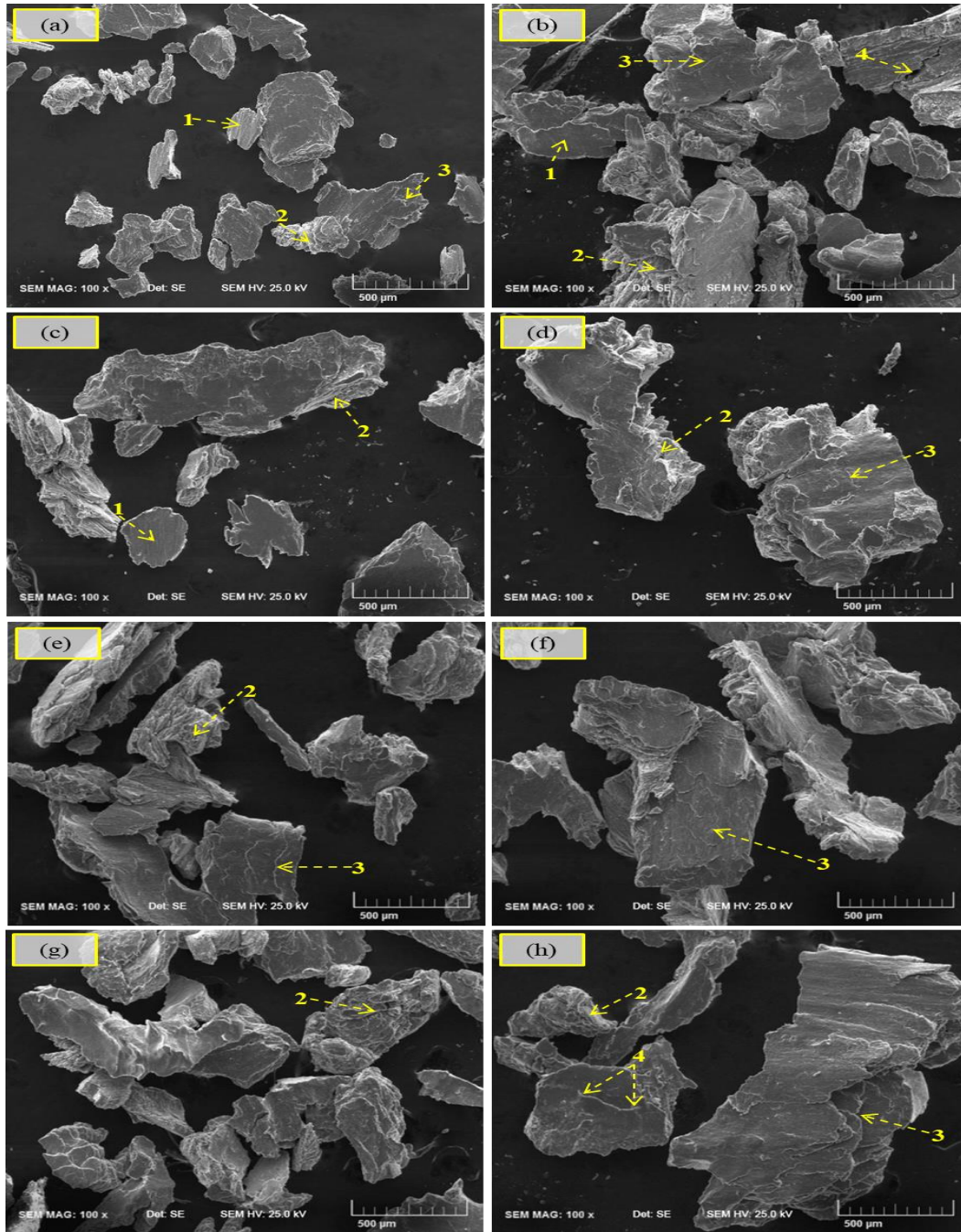


Figure 4.13: Wear debris of (a) and (b) A357 alloy, (c) and (d) DPS1 composite, (e) and (f) DPS2 composite, and (g) and (h) DPS3 composite at loads of 10N and 30N, respectively.

On the other hand, all composites showed flake like morphology and the size and quantity of these flakes increase with the increase in load from 10 N to 30 N. This is mainly due to the fact that at higher loads the shear force generated is quite larger than

that at lower loads leading to larger strain gradient between two contact surfaces and the interface. Careful examination of wear debris especially in case of DPS2 composite (Figure. 4.13 (f)) indicates microlevel delamination on flakes of the wear debris which is mainly due to numerous cracks. Further, the debonding of SiC particles from the surface of the composites takes over a period of time during the sliding test. These particles are entrapped in between the two mating surfaces and cause wear grooves. These wear grooves are clearly visible on the surface of the composites as shown in Figures. 4.13 (d), (f) and (h). Cutting action by the hard asperities and debonded particles cause composite flake generation along with that of delamination flakes. While in case of DPS3 composite, the flakes show extensive cracks displaying microcutting behavior (Rajmohan et al.2013 ; Uthayakumar et al. 2013).

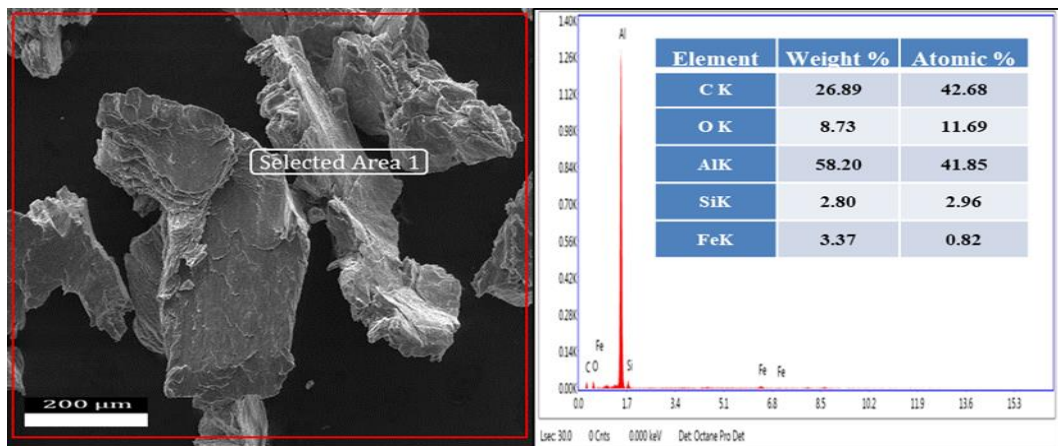


Figure 4.14: EDAX analysis of selected area on wear debris of DPS2 composite at a load of 30 N.

Figure. 4.14 shows the SEM image and EDAX analysis of DPS 2 composite taken at load of 30 N. The wear debris indicates the formation of micro-cracks at the subsurface level which eventually join together to cause the delamination of material. The EDAX analysis shows the presence of various peaks of Al, Si, Fe and O. Here Al and Si are of matrix material. The presence of Fe can be correlated to wear of the countersurface. In addition to this, presence of oxygen peak could be from oxidation of the composite surface resulting from increase in temperature due to wear testing at higher loads.

CHAPTER-5

RESULTS AND DISCUSSION

Effect of solutionizing temperature on microstructure, physical, mechanical and wear properties of dual particle size SiC reinforced A357 composites

In this chapter, the effect of solutionizing temperature (which is varied from 500°C to 540°C in steps of 20°C for 9 h at constant aging temperature of 150°C for 6 h) on the microstructure, mechanical and wear properties of A357 alloy and the developed DPS composites are discussed. Results also include wear debris and worn surface analysis.

5. 1. Density of A357 alloy and the developed DPS composites

Table 5.1: Theoretical and experimental densities of A357 alloy and the developed DPS composites at varying solutionizing temperature

S/No	Alloy/Composite	Designation	Theoretical Density (ρ_{th}) (gm/cc)	Experimental Density (ρ_{exp}) (gm/cc)
1	A357 Alloy	A357-9H-500°C	2.700	2.672
2	DPS1 Composite	DPS1- 9H-500°C	2.730	2.705
3	DPS2 Composite	DPS2- 9H -500°C	2.730	2.709
4	DPS3 Composite	DPS3- 9H -500°C	2.730	2.704
5	A357 Alloy	A357- 9H -520°C	2.700	2.675
6	DPS1 Composite	DPS1- 9H -520°C	2.730	2.709
7	DPS2 Composite	DPS2- 9H -520°C	2.730	2.711
8	DPS3 Composite	DPS3- 9H -520°C	2.730	2.707
9	A357 Alloy	A357- 9H -540°C	2.700	2.682
10	DPS1 Composite	DPS1- 9H -540°C	2.730	2.711
11	DPS2 Composite	DPS2- 9H -540°C	2.730	2.712
12	DPS3 Composite	DPS3- 9H -540°C	2.730	2.710

Table. 5.1 shows the theoretical and measured experimental density values of A357 alloy and the developed DPS composites at varying solutionizing temperatures (500°C, 520°C, and 540°C) and at a constant aging temperature. The higher density values for DPS composites over A357 alloy can be attributed to the higher density of SiC particles, which is 3.21 g/cm³. The increase or decrease in density of composites over the unreinforced counterpart depends on the density value of the reinforcing phase (Hassan et al., .2009; Veeresh Kumar et al. 2011). It can be seen that the experimental densities of A357 alloy and DPS composites are lower than that of theoretical density and the difference in densities is < 1%. This indicates that all the materials considered have dense microstructure with minimal porosity (Zakaria, 2014). The presence of a small percentage of porosity could be due to atmospheric air intake during the holding of molten metal in furnace or entrapment of atmospheric air during pouring (Kandpal et al. 2017). Another reason could be hydrogen evolution and shrinkage due to alloy solidification (Prasad et al. 2014). With respect to reinforcement combination, DPS2 composite showed higher density compared to that of A357 alloy and other DPS composites. With increase of solution temperature, the density of all the materials is found to increase marginally i.e., highest density values were exhibited by materials heat treated at solution temperature of 540°C while lowest density values were exhibited by materials heat treated at solution temperature of 500°C. Similar trends have been reported in literature (Das et al. 2014; Khalifa and Mahmoud 2009).

5.2 Microstructural analysis of A357 alloy

Figures. 5. 1 (a) - (f) show optical and scanning electron micrographs of A357 alloy at different solution temperatures (500, 520, and 540°C) and at constant aging temperature of 150°C, respectively. The microstructure analysis was carried out to enable the understanding of the effect of varying solution temperatures on the microstructure of A357 alloy. The main features of the alloy seen in all the micrographs are that it consists of α -Al solid solution and Al-Si eutectic. The morphology of silicon in A357 alloy is different for different solution temperatures, as shown in Figure. 5.1.

Silicon exhibits a plate type morphology in the A357 alloy, which was solution treated at 500°C, as shown in Figures. 5.1 (a) and (b). While it exhibits a rod-shaped morphology for the alloy, that was solution treated at 520°C (Figures. 5.1 (c) and (d)). For the case of the A357 alloy solution treated at 540°C, (Figures. 5.1 (e) and (f)) silicon exhibits a spherical morphology, indicating its spheroidization. Similar observations were reported by researchers (Rajesh Sharma et al. 2006; Eva et al. 2018; Faccoli et al. 2017; Shivkumar et al. 1990). It is well known that solution temperatures well below 495°C are not capable of changing the morphology of silicon (Apelian et al. 1989). But when the solution temperature is increased beyond 500°C i.e., 520°C the micrographs have shown that the morphology of silicon changes from plate type to rod type as seen in Figures. 5.1 (c) and (d). When the solution temperature was increased further to 540°C, the silicon particles had ellipsoidal morphology which can be seen in Figures. 5.1 (e) and (f). Decrease in surface energy is the main driving force for the formation of ellipsoidal shaped silicon particles (Jiaqing et al. 2017). In addition to this, the increase in diffusion rate with the increase in solution temperature tends to increase the spheroidization rate of silicon particles. So here it is quite clear that with the increase in solution temperature, the morphology of silicon changes and the time needed for spheroidization is shortened (Apelian et al. 1989; Lados et al. 2011). The shape as well as size of Si particles changes when solution treatment is done.

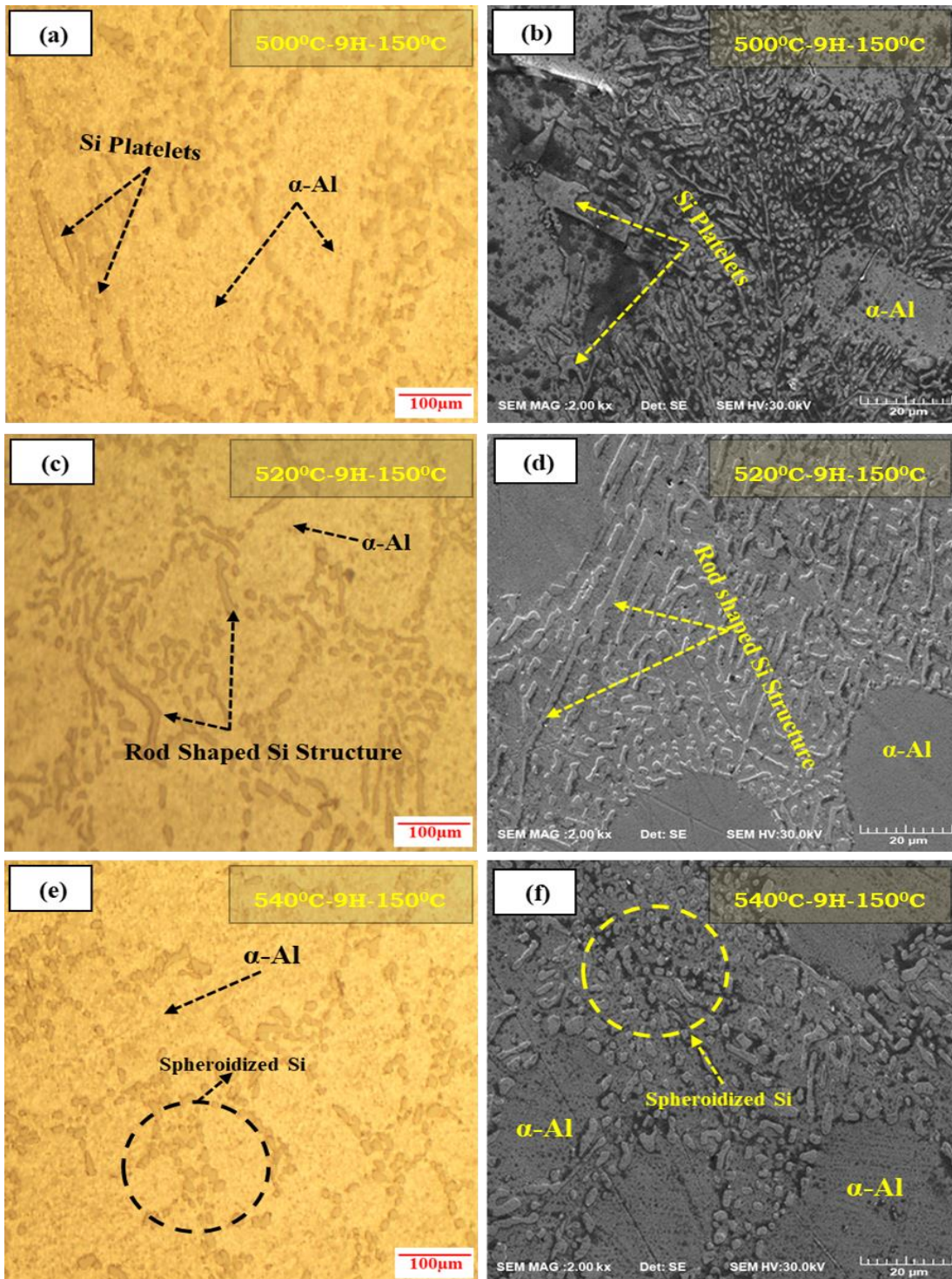


Figure 5.1: (a) and (b) shows optical and SEM micrograph of A357 alloy solutionized at 500°C, (c) and (d) shows optical and SEM micrograph of A357 alloy solutionized at 520°C, and (e) and (f) shows optical and SEM micrograph of A357 alloy solutionized at 540°C.

5. 3 Microstructural analysis of the developed DPS composites

Figures. 5.2 (a), (b), (c), and (d) present the optical micrographs of all the three DPS composites that were solution treated at 540°C and aged at 150°C. In these figures, number 1 represents coarse SiC and 2 represents fine SiC. Optical microscopy analysis was used to check the dispersion and interfacial bonding of dual size SiC particles in the A357 matrix. The interfacial bonding between the dual size SiC particles and A357 matrix is important from the mechanical and tribological performance point of view. The dispersion of dual particle size is found to be fairly uniform throughout the A357 matrix with minimal clustering. Although, there were few particles which are found to be closer to one another, this can be attributed to the moving solidification front which pushes them until molten metal is solidified completely. The solidification front tends to push the smaller and lighter particles while the large particles get entrapped in between the solidification interfaces. In addition to this, small sized SiC particles were found to be in the vicinity of large particles. Though the solidification front pushes the smaller particles, the presence of large particles is inhibiting their movement eventually allowing them to segregate near them. This is quite evident from the optical micrograph of DPS2 composite shown in Figure. 5.2 (d). From the figure, it can be inferred that the fine size SiC particles have encircled the large size SiC particles leaving behind a segregated region of particles. From Figures. 5.2 (a), (b) and (c) it can be seen that the interface between the SiC particles and A357 matrix is clean with no interfacial products. The bonding was in general found to be good with no discontinuities such as cracks or porosity with few exceptions at some regions. The good bonding is helpful in efficient load transfer from soft matrix to hard SiC particles (Shen et al. 2013; Bindumadhavan et al. 2001; Lakshmikanthan et al. 2019).

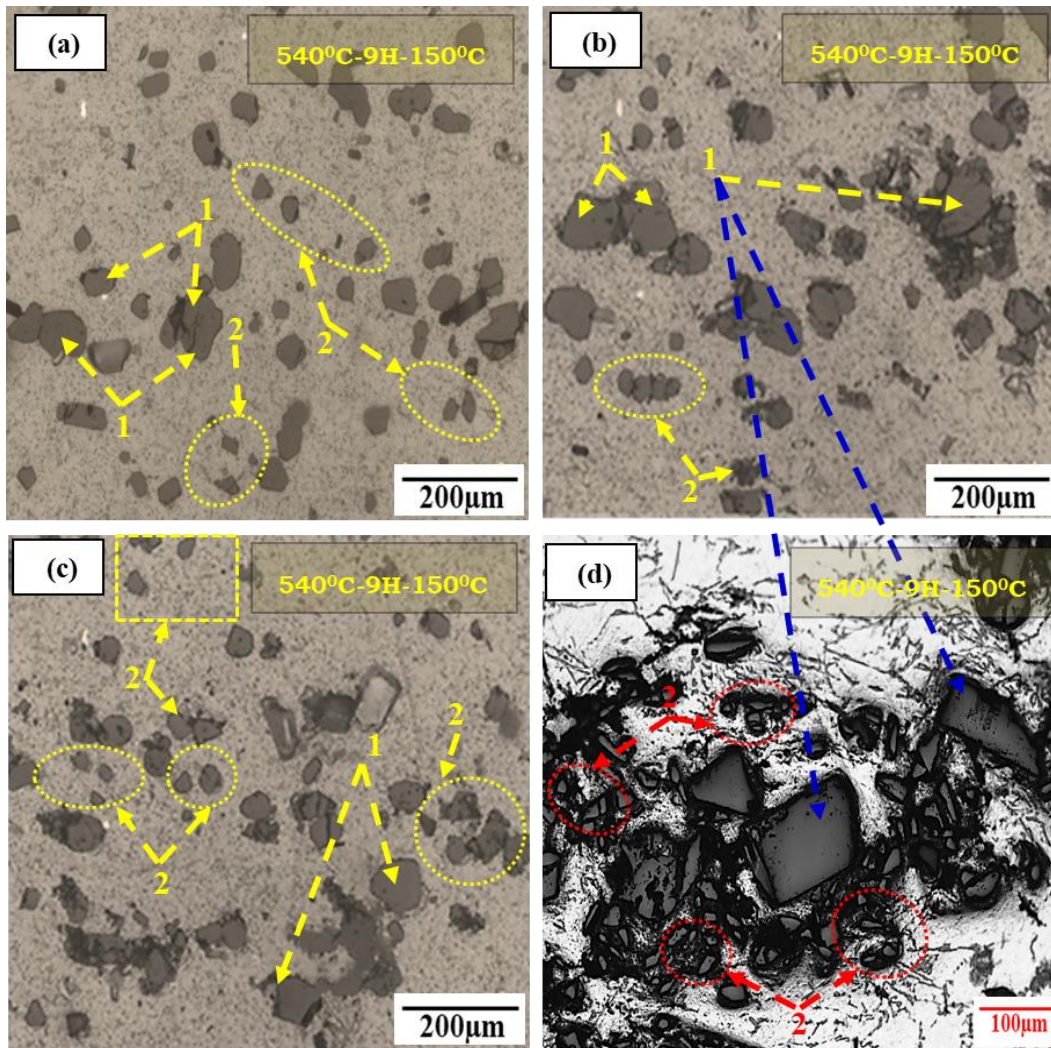


Figure 5.2: Optical micrographs of the developed DPS composites solutionized at 540°C . Where (a) DPS1 composite, (b) DPS2 composite,(c) DPS3 composite, and (d) DPS2 composite at higher magnification showing interfacial bonding.

EDAX analysis of the DPS1 composite solution treated at 540°C was carried out, and spectra were taken at multiple locations. As shown in Figure. 5.3 (a), the first EDAX spectrum was taken exactly on SiC particle, and the two distinct peaks of Si and C are seen. This confirms that the particle observed in SEM is SiC particle. The second EDAX spectrum was taken on the whole area of the composite, and three distinct peaks related to Al, Si, and C were seen in Figure. 5.3 (b). Out of the three elements, aluminium corresponds to A357 alloy, and Si and C correspond to SiC particles. The final EDAX spectrum was taken at the interface between matrix and SiC particles and

is shown in Figure. 5.3 (c). It can be seen that Al, Mg, Si, and C were the main elements seen in the spectrum. As mentioned earlier, the Al peak corresponds to the matrix, while the C peak corresponds to SiC particles. Mg and Si are the principal alloying elements of the alloy, and the peaks observed could be from the A357 alloy. On the other hand, it is well known that the Mg and Si could be related to Mg_2Si precipitates, which could have formed at the interface between SiC particles and matrix. Similar observations were reported by the thesis author (Lakshmikanthan et al. (2020).

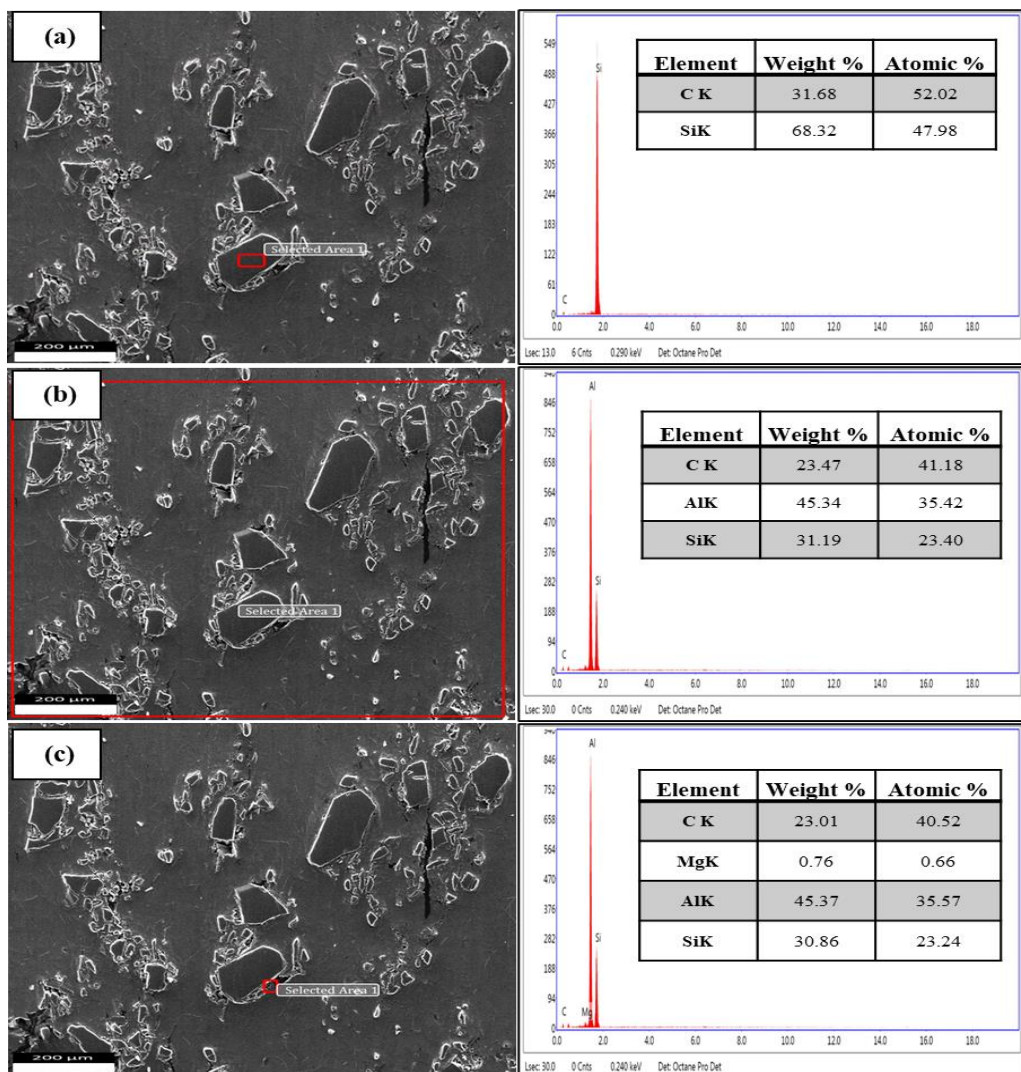


Figure 5.3: EDAX of DPS 1 composite solutionized at 540°C. Where (a) EDAX spectrum taken exactly on SiC particle, (b) EDAX spectrum taken on DPS 1 composite and (c) EDAX spectrum taken at Al/SiC interface.

5.4 TEM analysis of A357 alloy and the developed DPS composites

Figure 5.4 shows the bright-field TEM images of both A357 alloy and the developed DPS composites that were solutionized at 540°C and aged at 150°C. During heat treatment (T6) process supersaturated solid solution is formed after solution treatment and quenching. This is followed by the aging process which leads to the formation of nanosize and sometimes submicron size precipitates from supersaturated solute atoms (Edwards et al. 1998; Lendvai et al. 1974; Es-Said et al. 2002).

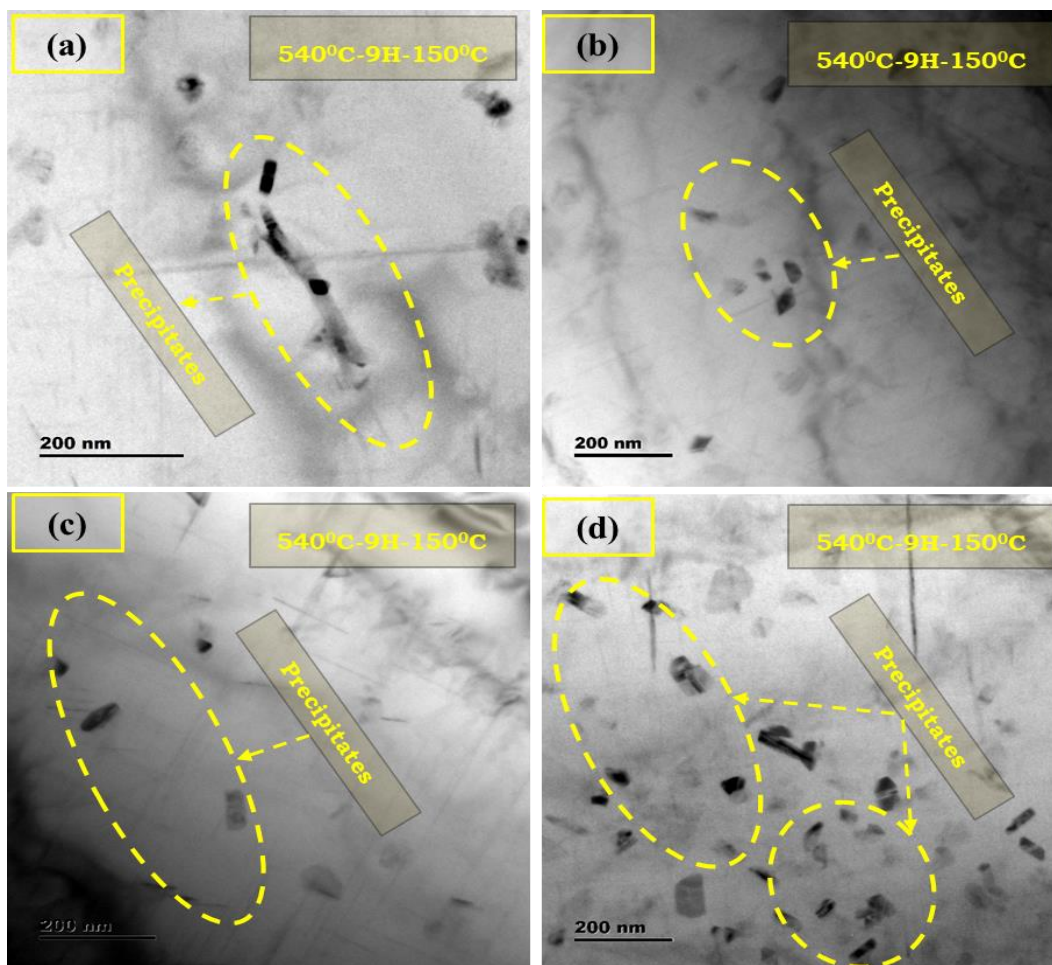


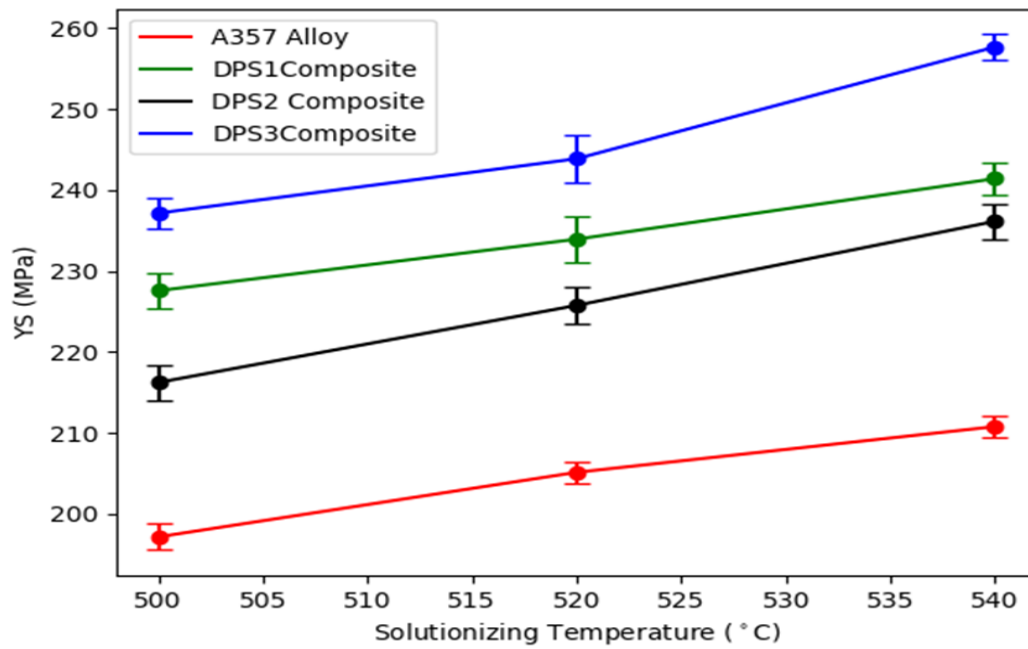
Figure 5.4 : Bright-field TEM images of (a) A357 alloy, (b) DPS1 composite, (c) DPS2 composite, and (d) DPS3 composite, after heat treatment at solutionizing temperature of 540°C.

In the present work, samples are aged for about 6 hours, which helps in the formation of more number of GP zones. In order to check the type and shape of precipitates

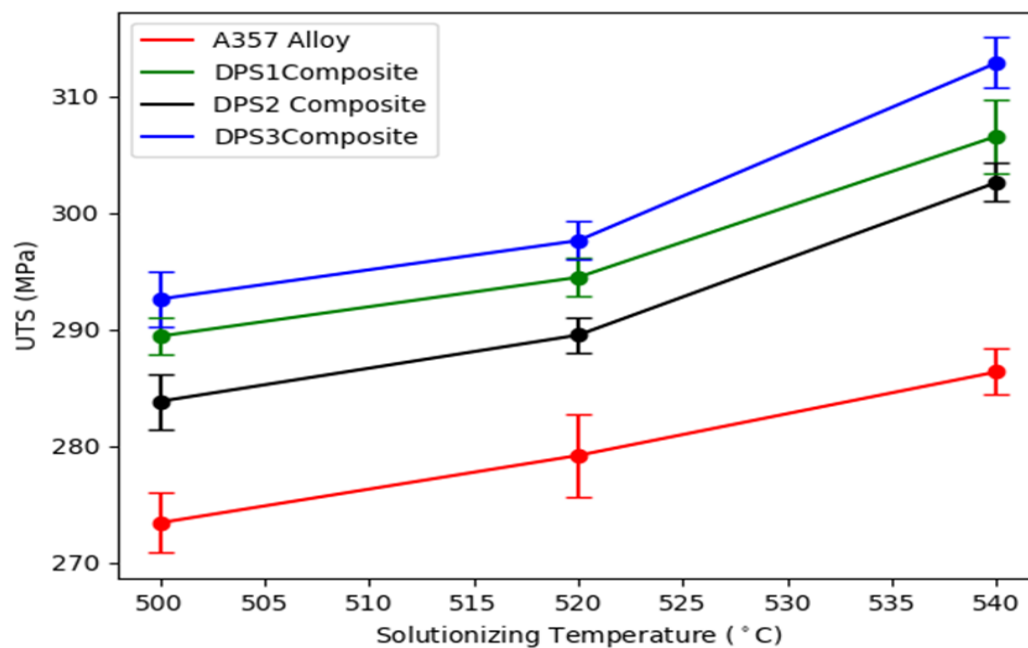
formed, the TEM investigation of A357 alloy and the developed DPS composites was carried out. In case of A357 alloy, the TEM micrograph as shown in Figure. 5.4 (a) shows very few precipitates corresponding to β -Mg₂Si. The black-colored particles seen in the micrograph represent the β -Mg₂Si precipitates which are formed at the end of the transformation. In case of DPS1, DPS2 and DPS3 composites the microstructure consisted of both β'' and β -Mg₂Si precipitates as shown in Figures 5.4 (b), (c) and (d). Here the β'' are known as GP-II zone and are in the form of needles and are found to be uniformly dispersed in the A357 matrix (Mohamed and Samuel , 2012). The β'' -Mg₂Si and β -Mg₂Si precipitate embedded in the matrix helps to strengthen the matrix.

5.5 Tensile strength

Figures. 5.5 (a) & (b) show the strength values of (yield and ultimate) of A357 alloy and the developed DPS composites at different solutionizing temperatures (500°C, 520°C, and 540°C). From Figures. 5.5, it can be observed that the strength (both YS and UTS) of A357 alloy and the developed DPS composites increases with increase in solutionizing temperatures. The DPS3 composite exhibited better tensile strength values when compared with DPS2 and DPS1 composites. All the composites had higher tensile strength than the unreinforced A357 alloy. The higher strength values of composites can be attributed to the presence of SiC particles (6%). DPS3 composite which exhibits the highest tensile strength has a higher ratio of smaller particles (Lakshmikanthan et al. 2019). Also, DPS1 and DPS2 composites show a considerable amount of clustering, while in the case of DPS3 composite, the clustering was not so significant, which was quite evident from the microstructure shown in Figure. 5.2. Better dispersion of SiC particles in case of DPS3 composite was one of the main reasons for significant increment in strength values over A357 alloy and other DPS composites. Both A357 alloy and the developed DPS composites exhibited higher yield and ultimate tensile strength values with an increase in solutionizing temperature from 500°C to 540°C. This may be due to full dissolution of Mg atoms in the solid solution to form Mg₂Si precipitates.



(a)



(b)

Figure 5.5: (a) Yield and (b) Ultimate tensile strengths of A357 alloy and the developed DPS composites at different solutionizing temperatures.

The lower strengths exhibited by A357 and the DPS composites at 500°C can be attributed to incomplete dissolution of particles and low solute concentration in the

matrix (Arsenault and Shi 1986). Also, with the increase in solution temperature, both the activation energy for GP zone nucleation and dislocation density tends to increase (Rong et al. 2000; Das et al. 2008 ;Sankaranarayanan et al. 2011; Lei et al. 2013). When all the materials are cooled to room temperature from solution temperature strain mismatch occurs. This strain mismatch is due to the difference in thermal expansion coefficient of SiC and A357 matrix.

Due to strain mismatch, the matrix undergoes large plastic deformation which in turn produces high dislocation density. So greater the solution temperature, greater is the density of dislocations (Ma et al. 2014; Arsenault and Shi ,1986). This is the reason why all the materials (A357 alloy and DPS composites) showed highest yield and ultimate tensile strength values at a solution temperature of 540°C. In addition to this, the other strength mechanisms responsible for increment in strength are precipitation hardening and load transfer mechanisms (Mirjavadi et al. 2017; Cai et al. 2018). Evidence for formation of precipitates which strengthen the matrix material especially for composites are shown in Figure. 5.4. These mechanisms work together to enhance the strength values especially at solution temperature of 540°C and for DPS3 composite.

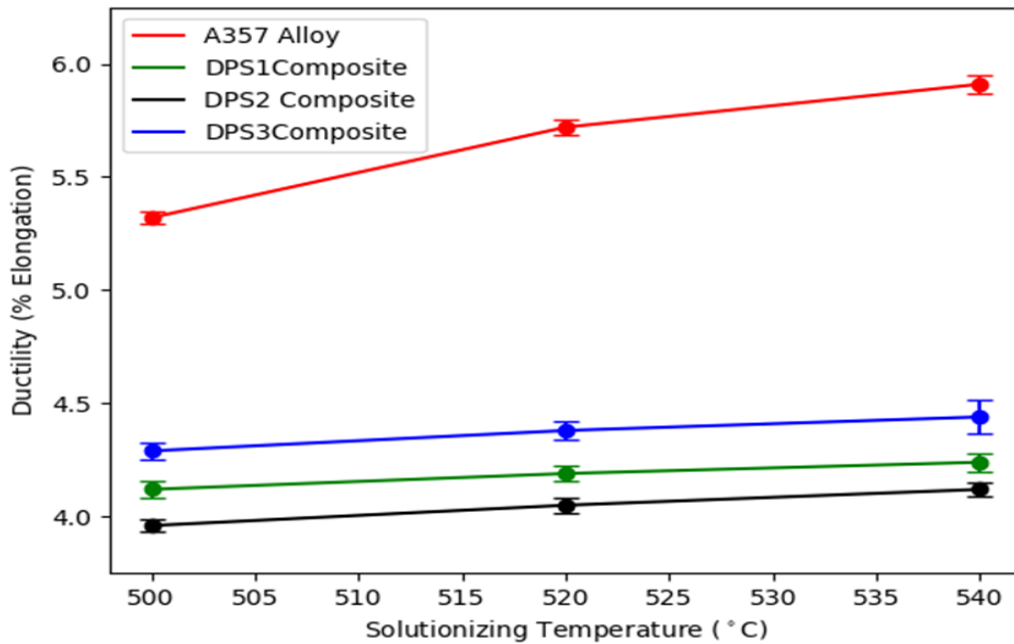


Figure 5.6: Percent elongation (%) of A357 alloy and the developed DPS composites at varying solutionizing temperatures.

Figure. 5.6 shows the variation of percentage elongation of A357 alloy and the developed DPS composites at varying solutionizing temperatures. From Figure. 5.6, it can be seen that the composites exhibit lower ductility when compared to the alloy at all solutionizing temperatures. The addition of hard ceramic particles (SiC) to the soft aluminium matrix (A357 alloy) has to lead to significant loss of ductility in DPS composites. From the figure, it is also observed that ductility values of A357 alloy increase substantially while it increases marginally for DPS composites with an increase in solutionizing temperature. Highest and lowest values of ductility were observed for A357 alloy (5.91%) and DPS3 composite (4.44%) respectively. The reason for increase in ductility at a solution temperature of 540°C compared to other solution temperatures (500°C and 520°C) is due to the softening effect of the matrix (Moller et al. 2008). Due to this effect, dislocation motion is facilitated upto a certain extent resulting in increase in ductility (Ragab et al. 2018). Similar trends have been reported in literature (Moller et al. 2008).

5.6. Tensile fracture surface analysis

Figures. 5.7 (a) – (l), show the tensile fracture surfaces of A357 alloy and the developed DPS composites after the tensile test at varying solutionizing temperatures of 500°C, 520°C, and 540°C. The tensile fracture surfaces of A357 alloy taken at all the three solutionizing temperatures of 500°C, 520°C, and 540°C, showed crack nucleation at the inter-dendritic regions as shown in Figures. 5.7 (a), (b) and (c). For the case of A357 alloy, the inter-dendritic cracking is regarded as the main fracture mechanism irrespective of solution temperature. The crack nucleation occurs at these inter-dendritic regions and propagates along these dendrites, causing its failure. For instance, the sample solutionized at 500°C (Fig. 5.1 (a)) was wholly comprised of cracks propagating through weak dendritic regions. Similar observations were made in the case of other two solution temperatures (520°C, and 540°C). In case of DPS1 composite, the fracture surface for all three solutionizing temperatures (500°C, 520°C, and 540°C), as shown in Figures. 5.7 (d), (e), and (f) show a large number of dimples. The fracture surface of DPS1 composite solution treated at 500°C (Figure. 5.7 (d)) is comprised of dimples with particle pull-out at few regions. Compared to the composite solution treated at both 500°C and 520°C, the composite solution treated at 540°C showed a slightly higher number of dimples indicating higher ductility for the later condition. Owing to dense microstructure and stable stress state, the plastic deformation took completely resulting in fracture surface filled with fine dimples. The presence of both dimples and cleavage planes in the fractured surfaces illustrate mixed mode fracture in DPS1 composite. DPS2 composite also exhibited similar fracture characteristics at all three solutionizing temperatures, as shown in Figures. 5.7 (g), (h) and (i). DPS2 composite solution treated at 500°C (Figure. 5.7 (g)) exhibited cracked eutectic silicon particle regions and interfacial cracks at a few spots. Some regions of DPS2 composite showed SiC particle pull-out, which is shown in Figures. 5.7 (h) and (i). The particle pull-out is attributed to the weakening of interfacial bond strength between the A357 matrix and the SiC particles. With the increase in loading the matrix friction stress increases which in turn enhances the work hardening rate leading to SiC particle pull-out (Zhang et al. 2019).

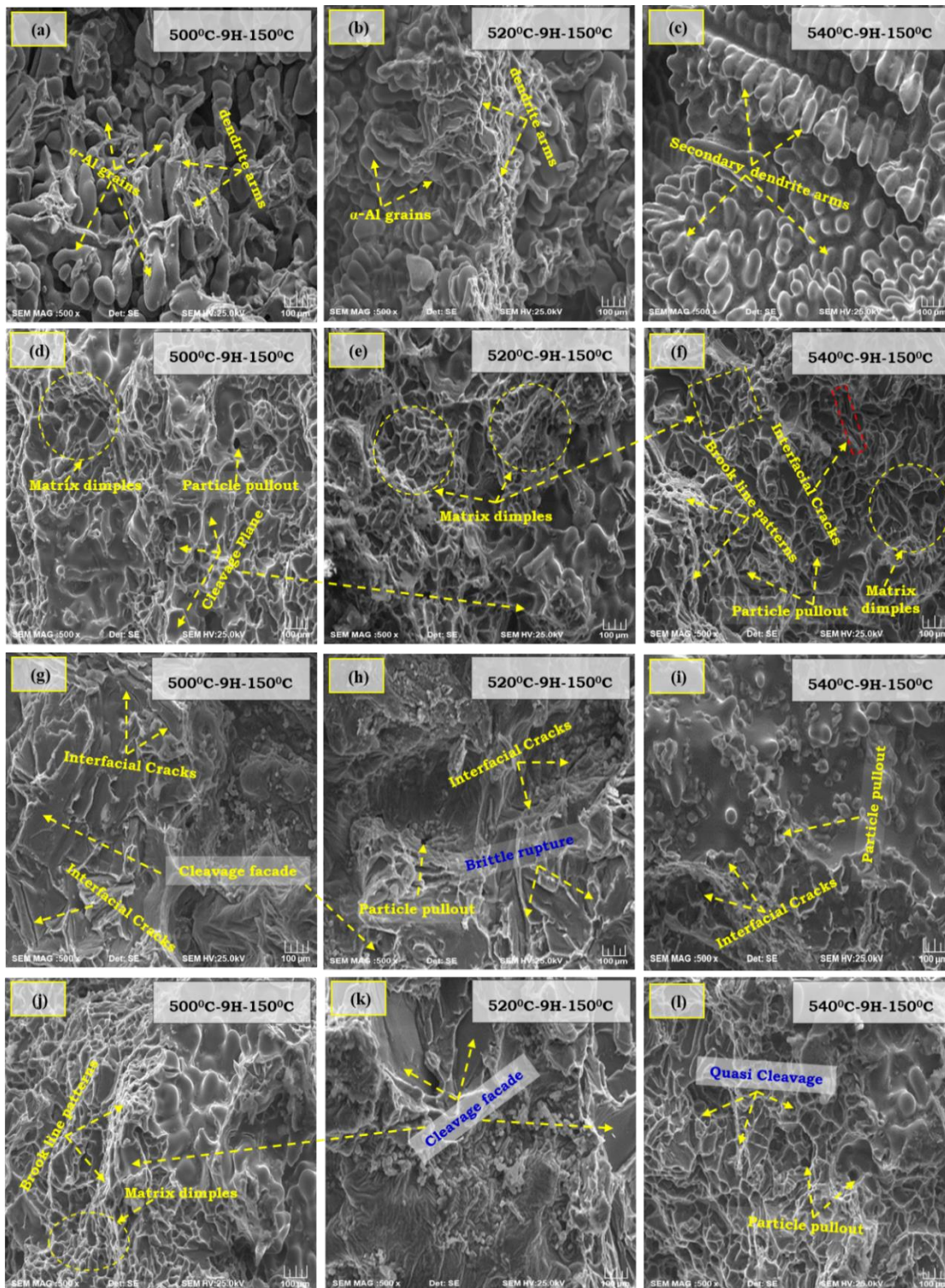


Figure 5.7 : Fractographs of (a), (b), and (c) A357 alloy, (d), (e), and (f) DPS1 composite, (g), (h), and (i) DPS2 composite, (j), (k), and (l) DPS3 composite solutionized at 500 °C, 520 °C, and 540 °C, respectively.

In addition to this, some eutectic silicon particles were also pulled-out from matrix surface which were accompanied by formation of secondary cracks that are shown in Figures. 5.7 (i). So, it can be presumed that the debonding of eutectic silicon particle and SiC particle were responsible for failure of DPS2 composite. Finally, for the case of DPS3 composite, the quasi-cleavage planes were visible on the surfaces of composite for all three solutionizing temperatures which are shown in Figures. 5.7 (j) (k) and (l). The fractography of DPS3 composite solution treated at 500°C (Figure. 5.7 (j)) comprises of inter-dendritic cracking and fine dimples. At few regions, both particle pull-out and particle de-bonding were seen. Unlike for composite solution treated at 500°C and 520°C, the one solution treated at 540°C showed more particle cracking. This implies that the SiC particles participated in the fracture process. The reason for SiC particle cracking is attributed to increasing internal stress and particle fracture stress. During tensile loading, stresses are being imposed on the SiC particles by the A357 matrix. The internal stress which is induced on the SiC particles tends to increase and reach particle fracture stress eventually leading to cracking of SiC particles. However, one can see that the number of dimples on DPS3 composite solution treated at 540°C was more when compared to that of composite solution treated at 500°C and 520°C, respectively. More number of dimples is due to reduction in morphology of eutectic silicon and indication of increased ductility for DPS3 composite shown in Figure. 5.7 (h). Overall, all DPS composites showed mixed mode fracture due to presence of dimples and cleavage planes. Similar trends have been reported in literature (Pramod et al. 2008; Lakshmikanthan et al. 2020).

5.7 Hardness results

Figure. 5.8 shows the variation of hardness of A357 alloy and the developed DPS composites at varying solutionizing temperatures (500°C, 520°C, and 540°C). The DPS composites showed higher hardness than A357 alloy at all solutionizing temperatures. This can be attributed to the presence of hard SiC particles. Among the composites, the highest hardness was exhibited by DPS2, whereas DPS3 exhibited the

lowest hardness. This was observed for all the three solutionizing temperatures. From Figure. 5.8, it can be seen that hardness increases with increase in solutionizing temperature. The possible reason for increment in hardness is attributed to effective refinement of silicon particles from plate shaped morphology at 500°C to fine ellipsoidal at 540°C (Faccoli et al. 2017). In addition to this aging kinetics tend to accelerate with the increase in solution temperature which is why all the materials showed higher hardness values at 540°C.

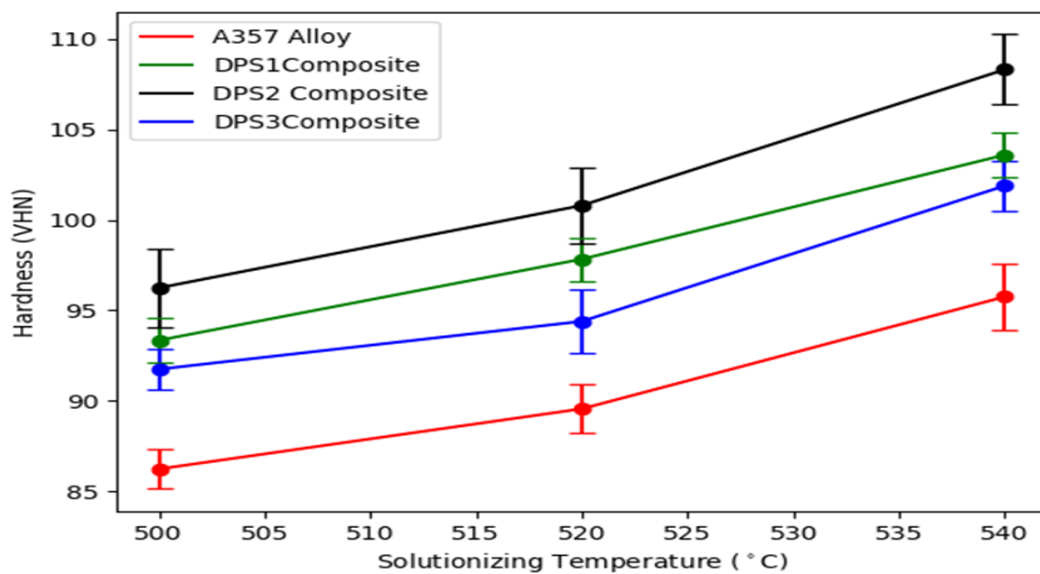


Figure 5.8: Hardness test results of A357 alloy and the developed DPS composites at different solutionizing temperatures.

However, this is not the only reason for increment of hardness, but other contributors working along with this such as dispersion and dislocation strengthening mechanisms (Ajith kumar et al. 2014; Deng et al. 2012). Jin et al.(2011) in their work showed highest hardness values for a solution temperature of 530°C when compared to other solution temperatures of 495 and 560°C, respectively. Increase in solution temperature from 530°C to 560°C, led to both precipitate and grain coarsening which is why the hardness didn't increase with further increase in solution temperature. The hardness results obtained in the present work are in good agreement with the results reported by Jin et al.(2011).

5.8 Specific wear rate

Figure. 5.9 shows the plot of specific wear rate (at 30 N) v/s solutionizing temperature of A357 alloy and the developed DPS composites. From Figure 5.9, it can be observed that A357 alloy displays the highest wear rate. The reason for high wear rate in A357 alloy can be attributed to increased contact area between the two contact surfaces which further leads to interlocking or possible local welding between the asperities of the two contact surfaces resulting in increased specific wear rate (Vieira et al. 2009; Suresh and Sridhara, 2010). In addition to this, absence of load-bearing material can cause thermal softening of surface due to increase in temperature at the interface of contact surfaces.

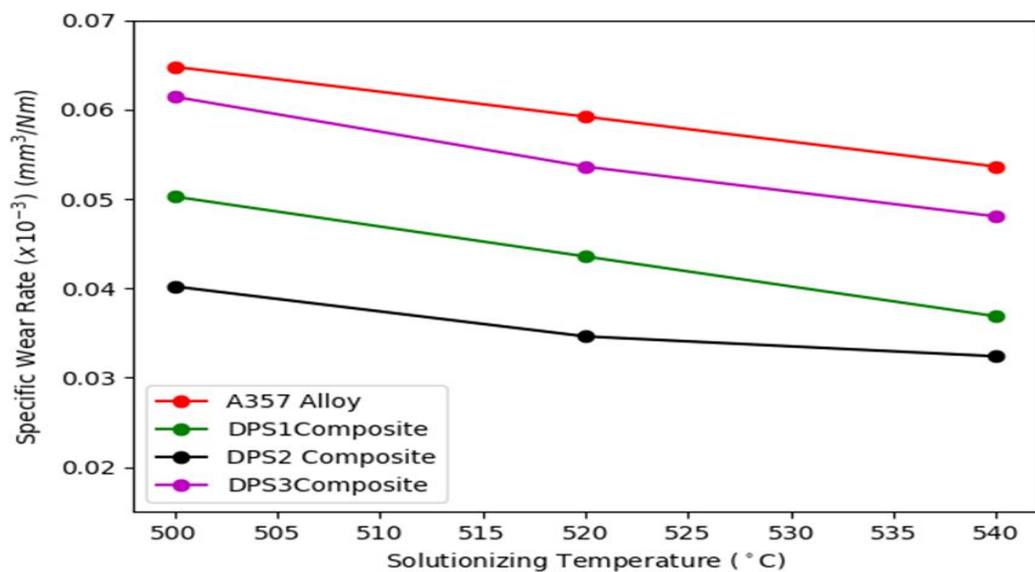


Figure 5.9 : Effect of solutionizing temperature on the wear rate of A357 alloy and the developed DPS composites.

From Figure. 5.9, it can also be observed that DPS composites exhibit lower wear rate when compared to A357 alloy. This can be attributed to the presence of hard SiC particles in DPS composites. In addition to this, the strain hardening effect due to the presence of SiC particles also contributes to lower wear rate (Guo et al. 2002). Among the composites, the DPS2 composite displayed least wear rate when compared to

DPS1 and DPS3 composites at all solutionizing temperatures. The better wear resistance of DPS2 composite over the others (DPS1 and DPS3 composites) is attributed to its high hardness. From Figure. 5.8, it is evident that the hardness of DPS2 composite is higher for all cases of solution temperatures. The wear behavior of A357 alloy and its DPS composites can be directly related to their hardness. According to Archard's law, the wear volume is inversely proportional to the hardness of a material (Archard,1953). To this end, the DPS2 composite exhibited higher hardness value over the other two DPS composites and the A357 alloy. It is quite clear that due to its high hardness, DPS2 composite displayed lower specific wear rate while A357 alloy with low hardness exhibited high specific wear rate. It is interesting to note the relation between solutionizing temperature and wear resistance.

From Figure. 5.9, it can be observed that with increase in solution temperature from 500°C to 540°C, the specific wear rate of A357 alloy and the developed DPS composites tends to decrease. It is well known that increase in solution temperature increases both the activation energy for GP zone nucleation and dislocation density (Rong et al. 2000; Das et al. 2008 ; Sankaranarayanan et al. 2011; Lei et al. 2013). Due to this, both the hardness and the strength of all materials tend to increase with increase in solution temperature. Similar results were reported by several researchers (Li et al. 2018; Gupta et al. 2012).

5.9. Worn surface analysis

Figures. 5.10 (a) – (l) show the SEM micrographs of worn surfaces of both A357 alloy and the developed DPS composites at varying solutionizing temperatures (500°C, 520°C, and 540°C), at a load of 30N, sliding velocity of 2.5 m/sec and sliding distance of 1500 m. In these figures, number 1 represents sliding direction, 2 represents abrasion region, 3 represents coarse ploughed grooves ,4 represents narrow ploughed grooves , 5 represents craters and 6 represents specks, respectively. In case of A357 alloy, the worn surface as seen in Figures. 5.10 (a), (b), and (c) show abrasive grooves running parallel to the sliding direction. Worn surface of A357 alloy solutionized at 500°C (Figure. 5.10 (a)) showed a few delaminated regions along with

specks in between the parallel grooves. The width and number of abrasive grooves in case of A357 alloy solutionized at 500°C and 520°C were higher than that solutionized at 540°C. In addition to this, large patches of delaminated regions were seen for A357 alloy solutionized at 520°C. This is due to the fact that the hardness of A357 alloy is higher at higher solutionizing temperatures which provides utmost resistance to plastic deformation and avoids formation of micro-cracks at the sub-surface level (Abouei et al. 2010). Formation of micro-cracks at the surface tends to coalesce at the subsurface region eventually removing the material in the form of flakes (Zhu et al. 2017). Due to high hardness this is avoided to certain extent which is why minimal delaminated regions were seen in Figure. 5.10 (c).

Worn surfaces of DPS1 composite presented in Figures. 5.10 (d), (e) and (f) show abrasive grooves running parallel to the sliding direction with minimal delaminated regions. Worn surface of DPS1 composite solutionized at 500°C (Figure. 5.10 (d)) showed relatively smooth surface along with few delaminated regions. It can be seen that compared to A357 alloy the number of abrasive grooves on the composite is lower indicating improved resistance to plastic deformation due to presence of SiC particles. Both eutectic silicon and SiC particles are known for their high hardness and they resist the plastic flow of material restricting the formation of abrasive grooves. Further, the delaminated regions are comparatively lesser for DPS1 composite, and their size is also quite smaller when compared with that of A357 alloy. The DPS1 composite solution treated at 540°C showed no delaminated regions which can be attributed to its high hardness.

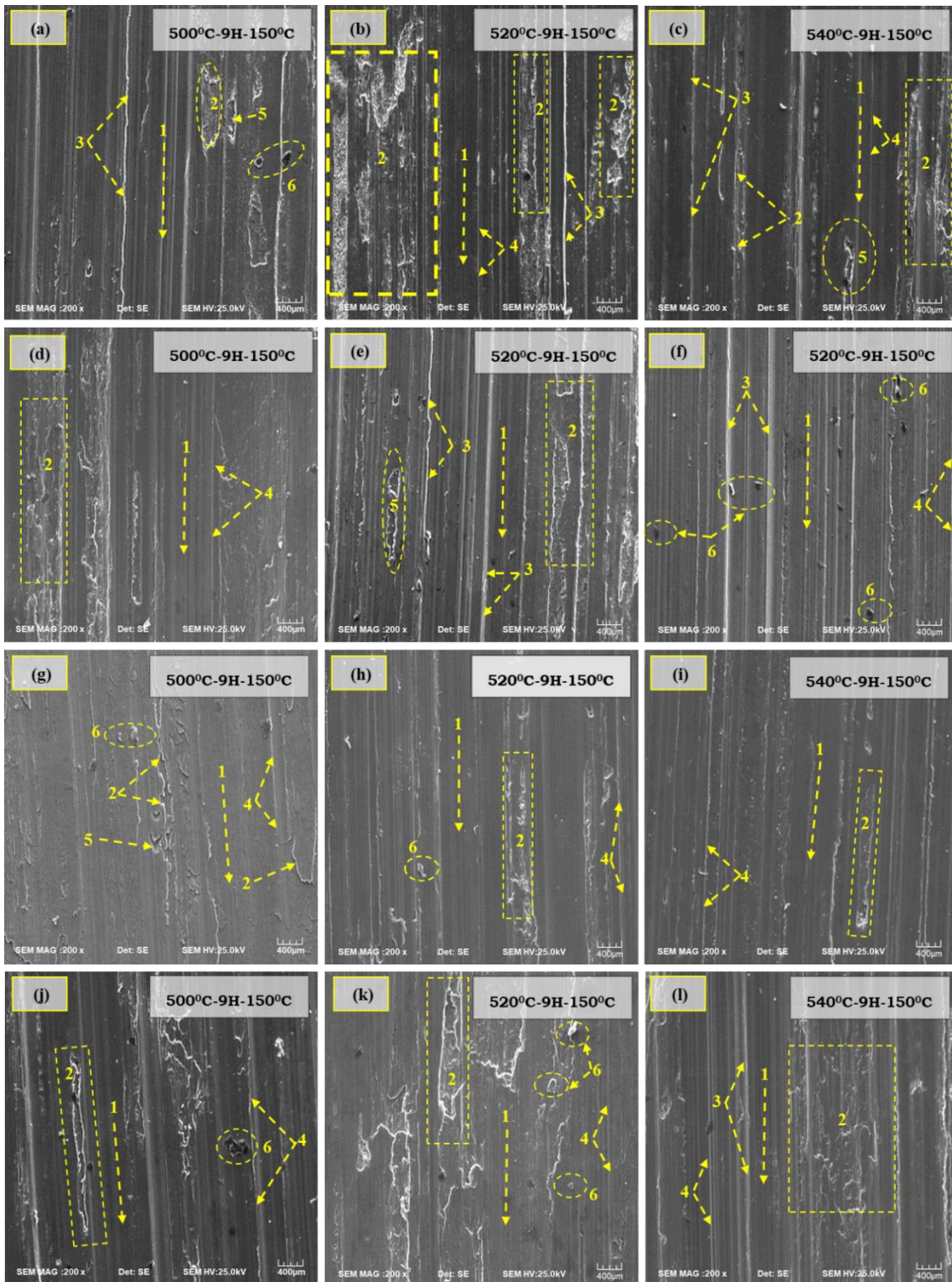


Figure 5.10: Wear tracks of (a), (b), and (c) A357 alloy, (d), (e), and (f) DPS1 composite, (g), (h), and (i) DPS2 composite, (j), (k), and (l) DPS3 composite solutionized at 500 °C, 520 °C, and 540 °C, respectively.

Worn surfaces of DPS2 composite presented in Figures. 5.10 (g), (h), and (i) show thin abrasive grooves running parallel to sliding direction, indicating abrasive wear. However, one can observe that the worn surface of DPS2 composites is quite smooth compared to the other two DPS composites. For instance, the worn surface of DPS2 composite solutionized at 500°C (Figure. 5.10 (g)) showed relatively smooth surface with fine abrasive grooves. The main reason is the high hardness observed in DPS2 composites for all solution treatment temperatures. Due to its high hardness, the asperities of countersurface find it very hard to dig the surface of composite and because of this the extent of delamination is also decreased. Also, the contact surfaces and sliding surface temperatures are not increased to an extent such that the composite surface is softened; due to this, adhesion is largely avoided thereby reducing the area of delamination.

The worn surfaces of DPS3 composite are shown in Figures. 5.10 (j), (k) and (l). This surface is found to be composed of parallel abrasive grooves and large delaminated regions. The width of abrasive grooves in DPS3 composite is found to be quite larger than that of DPS2 composite. The possible reason for severe delamination is attributed to an increase in the higher normal load applied during testing (Asl et al. 2010). The higher load ensures that the effective stress applied by the countersurface exceeds the yield strength of composite which results in yielding and breaking the asperities. In addition to this, the asperities of countersurface penetrate deeper into the composite surface thereby digging more material. Further, increasing the surface temperature causes softening and adhesion, which in turn leaves behind a large crater due to delamination of the composite surface. Overall, delamination wear was found to be the primary wear mechanism operating in A357 alloy and the developed DPS composites followed by abrasion (Li et al. 2018; Suh , 1977).

5.10 Three-dimensional surface topographies of worn surfaces

Figures. 5.11 (a) – (h) show three-dimensional surface topographies of the worn surfaces of A357 alloy and the developed DPS composites solutionized at different temperatures of 520°C and 540°C taken at 30 N load, sliding velocity of 2.5 m/sec, and sliding distance of 1500 m. The surface topography of A357 alloy shows very high roughness values for both solutionizing temperatures indicating severity of wear as seen in Figures. 5.11 (a) and (b). The topography showed large regions of material delamination along with wide abrasive grooves running along the sliding direction. Many grooves on the worn surface were found to be several hundred micrometers wide and up to ~40 µm depth. Due to the soft nature of A357 alloy, the asperities of the countersurface were able to remove material much easier and at large depths. This is why the surface roughness of A357 alloy at solutionizing temperatures of 520°C and 540°C was about 12.53 and 11.06 µm, respectively.

DPS1 composite showed considerably lesser surface roughness than A357 alloy indicating good resistance to plastic deformation. The surface roughness values were about 6.24 and 5.86 µm for 520°C and 540°C solution treated DPS1 composite as shown in Figures. 5.11 (c) and (d). The presence of SiC particles ensures minimal contact between the countersurface and the composite surface during testing. Less number of asperities from countersurface will have contact with the composite surface due to which the material loss is less as well as the surface roughness will be low which is quite evident from surface topographies. With the increase in material hardness, the asperities from countersurface find it very difficult to penetrate the surface of DPS2 composite due to which the surface will have fewer groove marks. Even though few abrasive grooves are present, the depth of the grooves is negligible. This is evident from the surface topography of DPS2 composite, as shown in Figures. 5.11 (e) and (f). The surface roughness of DPS2 composite was found to be 3.88 and 2.99 µm respectively for 520°C and 540°C solution temperature, respectively. The hardness of DPS2 composite was found to be higher than that of other composites and A357 alloy. Therefore, the composite provides utmost resistance to penetration of asperities of countersurface as well as minimizes the material loss.

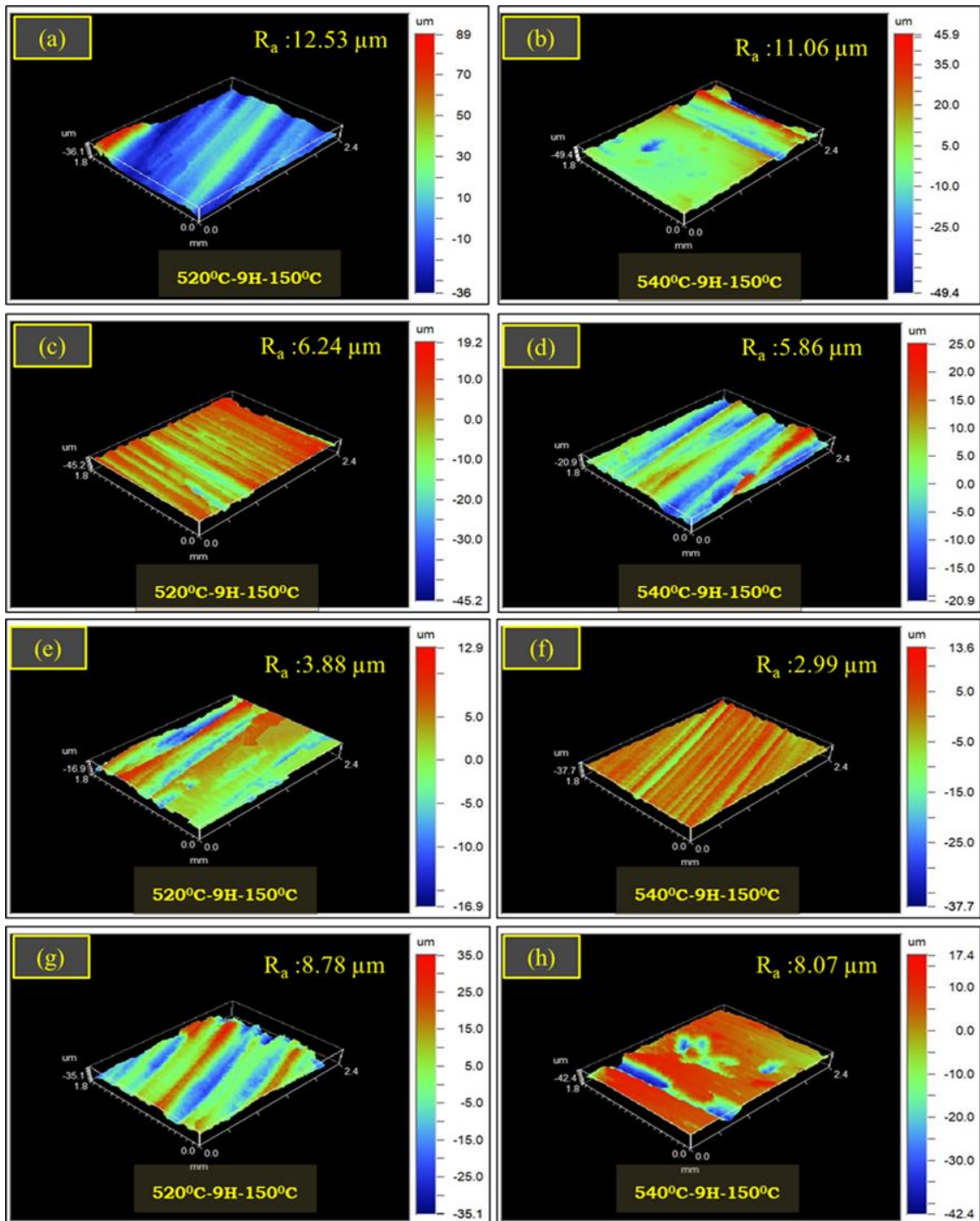


Figure 5.11: Three-dimensional surface topographies of worn surfaces of (a) and (b) A357 alloy, (c) and (d) DPS1 composite, (e) and (f) DPS2 composite, (g) and (h) DPS3 composite, solutionized at 520°C and 540°C, respectively.

The DPS3 composite (Figures. 5.11 (g) and (h)) showed abrasive groove marks with few delaminated regions in the topographies. The depth of the grooves for DPS3 composite solution treated at 520°C was found to be in the range of 15-35 µm while the one solution treated at 540°C showed depth of grooves in the range of 20-43 µm. The depth of delaminated region in case of DPS3 composite suggest the nucleation of large number of micro-cracks at the surface and propagating through the sub-surface where they tend to coalesce. This region covered with micro-cracks is delaminated from the composite surface leaving behind craters. Further among composites, DPS3 composite has shown highest surface roughness values which is well in line with the specific wear rate results. In addition to this, the surface topography results as shown in Figures. 5.11 (g) and (h) are almost similar to the SEM micrographs showing worn surfaces in Figures. 5.10 (k) and (l). Overall, the surface topography and the surface roughness values of A357 alloy and its DPS composites are well in line with the worn surfaces shown in Figures. 5.10.

5.11 Wear debris analysis

Figures. 5.12 (a) – (l) show the SEM images of wear debris collected from both A357 alloy and the developed DPS composites at solutionizing temperatures of 500°C, 520°C and 540°C respectively at a load of 30N, sliding velocity of 2.5 m/sec and sliding distance of 1500 m. In these figures, number 1 represents yarn-like debris, 2 represents micro-cracks, 3 represents wrecked debris, 4 represents wavy form debris, and 5 represents scale-like debris, respectively. The wear debris observed for A357 alloy solutionized at 500°C was found to be several hundred microns in size with large parallel grooves on them (see Figure. 5.12 (a)). Large, delaminated regions in the form of flakes were observed for A357 alloy as shown in Figures. 5.12 (b) and (c). Many of these regions were over 500 µm in length, indicating severity of the applied load. In case of low loads, the wear rates were low, and the debris formed is also fine in size. However, in the present case, the debris formed were quite large in size and in the form of metallic flakes indicating severe wear. The debris also showed presence of abrasive grooves on the surface which was the main wear characteristic seen in the

worn surfaces. Apart from few large, delaminated regions small powdered shaped debris was also extracted from the countersurface. This is attributed to ploughing action of asperities of countersurface over the composite surface repetitively.

On the other hand, the formation of large-scale debris which had micro-cracks on the surface showed that delamination wear was primary wear mechanism in A357 alloy followed by abrasion. In case of DPS composites the debris, and their size was considerably lower than that of A357 alloy except for DPS3 composite. The SEM micrographs of DPS1 and DPS2 shown in Figures. 5.12 (d), (e) (f), (g), (h) and (i) indicate that the size of debris was few hundred microns or lower than that. Here, formation of small size debris indicates that SiC particles were able to prevent the severe wear of A357 matrix. Careful observations of debris surface show the presence of abrasive grooves and their flake type morphology explains metallic wear. In addition to this, another characteristic feature was seen in case of DPS1 and DPS2 composites, where the debris is formed in shape of ductile ribbons (Kaur and Pandey, 2010). Due to predominance of abrasive wear such type of metallic ribbon debris is observed in these two composites.

In case of DPS3 composite, the large wear debris observed was similar to that seen for A357 alloy and are shown in Figures. 5.12 (j), (k) and (l). Presence of large metallic flakes with a number of micro-cracks over them suggest sub-surface delamination mechanism. Localized stresses on the composite surface over a period of time tend to become higher than that of the yield strength of the composite. Due to this, deformation occurs in large scale such that the fracture of sub-surface and surface takes place simultaneously leading to formation of large size debris. This is well in line with the specific wear rate observed for DPS3 composite which is considerably higher than other two composites. Overall, the DPS composites, showed delamination wear as primary wear mechanism followed abrasion (Kaur and Pandey, 2010).

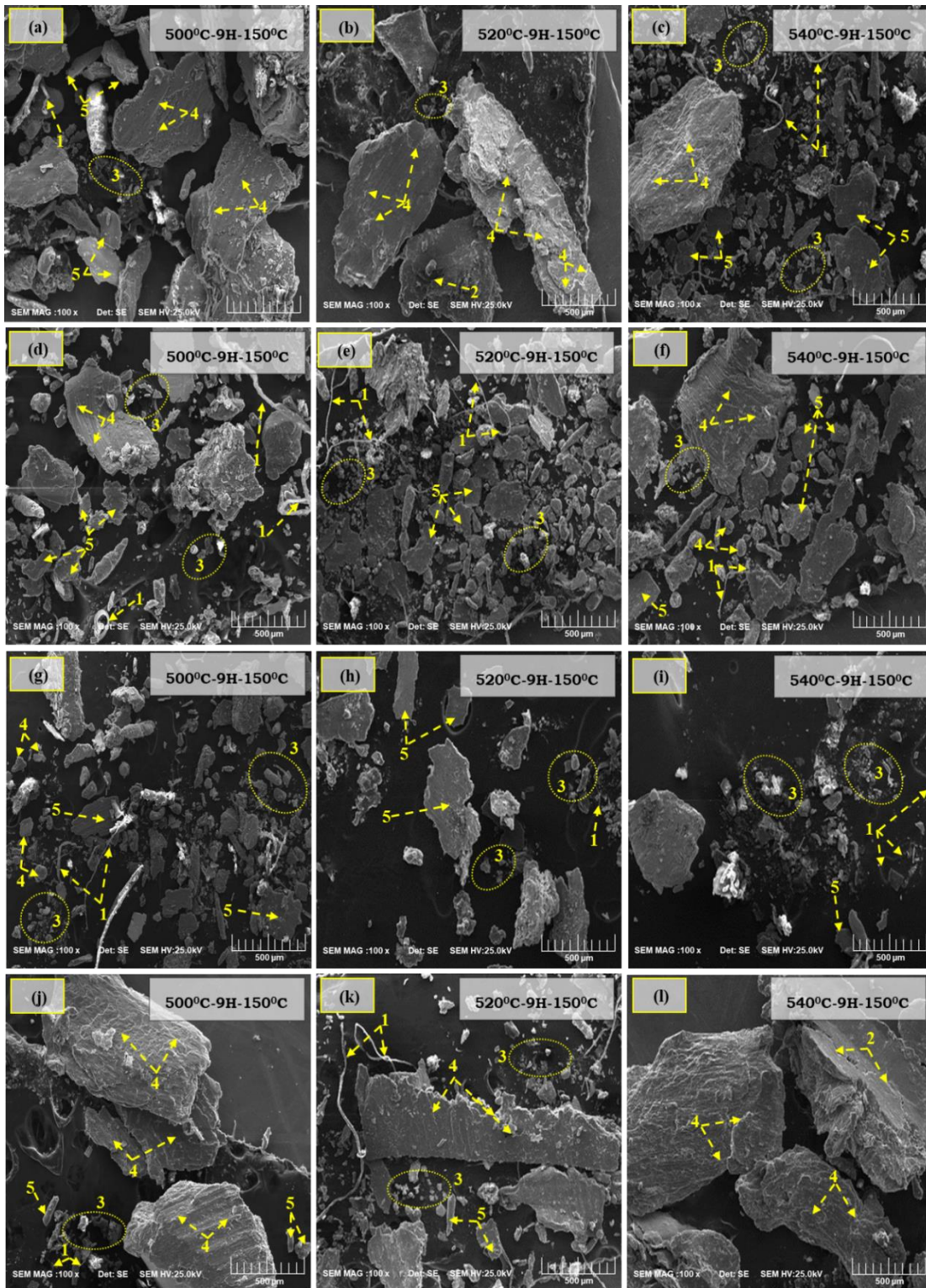


Figure 5.12: Wear debris of (a), (b), and (c) A357 alloy, (d), (e), and (f) DPS1 composite, (g), (h), and (i) DPS2 composite, (j), (k), and (l) DPS3 composite aged at 500 °C, 520 °C, and 540 °C respectively.

CHAPTER-6

RESULTS AND DISCUSSION

Effect of aging temperature on microstructure, physical, mechanical and wear properties of dual particle size SiC reinforced A357 composites

In this chapter, the effect of aging temperature (which is varied from 160°C to 200°C in steps of 20°C for 6 h at constant solutionizing temperature of 540°C for 9 h.) on the microstructure, mechanical and wear properties of A357 alloy and the developed DPS composites are discussed. Results also include wear debris and worn surface analysis.

6.1 Density of A357 alloy and the developed DPS composite

Table 6.1: Theoretical and experimental densities of A357 alloy and the developed DPS composites at varying aging temperatures.

S/No	Alloy/Composite	Designation	Theoretical Density (ρ_{th}) (gm/cc)	Experimental Density (ρ_{exp}) (gm/cc)
1	A357 Alloy	A357-160°C - 6H	2.700	2.685
2	DPS1 Composite	DPS1-160°C - 6H	2.730	2.713
3	DPS2 Composite	DPS2-160°C - 6H	2.730	2.715
4	DPS3 Composite	DPS3-160°C - 6H	2.730	2.713
5	A357 Alloy	A357-180°C - 6H	2.700	2.691
6	DPS1 Composite	DPS1-180°C - 6H	2.730	2.720
7	DPS2 Composite	DPS2-180°C - 6H	2.730	2.721
8	DPS3 Composite	DPS3-180°C - 6H	2.730	2.720
9	A357 Alloy	A357-200°C - 6H	2.700	2.688
10	DPS1 Composite	DPS1-200°C - 6H	2.730	2.717
11	DPS2 Composite	DPS2-200°C - 6H	2.730	2.718
12	DPS3 Composite	DPS3-200°C - 6H	2.730	2.716

Table. 6.1 shows the density measurements (theoretical and experimental) of A357 alloy and the developed DPS composites at varying aging temperatures (160°C, 180°C, and 200°C). The density values of the DPS composites are slightly higher compared to the A357 alloy. This is due to the presence of a high-density ceramic material (SiC) (Aykut Canakci et al. 2014; Youg Hu et al. 2019). Variations in density among the composites heat treated to different conditions are negligible. From Table. 6.1, it can be observed that the difference in the theoretical and experimental densities is insignificant. Thus, it can be concluded that the dispersion of SiC particles was found to be good with almost no observable porosity or any casting defects (Rao et al. 2012; Ramprabhu et al.2019).

6.2 Microstructural analysis of the A357 alloy

Figures. 6. 1 (a) and (b) show optical and SEM micrographs of A357 alloy solution treated at 540°C and aged at 180°C. Figures. 6. 1 (c) and (d) show optical and SEM micrographs of A357 alloy solution treated at 540°C and aged at 200°C, respectively. In Figures. 6.1 (a) and (b) fine globular morphology of eutectic silicon particles due to heat treatment can be observed. Similar results were reported by researchers (Akhter et al. 2007; Maube et al. 2014). Heat treatment results in the transformation of fibrous shape eutectic Si into fine spheroidized Si particles uniformly distributed in the A357 matrix. Heat treatment also dissolves Mg₂Si particles, resulting in structural homogenization, and alters the shape of eutectic Si particles. Upon heat treatment necking can be seen in Si particles. With further increase in temperature from 160-180°C, particle fragmentation and spherodization takes place (Figures. 6.1 (a) and (b)) (Apelian et al.1989; Shivkumar et al.1990). Further, from Figures. 6.1 (c) and (d) it can be observed that the Si particles are smaller and more uniformly distributed. The fragmentation of Si particles reduces particle size and increases particle number, which in turn leads to the strengthening of the alloy. As the aging temperature is increased from 180°C to 200°C, coarsening of Si particles can be observed (Figures. 6.1 (c) and (d)).

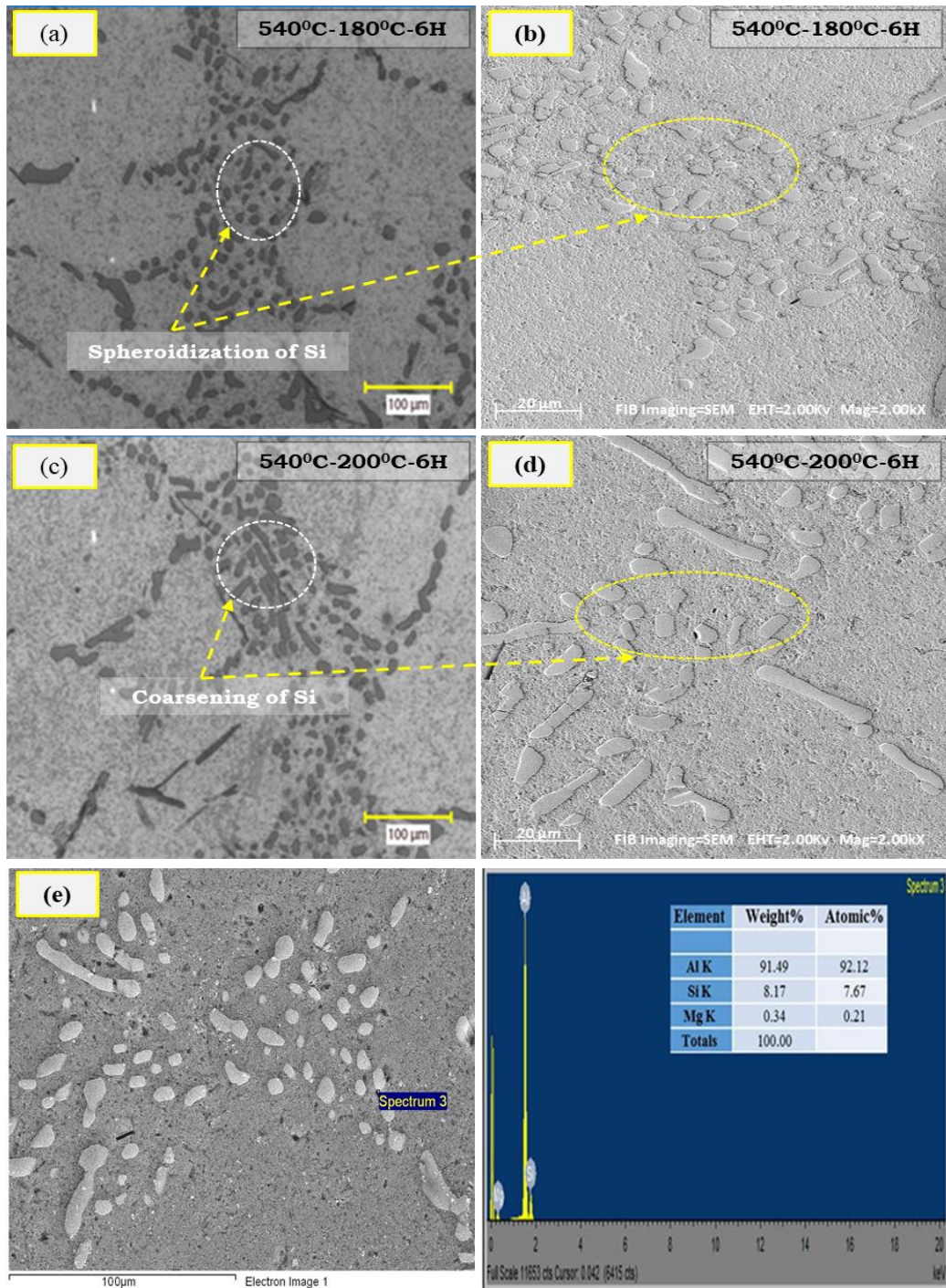


Figure 6.1: (a) and (b) shows optical and scanning electron micrographs of A357 alloy aged at 180°C. (c) and (d) shows optical and scanning electron micrograph of A357 alloy aged at 200°C. (e) EDS spectrum of A357 alloy taken on Al-Si interface at 180°C.

Figure 6.1 (e) shows the SEM micrograph with EDAX spectrum of A357 alloy solution treated at 540°C and aged at 180°C. From the EDAX spectrum, traces of Mg located at the Al-Si interfaces can be found. Typically, Mg is added to the Al-Si alloy for age hardening through the precipitation of Mg₂Si precipitates. In Figure 6.1 (e), magnesium peak from the EDAX analysis confirms that Mg₂Si precipitates form as a result of heat treatment.

6.3 Microstructural analysis of the developed DPS composites

Figures 6.2 (a), (b) and (c) show the optical micrographs of heat-treated composites (DPS1, DPS2 and DPS3) that were solution treated at 540°C and aged at 180°C. In these Figures, number 1 represents fine SiC, 2 represents coarse SiC and 3 shows clustering of fine SiC. It can be observed from all the micrographs that both dual size SiC particles were found to be fairly uniformly distributed in the A357 matrix. Figure 6.2 (a) shows micrograph of DPS1 composite where the dispersion of SiC particles was found to be very good with almost no observable porosity or any casting defects. However, a small extent of clustering of small size SiC particles was observed in the case of DPS2 composite as shown in Figure 6.2 (b). Here, most of the SiC particles seen in the microstructure are of large size, which is due to the high content of large size particles when compared to small size particles. On the other hand, the dispersion of particles in DPS3 composite was reasonably uniform, as shown in Figure 6.2 (c). Small-scale cluster formation of small size SiC particles were seen at few spots closer to large size SiC particles in DPS3 composite. High shear rate generated during melt-stirring process pushes small size particles at a faster rate when compared to large particles. However, the movement of small particles is restricted by large particles due to which they get settled near the large particles, and same is seen in Figure 6.2 (c). Overall, dispersion of dual particle size SiC was found to be reasonably uniform in all the composite systems, and hardly any casting defects such as porosity was seen on the surface. The addition of SiC as reinforcement enhances aging kinetics, phase transformation reaction and it also acts as seeding for precipitation during the heat treatment process, which further leads to alloy strengthening (Cottu et al. 1992; Yamanoglu et al. 2013; Myriounis et al. 2008).

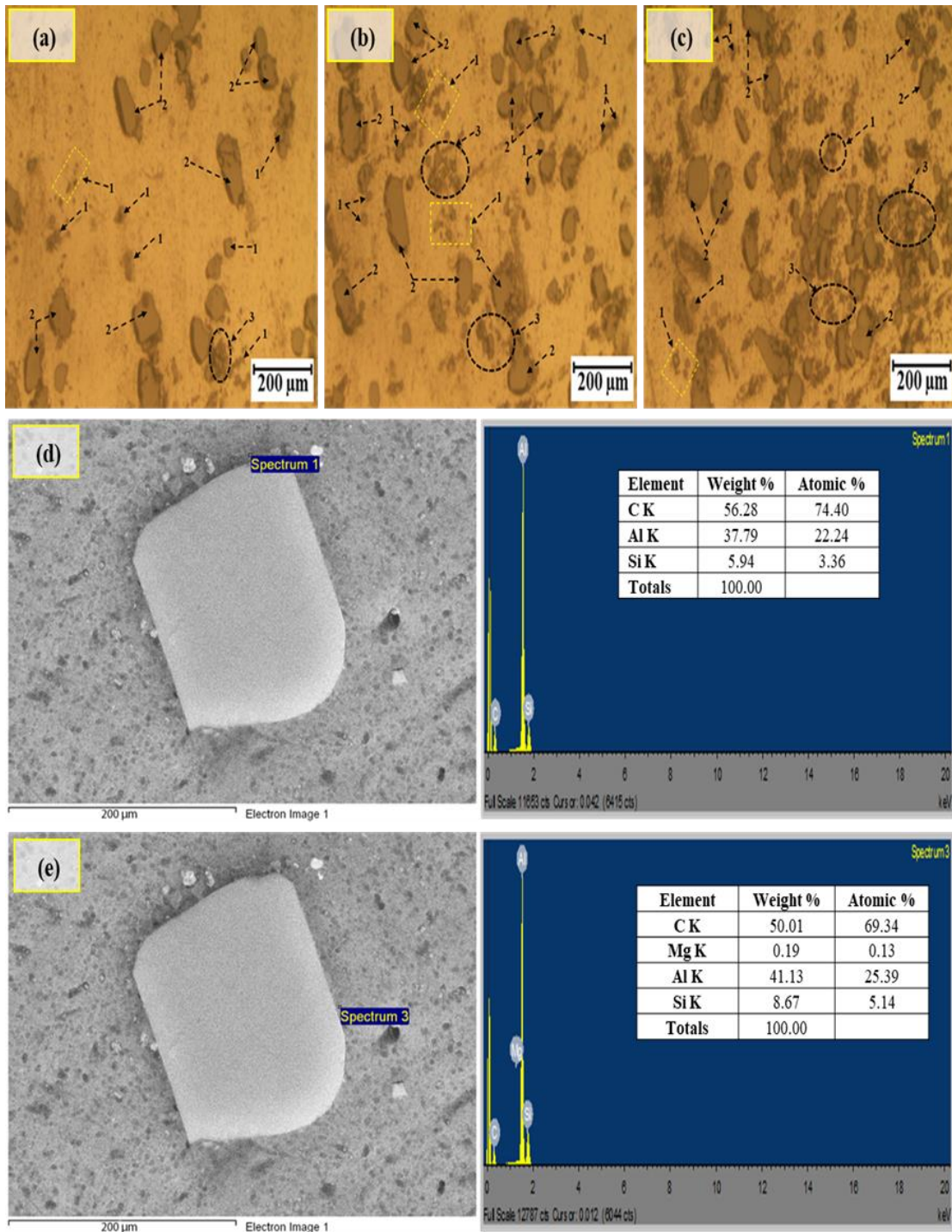


Figure 6.2: Optical Micrographs of (a) DPS1 composite, (b) DPS2 composite, (c) DPS3 composite, all aged at 180°C, (d) EDS spectrum taken on DPS2 composite particle, and (e) EDS spectrum at Al/SiC interface.

These dual sizes SiC particles influence the strengthening of matrix material in a significant way during the heat treatment process (Myriounis et al. 2008; Christmas and Suresh, 1988; Manoharan and Lewandowski, 1989, Karuppusamy et al. 2019).

Figure. 6.2 (d) shows the EDAX analysis of composite particle in DPS2 composite. From the figure, Si and C peaks can be observed. Si, C peaks confirm the presence of SiC particles in the A357 matrix. Figure. 6.2 (e) shows EDAX analysis at the Al/SiC interface. The interface shows the presence of Mg peak along with Al, Si and C peaks. The presence of four elements Al, Mg, Si, and C confirms the presence of Mg₂Si at the Al-SiC interface.

6.4 TEM analysis of A357 alloy and the developed DPS composite

Figures. 6.3 (a), (b), (c), (d), and (e) show the bright-field TEM images of A357 alloy and the developed DPS composites, that were aged at 180°C for about 6 hours. In these figures, number 1 represent needle shaped β" phase. Precipitation is a very important aspect of age hardening which directly influences the mechanical properties of a material. TEM image of A357 alloy as shown in Figure. 6.3 (a) shows the presence of very fine sized precipitates consisting of Mg and Si atoms. These fine sized precipitates which are spherical in shape correspond to β-Mg₂Si with diameter in the range of 20-40 nm. Apart from these precipitates, few needles corresponding to β" phase were also observed in the A357 alloy. In case of DPS1 and DPS2 composites, along with the β-Mg₂Si precipitates, needles of β" phase were also observed as shown in Figures. 6.3 (b) and (c). Compared to A357 alloy, needle shaped β" phase was comparatively high in the case of these composites. Most of these fine needles had length in the range of 30-100 nm and a diameter of about ~5 nm in the peak-aged, heat-treated conditions. Due to high silicon content in the matrix, quenching gives rise to higher content of supersaturated Si which favors the formation of β" phase (Sjolander and Seifeddine, 2010). Further a high magnification TEM micrograph of DPS3 composite as shown in Figure. 6.3 (d) showed uniform dispersion of β-Mg₂Si precipitates in the entire α-Al matrix.

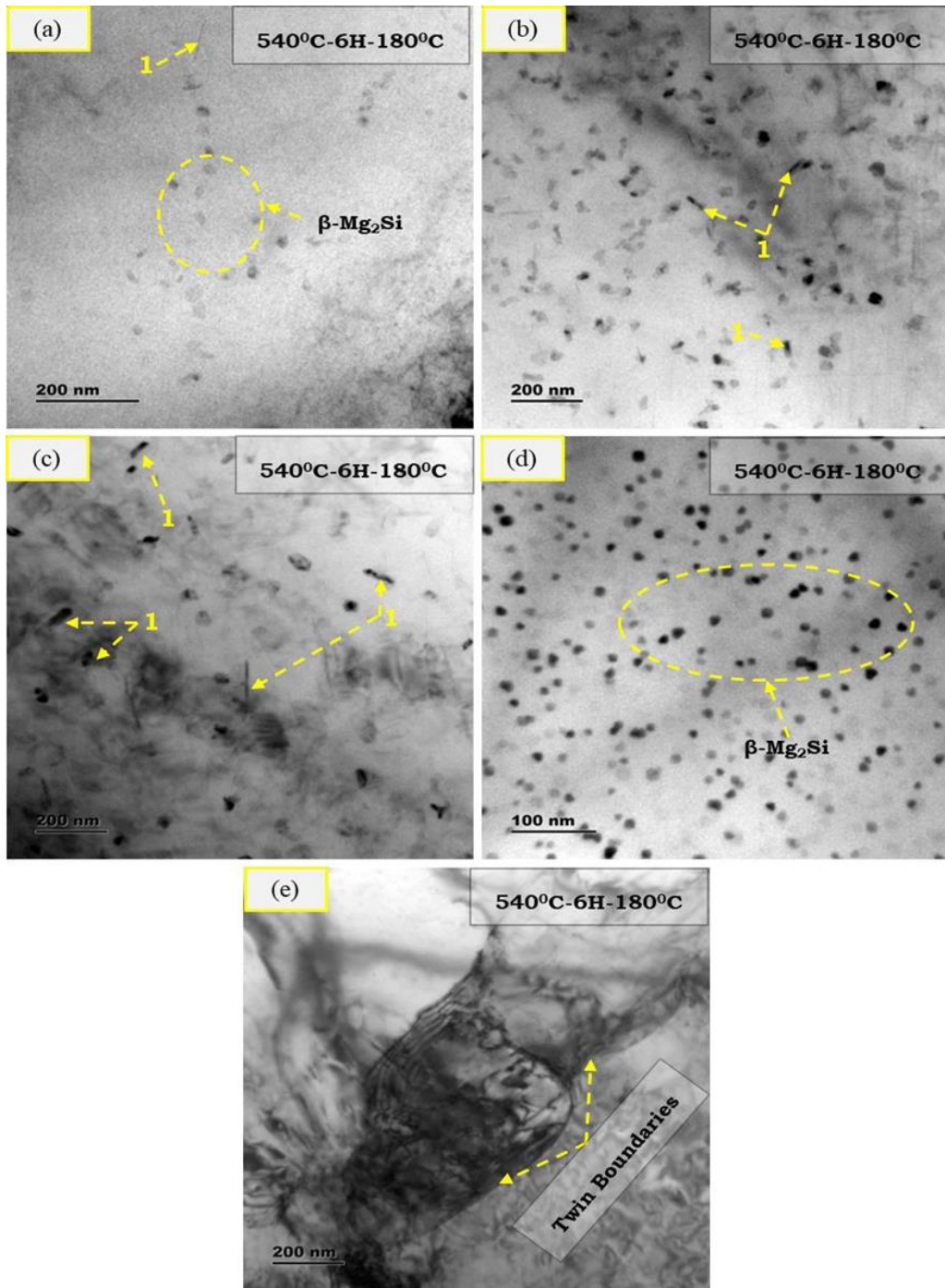
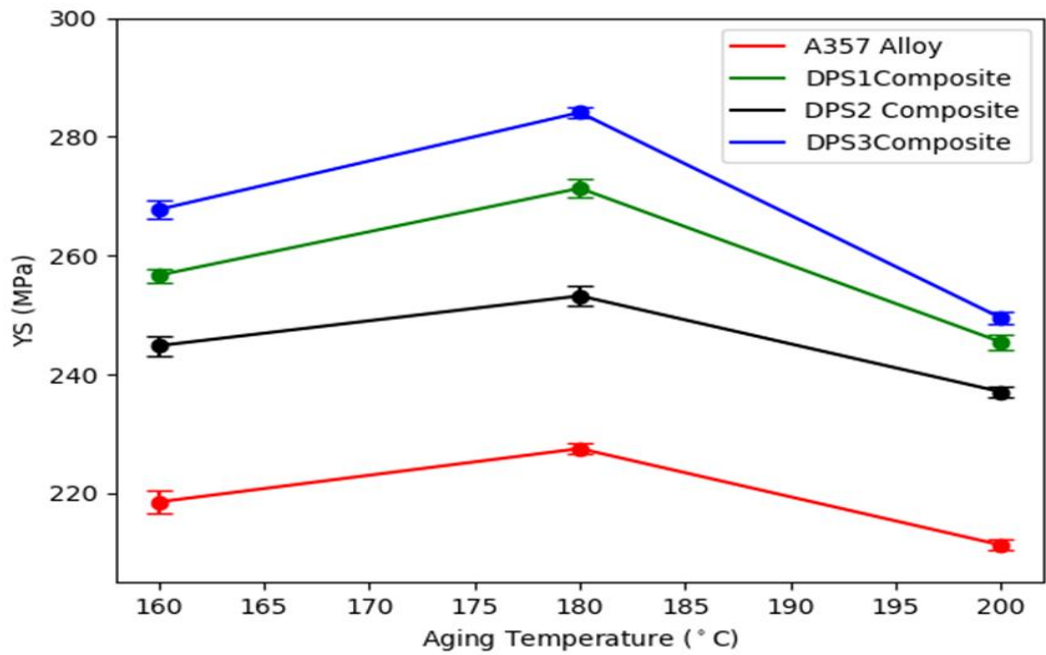


Figure 6.3: Bright-field TEM images of (a) A357 alloy, (b) DPS1 composite, (c) DPS2 composite, (d) DPS3 composite, and (e) Modified Si particles with twins in DPS2 composite after heat treatment at aging temperature of 180°C.

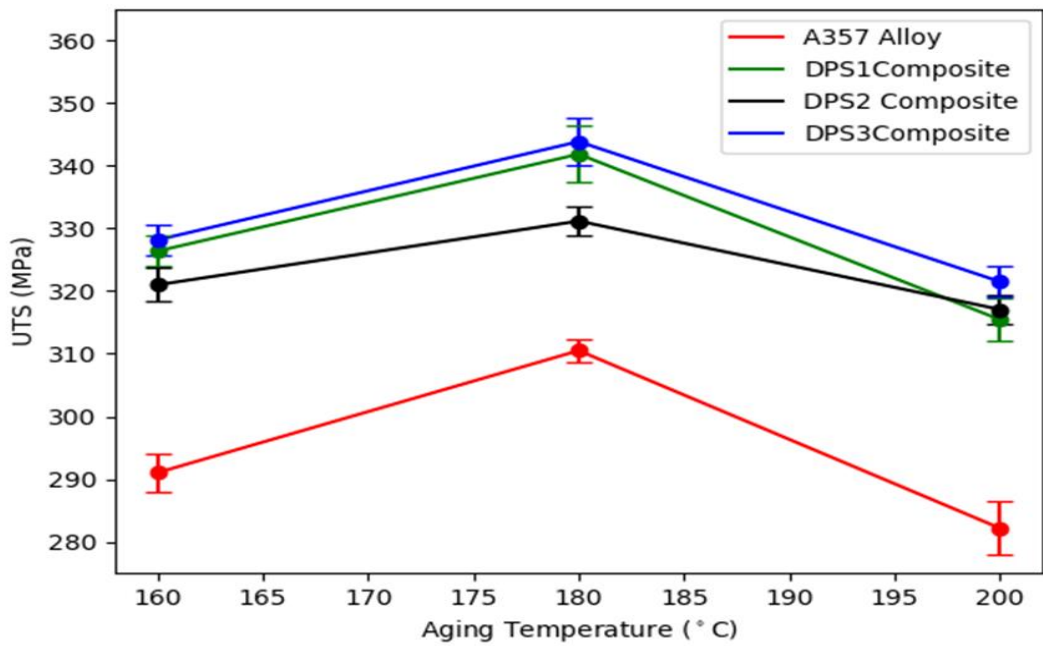
Also, presence of high silicon content in A357 matrix requires the above stoichiometric formation of β -Mg₂Si. This will not only favor the nucleation of these precipitates but also strength of both A357 alloy and DPS composites. However, it is interesting to note that in both A357 alloy and the developed DPS composites, no β' phase was observed which otherwise is considered to be nucleation site for β'' phase (Li et al. 2015; Liu et al. 2018). Figure. 6.3 (e) shows a small crystal of silicon particle whose edges are more rounded indicating spheroidization. Dark contrast structures resembling twin boundaries and dislocation networks are also seen inside the silicon particle. The morphological changes from irregular to nearly round shape and also decrease in size from coarse to small are mainly due to solution treatment. In addition to this, the formation of β' precipitates generates stresses in the matrix, which is compensated by the modification in silicon particle morphology. (Wang et al. 2015).

6.5 Tensile strength

Figures. 6.4 (a) and (b) show the variation of tensile strength (yield & ultimate) of A357 alloy and the developed DPS composites at varying aging temperatures (160°C, 180°C, and 200°C). From Figures. 6.4 (a) and (b) it can be observed that the addition of particulate reinforcement enhances the tensile strength of the DPS composites (Arsenault and Everett, 1991; Ganesh and Chawla, 2005). Although all DPS composites subjected to heat treatment exhibited nearly same tensile strength (yield & ultimate) values, the DPS3 composite exhibited slightly better strength properties at all three aging conditions followed by DPS1 and DPS2 composites. Strengthening effect in composites can be attributed to number of particles present in a composite. Even though, the weight fraction of SiC is same for all composites, number of particles are highest in DPS3 composite because of the higher concentration of smaller particles. After DPS3 composite, the next higher concentration of smaller particles are present in DPS1 composite. The least number of smaller particles are present in DPS2 composite. SiC particles act as dislocation pinning sites and hence can improve strength. Possible grain refinement due to SiC particles and effective load transfer from matrix to composite particles are also expected to play a role in the increase of the strength of composites.



(a)



(b)

Figure 6.4: (a) Yield and (b) Ultimate tensile strengths of A357 alloy and the developed DPS composites at different aging temperatures.

So, the strengthening of composites is a result of synergistic effect of grain refinement, precipitation hardening, Orowan looping and efficient load transfer

(Mirjavadi et al. 2017; Cai et al. 2018; Bembalge and Panigrahi, 2018; Umaru et al. 2016; Zhu et al. 2001; Ramprabhu, 2017). Further, from Figures. 6.4 (a) and (b), it can be observed that the strength values increase with increase in aging temperature from 160°C to 180°C but tend to drop as the temperature is further increased to 200°C, i.e., highest strength values are observed at 180°C aging temperature. Upon aging, increase in strength properties are due to precipitation of coherent β -Mg₂Si particles. Upon over aging i.e., at 200°C, loss in coherence leads to a loss in strength.

Figure. 6.5 shows the variation of percentage elongation of A357 alloy and the developed DPS composites at varying aging temperatures. From Figure. 6.5, it can be seen that the DPS composites exhibit lower ductility (% elongation) when compared to the A357 alloy at all aging temperatures. Presence of SiC particles could be attributed to reduction in ductility because they can act as nucleation sites for cracks and thus hasten failure. The mechanism of fracture appears to be changing from alloy to composites.

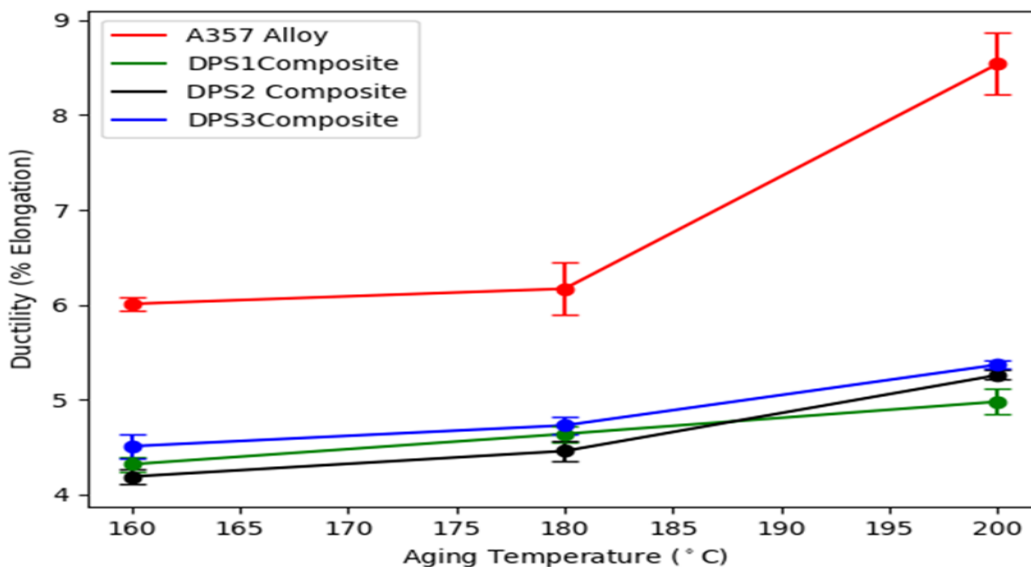


Figure 6.5: Percent elongation (%) of A357 alloy and the developed DPS composites at varying aging temperatures.

Also, from Figure. 6.5, it can be observed that as the aging temperature increases ductility increases substantially for A357 alloy whereas it increases marginally for

composites. Increase in ductility in A357 alloy with increase in aging temperature could be attributed to change in fracture mechanism from interdendritic to intradendritic upon over aging (Figures. 6.6 (a), (b) and (c)). Whereas for composites, aging temperature has little effect. This is because fracture is due to particle pull out irrespective of aging temperature (Figures. 6.6. (d), (e), (f), (g), (h), (i), (j), (k) and (l)). Analogous trends have been reported in literature (Wang et al. 2015).

6.6 Tensile fracture surface analysis

Figures. 6.6 (a) – (l) show the tensile fracture surfaces of A357 alloy and the developed DPS composites after the tensile test at varying aging temperatures of 160°C, 180°C, and 200°C. The fracture surface of A357 alloy at 160°C aging temperature (Figure. 6.6 (a)) showed a significant amount of dendritic shrinkage porosity. For the cases of 180°C, and 200°C, aging temperatures large numbers of dendrite fractured regions were observed in the fractographs of A357 alloy (Figure. 6.6 (b) and (c)). This confirms inter-dendritic cracking as the main fracture mechanism as these dendrite globules promote micro-crack propagation during the loading (Chen et al. 2014).

On the other hand, all DPS composites (DPS1, DPS2, and DPS3) at all the three aging temperatures, i.e., 160°C for 6h, 180°C for 6h, and 200°C for 6h, showed nearly identical fracture surfaces. For instance, the DPS1 composite aged at 160°C showed eutectic silicon particle cracking (Figure. 6.6 (d)). Also, DPS2 and DPS3 composites aged at 160 °C showed particle pull out and ductile failure, as shown in Figures. 6.6 (g) and (j) respectively. In case of 180°C and 200°C aging temperatures, the fracture surfaces of DPS composites consisted of a large number of dimples indicating ductile failure by void nucleation and coalescence mechanisms. The void nucleation takes place at Al matrix/SiC interface. When stress is applied, the plastic deformation starts by dislocation movement.

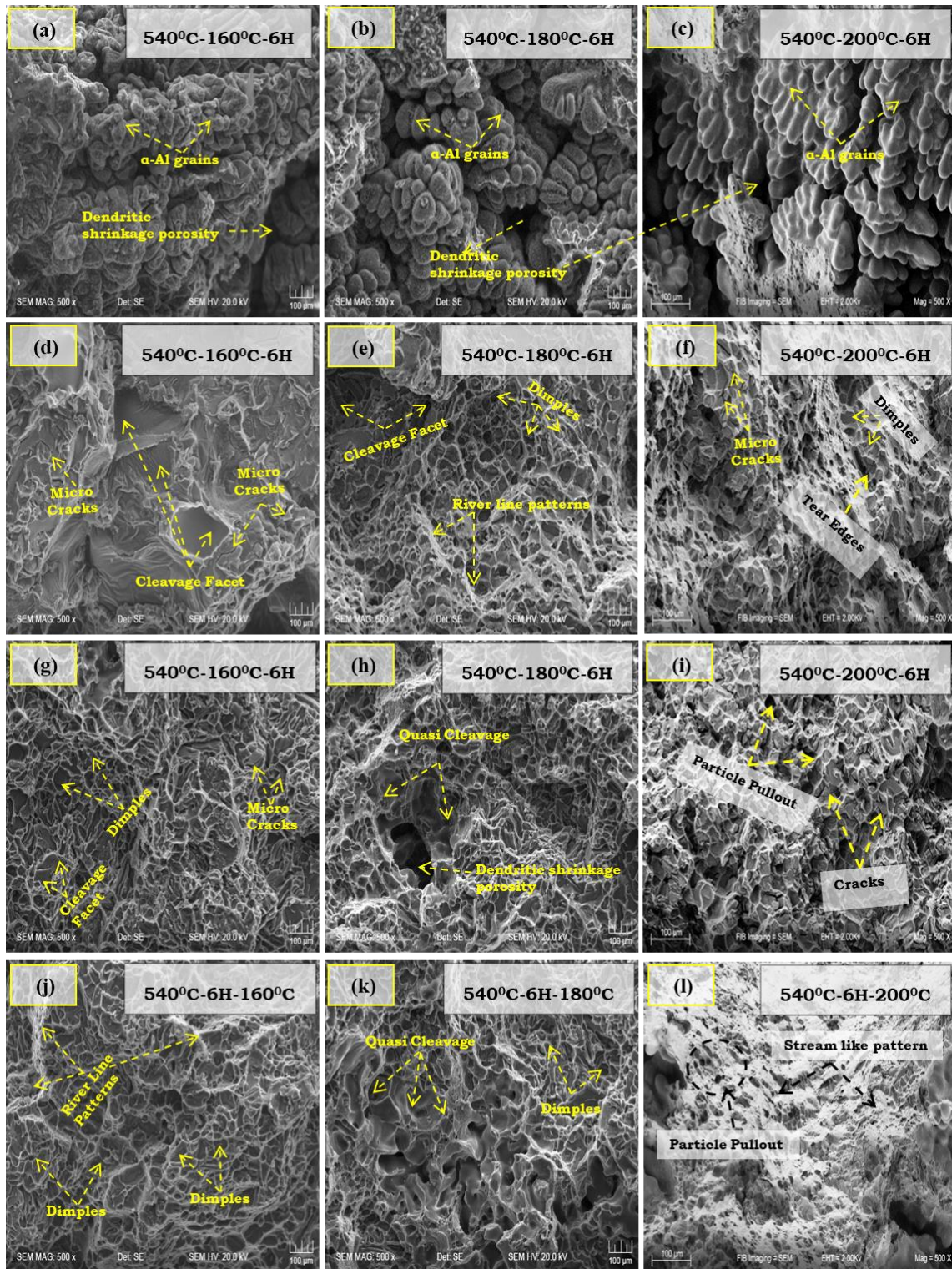


Figure 6.6 : Fractographs of (a), (b), and (c) A357 alloy, (d), (e), and (f) DPS1 composite, (g), (h), and (i) DPS2 composite, (j), (k), and (l) DPS3 composite, aged at 160 °C, 180 °C, and 200 °C respectively.

These dislocations are blocked by the Al matrix/SiC interfaces resulting in dislocation accumulation. This results in stress build up around the interface resulting in much higher stress than the applied stress. When the stress is sufficient to crack the interface, micro voids preferably nucleate at the interface due to strong stress gradient. Due to the creation of micro-voids, the crack initiates at the micro voids and propagates around the SiC particles. Eventually, the particles are pulled out of the A357 matrix leaving behind nearly circular shaped voids. These voids connect with each other through crack propagation and finally lead to fracture forming a dimpled fractured surface as seen in Figures. 6.6 (e), (f), (h), (i), (k), and (l).

6.7 Hardness results

Figure. 6.7 shows the variation of hardness of A357 alloy and the developed DPS composites at varying aging temperatures (160°C, 180°C, and 200°C). From Figure 6.7, it can be seen that the DPS composites show an increase in hardness when compared to A357 alloy at varying aging temperatures. Higher hardness of composites can be attributed to the presence of hard SiC particles.

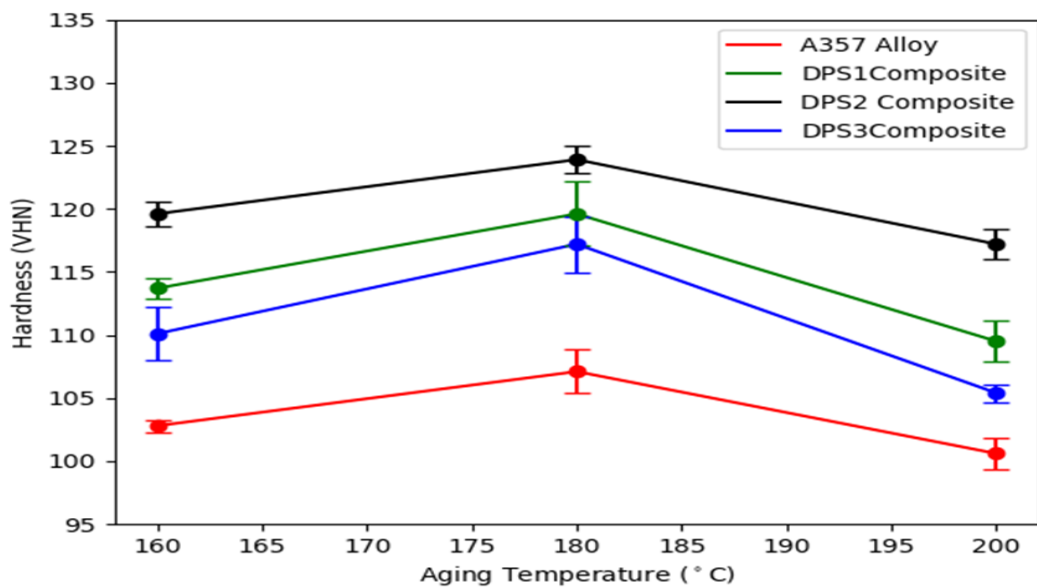


Figure 6.7: Hardness results of A357 alloy and the developed DPS composites at varying aging temperatures.

Among the composites, DPS2 composite exhibited highest hardness while the DPS3 composite exhibited the lowest hardness at all three aging temperatures. This trend in hardness among composites can be rationalized based on weight fraction of large SiC particles. Small size particles offer less resistance to deformation when compared to large size particles and this leads to lower hardness (Avinash et al. 2016; Lakshmikanthan et al. 2019). High hardness of DPS2 composite is due to the presence of maximum weight fraction of large sized particles. Similarly, lowest hardness values exhibited by DPS3 composite is due to the presence of minimum weight fraction of large sized particles.

From Figure. 6.7, it can be observed that the hardness values increase with aging temperature till 180°C and reduces beyond 180°C i.e., maximum hardness values are observed at an aging temperature of 180°C. The increase in hardness after heat treatment can be attributed to formation of hard Mg₂Si phase due precipitation hardening (Sharma et al. 2012). From the peak hardness variation with different aging temperatures, it was found that the composite is under aged at 160°C and overaged at 200°C. Analogous trends were reported in literature (Yamanoglu et al. 2013; Myriounis et al. 2008; Ravikumar et al.2018).

6.8 Specific wear rate

Figure. 6.8 shows the plot of specific wear rate (at 30 N) v/s aging temperature of A357 alloy and the developed DPS composites. From Figure. 6.8, it can be observed that A357 alloy exhibited the highest wear rate. The reasons for high wear rate of A357 alloy can be attributed to: extensive sub surface deformation, high adhesive metal-metal contact assisted surface shear strain, the increased contact area of matrix to counter surface, and the absence of load bearing particles (Avinash et al. 2016; Lakshmikanthan et al. 2019; Ramprabhu , 2016).

From Figure. 6.8, it can also be observed that DPS composites exhibit lower wear rate when compared to A357 alloy. This can be attributed to the presence of hard SiC particles in DPS composites. SiC particles are hard and hence they can resist abrasion.

Moreover, they also reduce contact between counter surface and soft matrix and share some load. Reduced contact between counter surface and matrix and load sharing leads to lower wear rate (Rao et al.2009; Rajeev et al. 2010). Among the composites, the DPS2 composite exhibits least wear rate when compared to DPS1 and DPS3 composites at all aging temperatures. Good wear resistance (least wear rate) of DPS2 composite is mainly due to presence of high weight percent of large size SiC particles which bear most of the applied pressure when compared to that of small size SiC particles and A357 matrix. Further, large sized SiC particle protect the fine size SiC particles from gouging out of the matrix thereby allowing them to provide protection against weight loss for a longer time (Bindumadhavan et al. 2001; Chung and Hwang, 1994; Chawla , 2006; Song et al. 1995).

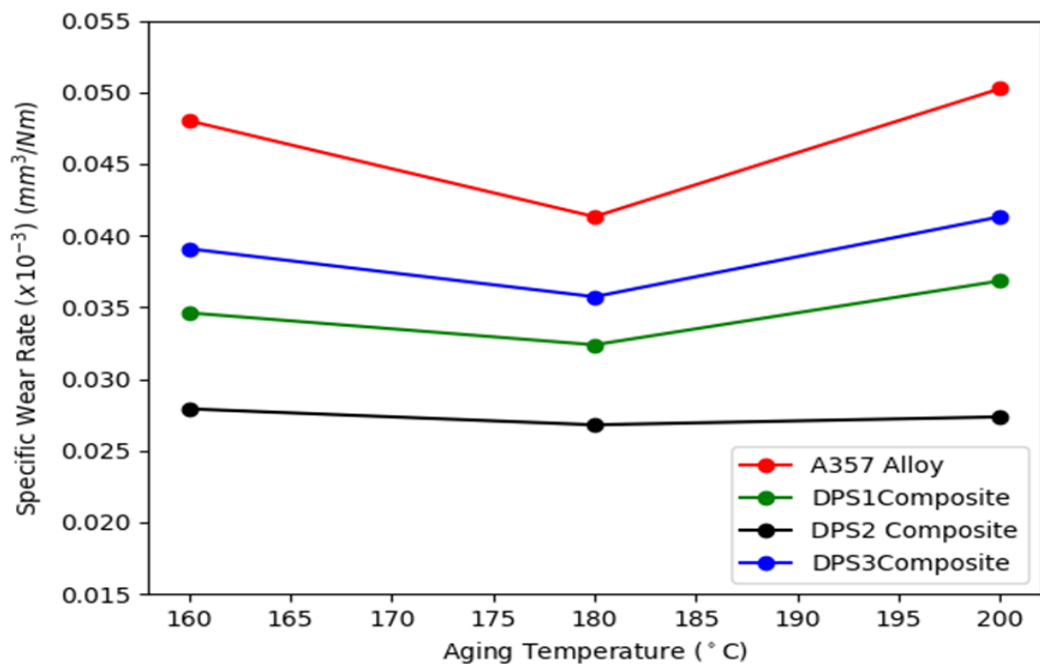


Figure 6.8: Effect of aging temperature on wear rate of A357 alloy and the developed DPS composites.

From Figure. 6.8, it can be observed that both A357 alloy and the developed DPS composites show decrease in wear rate with aging temperature till 180°C but beyond this temperature wear rate increases. The specimens aged at 180°C show better wear resistance compared to the specimens aged at 160°C and 200°C and it may be due to

the presence β'' and β - Mg_2Si precipitates (Pedersen and Arnnberg, 2001; Gaun et al. 2016). Thus, the specimens aged at $180^\circ C$ can be considered as peak aged, while the specimens which are aged at $160^\circ C$ are considered as under aged and the specimens which are aged at $200^\circ C$ are considered as over aged. Similar results were reported in literature (Ravikumar et al. 2018; Chacko and Nayak, 2014).

6.9 Worn surface analysis

Figures. 6.9 (a) – (l) show the SEM micrographs of worn surfaces of both A357 alloy and the developed DPS composites at varying aging temperatures of $160^\circ C$, $180^\circ C$, and $200^\circ C$, at a load of 30N, sliding velocity of 2.5 m/sec and sliding distance of 1500 m. In these figures, the number 1 represents a delaminated wear-out area, 2 represents abrasion, 3 represents thin ploughed trenches, 4 represents deep ploughed trenches, 5 represents craters, and 6 represents sliding direction, respectively. Worn surface of A357 alloy at different aging temperatures ($160^\circ C$, $180^\circ C$ and $200^\circ C$) is shown in Figures. 6.9 (a), (b) and (c). From these figures, it can be observed that wear mechanism changes with temperature. The A357 alloy aged at $160^\circ C$ showed large, delaminated areas along with abrasive grooves running along the sliding direction (see Figure. 6.9 (a)). Some of the delaminated areas were almost few hundred microns in size. At peak aging temperature of $180^\circ C$, wear is predominantly caused by the surface delamination. When temperature is increased to $200^\circ C$, instead of surface delamination, deep grooves are observed which is an indication of plastic deformation. So, at high temperatures, wear mechanism changes from surface delamination to intense plastic deformation and material removal. Both the worn surfaces show wide and parallel grooves running in sliding direction with large cavities in between them. The formation of cavities can be attributed to delamination of the surface material of the alloy. At a high load of 30 N, the softening of surface takes place due to frictional resistance as a result of surface material of the alloy getting welded to the counterface surface. Due to the increase in adhesive nature of pin and alloy, delamination occurs easily. It appears that the extent of delamination is higher in the case of $200^\circ C$ aged alloy. This may be due to its low hardness at $200^\circ C$ when compared to that at $160^\circ C$ and $180^\circ C$ aging conditions.

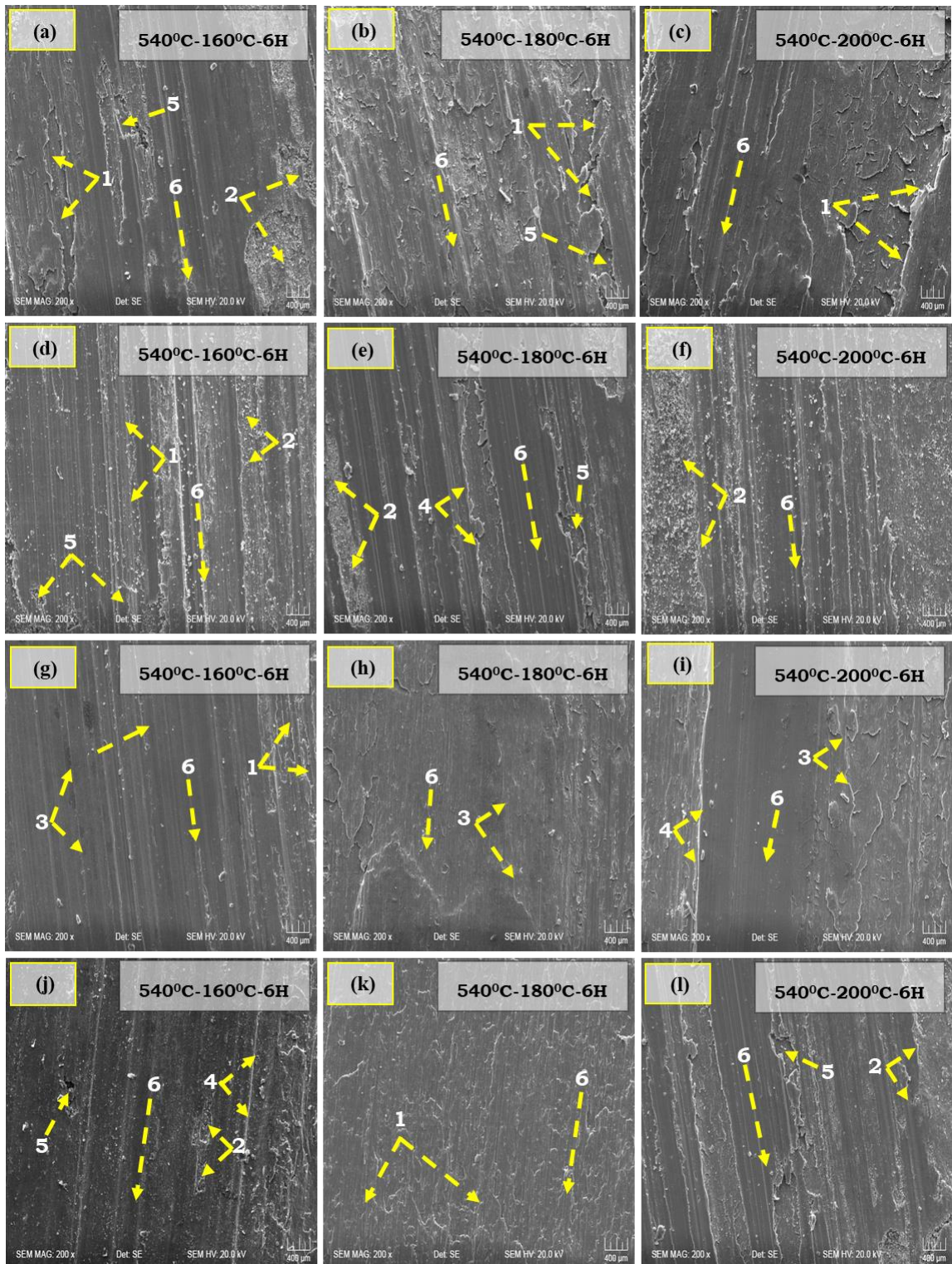


Figure 6.9: Wear tracks of (a), (b), and (c) A357 alloy, (d), (e), and (f) DPS1 composite, (g), (h), and (i) DPS2 composite, (j), (k), and (l) DPS3 composite, aged at 160 °C, 180 °C, and 200 °C, respectively.

The extent of delamination appears to be less in DPS1 composite compared to that of the alloy as seen in Figures. 6.9 (d), (e) and (f). The DPS1 composite aged at 160°C showed abrasives grooves of large width running along the sliding direction (Figure. 6.9 (d)). Hard SiC particles in DPS1 composite protrude out of composite surface during wear testing process and prevent direct contact between composite surface and counterface surface. Due to this, the extent of delamination is decreased.

The worn surface of DPS2 composite had a relatively smooth surface with fine abrasive groove marks. The width of abrasive grooves was quite small for all three aging temperatures (160 °C, 180 °C, and 200 °C), as shown in Figures. 6.9 (g) (h) and (i). This is mainly due to the presence of a higher weight fraction of large size SiC particles, which tend to take most of the applied load and protect small-sized SiC particles as well as the matrix (Rajmohan et al. .2013; Singh and Chauhan, 2016). These large particles avoid direct contact between the counterface surface and composite surface which is why the groove width is smaller when compared to that of A357 alloy and other two composites. On the other hand, the worn surface of DPS3 composite was almost similar to that of the DPS1 composite. Deformation grooves and delamination were the primary reasons for weight loss in this composite. The worn surface of DPS3 composite is nearly smooth with minimal abrasive grooves at all three aging temperatures of 160°C, 180°C, and 200°C respectively as shown in Figures. 6.9 (j), (k) and (l). The worn surface of DPS3 composite aged at 160°C, showed a relatively smooth surface with considerable amount of delamination. These figures show changes in the deformation mechanism from abrasion at 160°C to delamination at 180°C, to deformation at 200°C aging temperature.

6.10 Three-dimensional surface topographies of worn surfaces

Figures. 6.10 (a) – (h) show the three-dimensional surface topographies of worn surfaces of both A357 alloy and the developed DPS composites at varying aging temperatures of 180°C and 200°C, at a load of 30 N, sliding velocity of 2.5 m/sec and sliding distance of 1500 m.

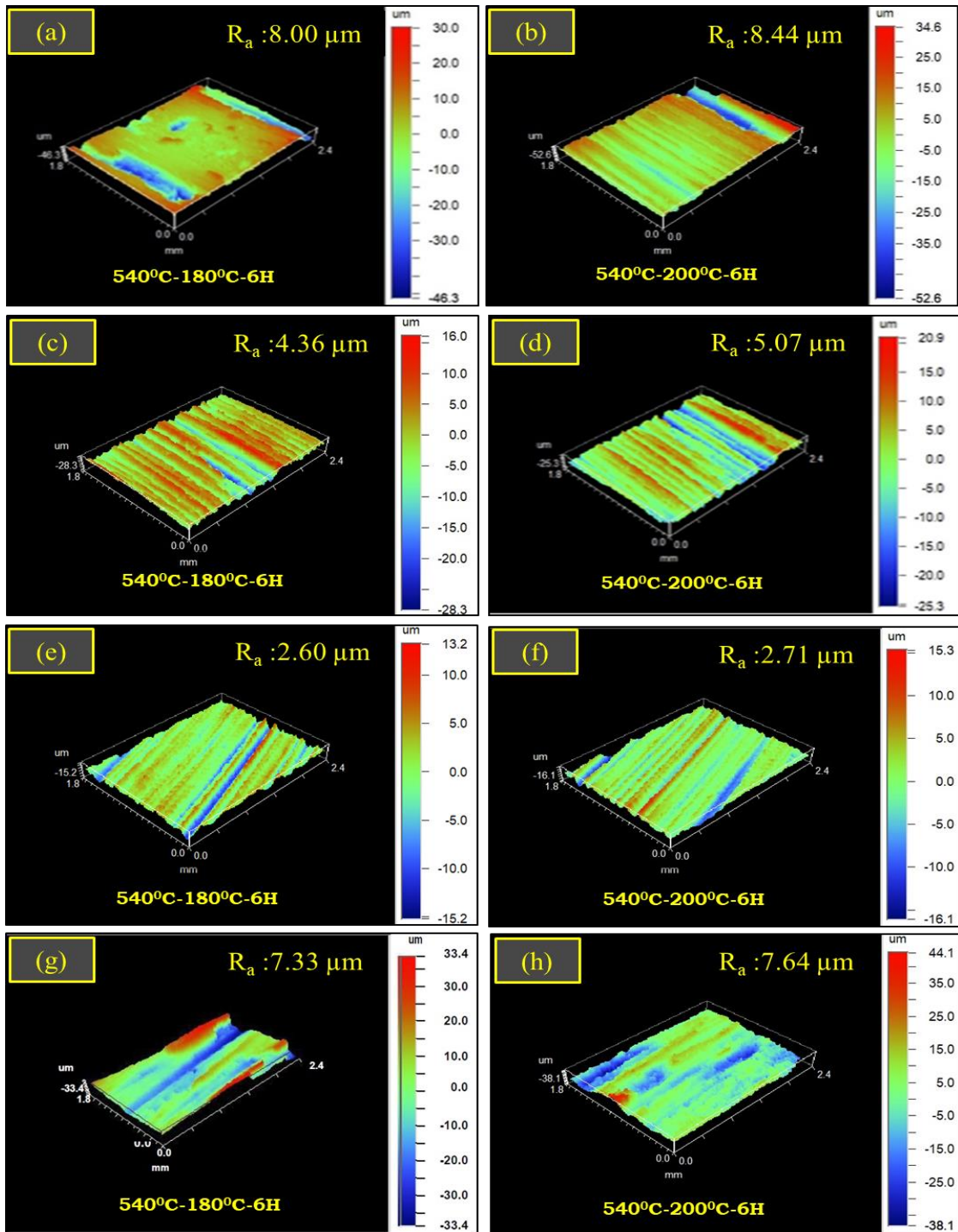


Figure 6.10: Three-dimensional surface topographies of worn surfaces of (a) and (b) A357 alloy, (c) and (d) DPS1 composite, (e) and (f) DPS2 composite, (g) and (h) DPS3 composite, aged at 180°C and 200°C, respectively.

In case of A357 alloy, it can be seen from Figures. 6.10 (a) and (b) that the surface showed features of surface delamination and formation of deep grooves supporting the evidence obtained using SEM (Figures. 6.9 (b) and (c)). The R_a values measured for the A357 alloy at 180°C and 200°C aging temperatures are 8.00 μm and 8.44 μm , respectively. On the other hand, lowest R_a values were measured for the DPS2 composite at 180°C (2.60 μm) and 200°C (2.71 μm) respectively. These observations are well in line with the low specific wear rate recorded for this composite.

Further, compared to A357 alloy and other DPS composites the undulations observed on the worn surface of DPS2 composite are significantly less (see Figures. 6.10 (e) and (f)). Also, compared to A357 alloy, the DPS composites showed lower R_a values which is attributed to the resistance offered by dual size SiC particles. The asperities of counterface surface are prevented from penetrating inside the matrix by the SiC particles due to which the surface roughness values are quite lower for DPS composites. The depth of valleys and width of grooves were found to be higher for A357 alloy compared to that of DPS composites. This is mainly because of higher hardness exhibited by DPS composites when compared to A357 alloy. Overall, these results are well in line with preceding sub-sections (6.1.8 and 6.1.9). Further, compared to the DPS composites, A357 alloy exhibited higher R_a values due to higher wear rate. Also, the surface topographies of the developed DPS composites showed no abnormal depth in the worn surface indicating absence of SiC particle pull-out.

6.11 Wear debris analysis

Figures. 6.11 (a) – (l) show the wear debris of worn surfaces of both A357 alloy and the developed DPS composites at varying aging temperatures of 160°C, 180°C, and 200°C, and at a load of 30 N, sliding velocity of 2.5 m/sec and sliding distance of 1500 m. In these figures, number 1 represents fleck-like debris, 2 fiber-like debris, 3 represents ruptured debris, 4 represents ribbed debris, and 5 represents coil-like debris, respectively. In the case of A357 alloy, the size of wear debris collected for 160°C aging temperature showed large debris having a size of several hundred microns (~500 μm), (Figure. 6.11(a)). The size of wear debris of A357 alloy collected

for 180°C aging temperature condition was smaller (~300 µm) than that collected for 200°C aging temperature condition (~600 µm) which are shown in Figures. 6.11 (b) and (c).

In the case of DPS1 composite, the size of wear debris showed similar trend as that of A357 alloy. Wear debris size of ~150 µm, ~100 µm, and ~180 µm were recorded for the DPS1 composite aged at 160°C, 180°C and 200°C respectively as shown in Figures. 6.11 (d) (e) and (f). On the other hand, the wear debris of the DPS2 composite (Figures. 6.11 (g), (h) and (i)) have sizes approximately ~80 µm, ~50 µm and 100 µm when aged at 160°C, 180°C and 200°C, respectively. The wear debris size of DPS2 composite is very small compared to that of A357 alloy and other two DPS composites. Most of the debris had irregular flake-like morphology with sharp edges indicating delamination as a primary wear mechanism. The small size of wear debris in the DPS2 composite can be attributed to the higher hardness exhibited by this composite at all three aging temperatures. Similarly, for DPS3 composite, wear debris has a size of 180 µm, 150 µm and 200 µm approximately for the samples aged at 160°C, 180°C and 200°C respectively as shown in Figures. 6.11 (j), (k) and (l). From these figures, it can be observed that the wear debris size and morphology of DPS3 composites is almost same for all three aging temperatures (Figures. 6.11 (j), (k) and (l)). Overall, it can be observed that at peak aging temperature of 180°C, both A357 alloy and the DPS composites showed smaller wear debris which is attributed to the presence of uniformly dispersed hardening phases such as β'' and β -Mg₂Si precipitates compared to the under aged (160°C) and over aged (200°C) conditions.

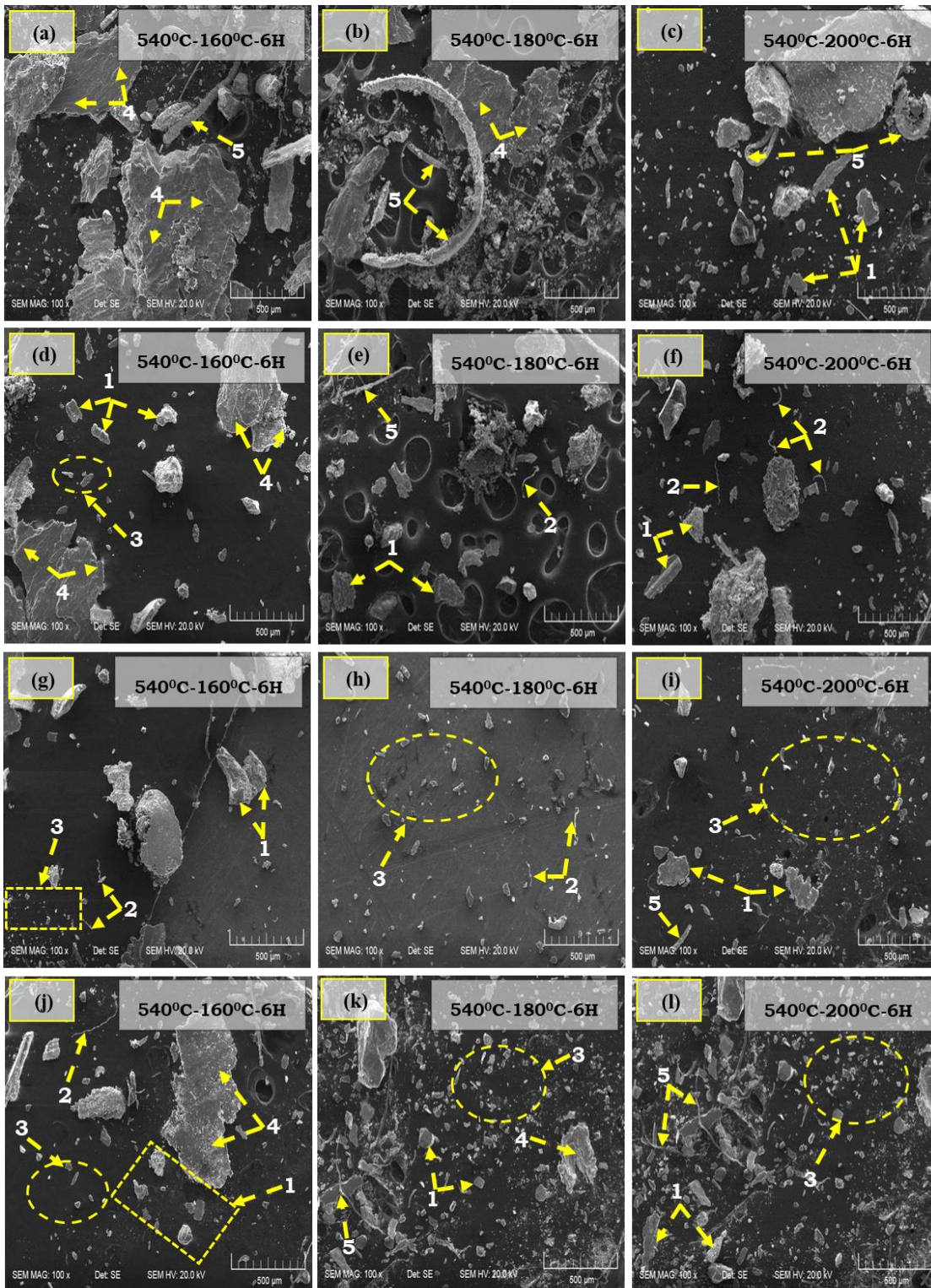


Figure 6.11: Wear debris of (a), (b) and (c) A357 alloy, (d), (e) and (f) DPS1 composite, (g), (h) and (i) DPS2 composite, (j), (k) and (l) DPS3 composite aged at 160 °C, 180 °C, and 200 °C respectively.

CHAPTER 7

CONCLUSIONS AND FUTURE WORK

7.1 Conclusions

This chapter presents the overall conclusions drawn from the various characterization studies and tests conducted on the A357 alloy and the developed DPS composites. This chapter also lists the various directions identified for future research.

This research focused on three aspects:

- 1) To understand the effect of dual particle size (DPS) SiC reinforcement on microstructure, mechanical and wear properties of A357 alloy and the developed composites.
- 2) To understand the effect of solution heat treatment on microstructure, mechanical and wear properties of A357 alloy and the developed DPS composites.
- 3) To study the effect of aging temperature on microstructure, mechanical and wear properties of A357 alloy and the developed DPS composites.

The key conclusions of each of the above aspects of the research are summarized separately below.

7.1.1 Effect of dual particle size (DPS) SiC reinforcements on microstructure, mechanical and wear properties of A357 alloy and the developed composites

- Optical microscopy analysis showed an almost uniform distribution of both fine and coarse size SiC particles in the A357 matrix with good interfacial bonding.
- The density measurements of A357 alloy and the developed DPS composites, revealed that the distribution of SiC particles in the A357 matrix was good with almost no observable porosity and casting defects.
- The hardness studies showed that all the developed DPS composites exhibited higher hardness than that of A357 alloy. Among the composites, the DPS 2 composite (4 wt. % of coarse SiC and 2 wt. % of fine SiC) (DPS2) exhibits the highest hardness. This is because of the higher probability for indentation to occur on large hard and stiff particles which are higher by weight fraction in DPS2 composite. Hence DPS2 composite exhibits highest hardness among the DPS composites.
- The yield and tensile strength of all composites were higher than that of the A357 alloy. Among the DPS composites, the DPS 3 composite (2 wt. % of coarse SiC and 4 wt. % of fine SiC) exhibited higher strength. Grain refinement and dislocation strengthening effects by the fine size SiC particles and load bearing effect from the coarse size SiC particles are responsible for the higher strength exhibited by the DPS3 composite.
- The wear resistance of all the developed DPS composites was higher than that of the A357 alloy. Effective load transfer from matrix to reinforcement particles and strengthening by dislocation generation and grain refinement are reasons attributed for the higher wear resistance of the DPS composites.
- Among the different dual particle size combinations, the DPS 2 composite (4 wt. % of coarse SiC and 2 wt. % of fine SiC) is found to show superior

wear resistance properties. This indicates that a combination of higher fraction of coarse size particles with a lower fraction of fine size particles is the optimum combination to derive the best of both coarse and fine sizes SiC particle effects.

- Overall, it can be concluded that small sized particles are good for strength properties while large sized particles are good for hardness and wear properties. Good hardness and wear properties are mainly due to large sized particles taking the load and hence composites with higher ratio of large size particles are good for wear properties. Whereas strength and ductility are mainly the result of dislocation pinning and bowing which are good when particle size is smaller. Hence smaller particles are good for strength properties.

7.1.2 Effect of solutionizing temperature on microstructure, mechanical and wear properties of A357 alloy and the developed DPS composites

- Microstructural analysis showed modification in silicon morphology from plate shape to ellipsoidal shape as the solution temperature increased from 500°C to 540°C. Further, the developed DPS composites showed fairly uniform dispersion of both size (coarse and fine size) SiC particles with good interfacial bonding with the A357 matrix.
- From the density measurements of A357 alloy and the developed DPS composites at varying solutionizing temperatures, it can be seen that the difference between experimental and theoretical densities values are less than 1%. This indicates that all the materials (A357 alloy and the DPS composites) have dense microstructure with minimal porosity.

- TEM analysis showed formation of β'' and β -Mg₂Si precipitates in A357 alloy and the developed DPS composites which help in strengthening of both the A357 alloy and the developed DPS composites.
- Highest hardness, strength, and wear resistance were observed in the DPS composites at a solution temperature of 540°C. Hardness, strength, and wear resistance were found to decrease with decrease in solution temperature.
- The developed DPS composites had higher hardness than that of A357 alloy. Among the DPS composites, DPS2 composite exhibited highest hardness followed by DPS1 and DPS 3 composites at all the solutionizing temperatures.
- The strength (UTS & YS) of the DPS composites were higher than that of the A357 alloy. Among the DPS composites, the DPS3 composite exhibited higher strength, followed by DPS1 and DPS 2 composites at all the solutionizing temperatures.
- The developed DPS composites had the highest resistance to wear for all conditions when compared to that of A357 alloy. Among the DPS composites, DPS2 composite displayed the highest wear resistance followed by DPS1 and DPS3 composites at all the solutionizing temperatures.
- Higher hardness and refined eutectic silicon structure led to better wear resistance of DPS composites compared to that of A357 alloy at all the solutionizing temperatures. Overall, delamination wear was found to be the primary wear mechanism operating in both the A357 alloy and the developed DPS composites followed by abrasion wear.

7.1.3 Effect of varying aging temperature on microstructure, mechanical and wear properties of A357 alloy and the developed DPS composites

- Microscopy analysis showed fairly uniform dispersion of dual particle size SiC in the A357 matrix.
- The density measurements of A357 alloy and the developed DPS composites at varying temperatures revealed that the dispersion of SiC particles was found to be good with almost no observable porosity or any casting defects.
- TEM analysis showed the formation of β'' -semi-coherent phase and Mg_2Si precipitate (β -phase) along with SiC particles. These phases lead to the improvement in mechanical & wear properties of both A357 alloy and the developed DPS composites.
- All the developed composites (DPS1, DPS2 and DPS3) showed improvement in hardness, strength (YS and UTS) and wear resistance when compared to A357 alloy.
- Overall, it can be concluded that for the same total weight percentage of SiC reinforcement, ratio of large to small particles influences mechanical and wear properties. Higher proportion of smaller particles improve strength and ductility whereas, higher proportion of larger particles improve hardness and wear properties.

7.2 Future work

The work carried out in the present research has led to certain inferences that have been documented in this chapter. The following areas have been identified as directions for future research:

- Detailed studies on high temperature wear of both untreated and heat treated A357 alloy and DPS composites can be carried out to evaluate their performance at elevated temperatures.
- Hot rolling of A357 composites wherein one can study the effect of rolling orientation and the effect of rolling percentage reduction to produce a surface with uniform thickness and grain refinement. Texture evolution in hot-rolled composites can be studied using electron backscatter diffraction (EBSD) technique to understand the possible mechanisms responsible for mechanical or tribological behavior of these materials.
- Investigation of thermal properties of hot rolled DPS composites to check their suitability for possible applications in engine components employed in the automotive sector.
- Investigation of erosion-corrosion of hot rolled DPS composites using air-jet erosion and slurry erosion test rigs to check their performance for possible applications in pipeline components employed in construction and transportation industry.

REFERENCES

- Archard, J. (1953) "Contact and rubbing of flat surfaces." *J Appl Phys.*, 24(8),981–988.
- Arsenault, R. J., and Shi, N. (1986) "Dislocation Generation Due to Differences between the Coefficients of Thermal Expansion." *Materials Science and Engineering.*, 81 , 175-187.
- Apelian, D., Shivkumar, S., and Sigworth, G. (1989) "Fundamental aspects of heat treatment of cast Al-Si-Mg alloys." *AFS Trans .*, 97:727–742.
- Arsenault, R., and Everett, R. (1991) "Tensile and compressive properties of metal matrix composites"., *Ed., Academic Press .*, 4. 133–167.
- Anderson, S. J., Zandbergen M. W., Jansen J., Traeholt C., Undal U., and Rieso O. (1998) "The crystal structure of the β' phase in Al–Mg–Si alloys.", *Acta Mater.*, 46(9), 3283–3298.
- ASTM Handbook (2002) "Standard Practice for Heat Treatment of Aluminum Alloy Castings from all Processes". B917.
- Arpon, R., Molina, J.M., Saravanan, R.A., Garcia-Cordovilla, C., Louis, E., and Narciso, J., (2003) "Thermal expansion behaviour of aluminium/SiC composites with bimodal particle distributions"., *Acta Materialia.*, 51(11) , 3145-3156.
- Akhter, R., Ivanchev, L., and Burger, H. (2007) "Effect of pre/post T6 heat treatment on the mechanical properties of laser welded SSM cast A356 aluminium alloy." *Mater. Sci. Eng. A*,447(1–2), 192–196.
- Abouei, V., Shabestari, S.G., and Saghafian, H. (2010) "Dry sliding wear behaviour of hypereutectic Al–Si piston alloys containing iron-rich intermetallics." *Mater. Charact.* 61(11), 1089–1096.

Asl, K.M., Masoudi, A., and Khomamizadeh, F. (2010) “The effect of different rare earth elements content on microstructure, mechanical and wear behavior of Mg–Al–Zn alloy.” *Mater. Sci. Eng. A.*, 527 (7-8), 2027–2035.

Ahmed, A., Neely, A.J., and Shankar, K.(2011) “Experimental comparison of the effects of nanometric and micrometric particulates on the tensile properties and fracture behavior of Al Composites at room and elevated temperatures”. *Metallurgical and Materials Transactions A.*, 42A ,795-815.

Ajith Kumar, K. K., Abhilash Viswanath., Rajan, T. P. D., Pillai, U. T. S., and Pai, B. C. (2014) “Physical, Mechanical, and Tribological Attributes of Stir-Cast AZ91/SiCp Composite”, *Acta Metall. Sin. (Engl. Lett.)*, 27(2), 295-305.

Aykut Canakci., Fazlı Arslan., and Temel Varol. (2014) “Physical and mechanical properties of stir casting processed AA2024/B₄Cp composites”, *Science and Engineering of Composite Materials.*, 21(4) , 505-515.

Arora, R., Kumar, S., Singh, G., Pandey O.P. (2015) “Influence of particle size and temperature on the wear properties of rutile-reinforced aluminium metal matrix composite”, *Journal of Composite Materials.*, 49(7) ,843-852.

Arora, R., Kumar, S., Singh, G., and Pandey O.P. (2015) “Role of Different Range of Particle Size on Wear Characteristics of Al–Rutile Composites”, *Particulate Science and Technology*, 33(3), 229-233.

Amne elahi, M., and Shabestari, S.G. (2016) “Effect of various melt and heat treatment conditions on impact toughness of A356 aluminum alloy”, *Transactions of Nonferrous Metals Society of China.*, 26(4), 956-965.

Avinash, L., Ramprabhu, T., and Bontha, S. (2016) “The Effect on the dry sliding wear behavior of gravity cast A357 reinforced with dual size silicon carbide particles”, in *Applied Mechanics and Materials.*, 829, 83–89.

Abdulwahab, M., Umaru, O.B., Bawa, M.A., Jibo, H.A. (2017) “Microstructural and thermal study of Al-Si-Mg/melon shell ash particulate composite”, *Results in Physics.*, 7, 947-954.

Alberta Aversa., Lorusso, M., Trevisan, F., Ambrosio, E P., Calignano, F., Manfredi, D., Biamino, S., Fino, P., Lombardi, M., and Matteo Pavese. (2017) “Effect of Process and Post-Process Conditions on the Mechanical Properties of an A357 Alloy Produced via Laser Powder Bed Fusion”, *Metals.*,7(2), 68.

Aluminium and its alloys (2015) - Designation www.azom.com/article.

Biswas, S.K., and Pramila Bai B.N. (1986) “Dry wear of aluminium graphite particle composites”, *Wear.*, 68(3), 347-358.

Bloyce, A., and Summers, J. (1991) “Static and dynamic properties of squeeze-cast A357-SiC particulate Duralcan metal matrix composite”, *Mater. Sci. Eng. A.*, 135, 231–236.

Bindumadhavan, P.N., Heng Keng Wah, and Prabhakar, O. (2001) “Dual particle size (DPS) composites: effect on wear and mechanical properties of particulate metal matrix composites”, *Wear.*, 248(1-2),112-120.

Blaza Stojanovic., and Lozica Ivanovic., (2015) “Application of aluminium hybrid composites in automotive industry”, *Technical Gazette.*, 22 (1), 247-251.

Badizi, R.M., Askari-Paykani, M., Parizad, A., and Shahverdi, H.R. (2018) “Effects of Electromagnetic Frequency and SiC Nanoparticles on the Microstructure Refinement and Mechanical Properties of Al A357-1.5 wt.% SiC Nanocomposites”, *International Journal of Metal casting.*, 12 ,565-573.

Berg, J.S. (2011) “Composite material advances in the golf industry”, *Proceedings, International Conference on Composite Materials.*, 338.

Bembalge, O., and Panigrahi S. (2018) “Development and strengthening mechanisms of bulk ultrafine grained AA6063/SiC composite sheets with varying reinforcement size ranging from nano to micro domain”, *J. Alloys Compd.*, 766, 355–372.

Chou, T.W., Kelly, A., and Okura, A. (1985) “Fibre-reinforced metal-matrix composites.” *Composites*. 16 (3),187-206.

Christman, T., and Suresh, S. (1988) “Microstructural development in an aluminum alloy-SiC whisker composite”, *Acta Metall.*, 36(7), 1691–1704.

Cottu, J.P, Couderc, J.J., Viguier, B., and Bernard, L, (1992).”Influence of SiC reinforcement on precipitation and hardening of a metal matrix composite.” *Journal of Materials Science.*, 27, 3068-3074.

Chung, S., and Hwang B. H. (1994) “A microstructural study of the wear behaviour of SiCp/Al composites”, *Tribol. Int.*, 27(5), 307–314.

Cocen, U., Onel, K., and Ozdemir, I. (1997) “Microstructures and age hardenability of Al-Si-Mg based composites reinforced with particulate SiC”, *Composites Science and Technology*, 57, 801-808.

Chawla, K.K. (1998) “Metal Matrix Composites. In: Composite Materials”. *Springer.*, New York, NY, 164-211.

Chakrabarti, D.J., and Laughlin, D.E. (2004) “Phase relations and precipitation in Al–Mg–Si alloys with Cu additions”, *Prog. Mat. Sci.*, 49, 389–410.

Chawla, N., and Chawla, K.K. (2006) “Metal-Matrix Composites in Ground Transportation”, *Journal of Metals.*, 58(11), 67-70.

Czerwinski, F. (2008) “Magnesium Injection Molding”, *Springer.*, New York.

Ceschini, L., Morri, A., Gamberini A., and Messieri, S. (2009) “Correlation between ultimate tensile strength and solidification microstructure for the sand cast A357 aluminium alloy”, *Mater. Des.*, 30(10), 4525–4531.

Chu, K., Jia, C., Liang, X., Chena, H., and Guo, H. (2009) “The thermal conductivity of pressure infiltrated SiC_p/Al composites with various size distributions: Experimental study and modeling”, *Materials and Design* 30., 3497-3503.

- Campbell, F.C. (2010) “Structural Composite Materials”, *ASM International*.
- Chawla, K.K. (2012) “Composite Materials: Science and Engineering”, 3rd Edn, *Springer*, New York.
- Chacko, M., and Nayak, J. (2014) “Aging behaviour of 6061 Al-15 Vol% SiC composite in T4 and T6 treatments”, *Int. J. Chem. Mol. Nucl. Mater. Metall. Eng.*, 8(3), 195–198.
- Chen, Hao X., Wang, Y., and Zhao, K. (2014) “In-situ observation of tensile fracture in A357 casting alloys”, *J. Mater. Sci. Technol.*, 30, 139-145.
- Colley, L. J., Wells, M. A., and Poole, W. J. (2014) “Microstructure–strength models for heat treatment of Al–Si–Mg casting alloys I: microstructure evolution and precipitation kinetics”, *Canadian Metallurgical Quarterly.*, 53(2), 125-137.
- Colley, Leo, J., Mary Wells, A., and Warren, J. Poole. (2014) “Microstructure–yield strength models for heat treatment of Al–Si–Mg casting alloys II: modelling microstructure and yield strength evolution”, *Canadian Metallurgical Quarterly*, 53(2), 138-150.
- Çam, S., Demir, V., and Ozyurek, D. (2016). “Wear Behaviour of A356/TiAl₃ in Situ Composites Produced by Mechanical Alloying”, *Metals.*, 6 ,34.
- Cai, C., Geng H., Wang S., Gong B., and Zhang, Z. (2018) “Microstructure Evolution of AlSi10Mg (Cu) Alloy Related to Isothermal Exposure”, *Materials*, 11(5), 809.
- Churyumov, A.Y., and Mohamed, I.A. (2019) “Microstructure and mechanical properties of composite materials based on the Al-Si-Mg system reinforced with SiC particles and obtained by pressure crystallization”, *Metal Science and Heat Treatment.*, 60 ,571-573.

- Christensen, R.M. (2005) “Mechanics of Composite Materials”, *Dover Publications.*, New York.
- Dieter, G.E. (1986). “Mechanical Metallurgy”, 3rd Edn., *Mc Graw-Hill Book Co.*, New York.
- Davis, J.R. (1993) “Aluminium and aluminium alloys”, *ASM International.*, 88-120.
- Deuis, R.L., Subramanian C., and Yellup J.M. (1997) “Dry sliding wear of aluminium composites”, - a review, *Comp. Sci. Technol.*, 57, 415-435.
- Dwivedi, D.K., Arjun, T.S., Thakur, P., Vaidya, H., and Singh, K. (2004) “Sliding wear and friction behaviour of Al–18% Si–0.5% Mg alloy”, *J. Mater. Proc. Technol.*, 152 323-328.
- Debdas, Roy., Bikramjit, Basu., and Amitava Basu Mallick. (2005) “Tribological properties of Tialuminide reinforced Al-based in situ metal matrix composite”, *Intermetallics.*, 13 733–740.
- Das, S., Mondal, D.P., Sawla, S., and Ramakrishnan, N. (2008) “Synergic effect of reinforcement and heat treatment on the two-body abrasive wear of an Al-Si alloy under varying loads and abrasive sizes”, *Wear.*, 264, 47–59.
- Das B, Eswar Prasad K, Ramamurthy U., Rao CNR. (2009) “Nano-indentation studies on polymer matrix composites reinforced by few layer grapheme”, *Nanotechnology.*, 20(12):125705.
- Deng, K.K., Wu, K., Wu, Y.W., Nie, K.B., and Zheng, M.Y. (2010) “Effect of submicron size SiC particulates on microstructure and mechanical properties of AZ91 magnesium matrix composites”, *J. Alloys Compd.*, 504, 542.
- Deng, K., Shi, J., Wang, C., Wang, X., Wu, Y., Nie, K., and Wu, K. (2012) “Microstructure and strengthening mechanism of bimodal size particle reinforced magnesium matrix composite”, *Composite Part A.*, 43 1280-1284.

- Dipti Kanta Das., Purna Chandra Mishra., Saranjit Singh., and Swati Pattanaik. (2014) “Fabrication and heat treatment of ceramic reinforced aluminium matrix composites – a review”, *International Journal of Mechanical and Materials Engineering.*, 1(6) , 15.
- Dora Siva Prasad., Chintada Shoba., Nallu Ramanaiyah,(2014) “Investigations on mechanical properties of aluminum hybrid composites”, *Journal of Materials Research and Technology*, 3, (1), 79-85.
- Ding, G., Xie, C., Zhang, J., Zhang, G., Song, C., and Zhou, Z. (2015) “Modal analysis based on finite element method and experimental validation on carbon fibre composite drive shaft considering steel joints”, *Materials Research Innovations.*, 19, S5-748-S5-753.
- Dhandapani, S., Thiagarajan Rajmohan., Palanikumar, K., and Charan, M. (2016) “Synthesis and Characterization of Dual Particle (MWCT+B₄C) Reinforced Sintered Hybrid Aluminium Matrix Composites”, *Particulate Science and Technology.*, 34 , 255-262.
- Dmitri, Kopeliovich. (2012) “Classification of aluminum alloys” *Subs tech forum* https://www.substech.com/dokuwiki/doku.php?id=classification_of_aluminum_alloys#classification_of_cast_aluminum_alloysb.
- Edwards, G.A., Stiller, K., Dunlop, G.L., and Couper, M.J. (1998) “The Precipitation Sequence in Al-Mg-Si Alloys”, *Acta Mater.*, 46(11), 3893–3904.
- Es-Said, O.S., Lee, D., Pfof, W.D., Thompson, D.L., Patterson, M., Foyos, J., and Marloth, R. (2002) “Alternative heat treatments for A357-T6 aluminum alloy”, *Engineering Failure Analysis.*, 9, 99–107.
- Eva Tillová¹., Mária Chalupová., Lenka Kuchariková., Juraj Belan¹., and Denisa Závodská. (2018) “Selection of optimal solution heat treatment of the casting cylinder heads”, *MATEC Web of Conferences* 157, 02053.
- Flemings, M.C. (1981) “Continuous Production of Strip by Rheocasting”, DOE/CS/40310-T1, 1-35, MIT, Cambridge, MA.

Faccoli, M., Dioni, D., Cecchel, S., Cornacchia, G., and Panvini, A. (2017) “Optimization of heat treatment of gravity cast Sr-modified B356 aluminum alloy”, *Trans. Nonferrous Met. Soc., China* 27, 1698–1706.

Gu, J., Zhang, X., and Gu, M. (2004) “Analytical modeling of damping at micromechanical level in particulate-reinforced metal matrix composites”, *Materials Letters.*, 58, 1952-1955.

Gomes, J.R., Ramalho, A., Gaspar, M.C., and Carvalho, S.F. (2005) “Reciprocating wear tests of Al– Si/SiCp composites: A study of the effect of stroke length”, *Wear.*, 259 545–552.

Ganesh, V., and Chawla, N. (2005) “Effect of particle orientation anisotropy on the tensile behavior of metal matrix composites: experiments and microstructure-based simulation”, *Mater. Sci. Eng. A.*, 391, 1–2, 342–353.

Geoffrey, K., Sigworth Timothy., and Kuhn, A. (2007) “Grain Refinement of Aluminum Casting Alloys”, *International journal of metal casting.*, 115(2):1-12.

Gupta, A.K., Prasad, B.K., Pajnoo, R.K., and Das, S. (2012) “Effects of T6 heat treatment on mechanical, abrasive and erosive-corrosive wear properties of eutectic Al-Si alloy”, *Trans. Nonferr. Met. Soc., China*, 22, 1041–1050.

Ghandvar, H., Farahany, S., and Idris, J. (2015) “Wettability Enhancement of SiCp in Cast A356/SiCp Composite Using Semisolid Process”, *Materials and Manufacturing Processes.*, 30(12), 1442-1449.

Guan, L.Y., Li, B.L., Qi, P., Wei, L.J., and Nie. (2016) “Effect of Heat Treatment on the Microstructure and Property of Al-Si-Mg Alloy”, in *Materials Science Forum*, 850, 768–772.

Husking, F.M., Folgar Portillo, F., Wunderlin, R., and Mehrabian, R. (1982) “Composites of aluminium alloys: fabrication and wear behaviour”, *J. Mater. Sci.*, 17, 477-498.

Hutchings, I.M. (1987) “Wear by particulates”, *Chemical Engineering Science.*, 42, 869-878.

A. Handbook (1991) “Heat treating”, *ASM Int.*, 4, (10).

Hull, D., and Clyne, T.W. (1996) “An Introduction to Composite Materials”, 3rd Edition. Cambridge, UK: Cambridge Univ. Press.

Harrigan, W.C. (1998) “Commercial Processing of Metal Matrix Composites”, *Materials Science and Engineering A.*, 224 75-79.

Hunt, W.H., and Miracle, D.B. (2001) “Automotive applications of metal matrix composites”, In: Miracle DB, Donaldson SL, editors. *ASM Handbook: Composites*. Vol. 21. Materials Park, Ohio: *ASM International.*, 1029-1032.

Holleman, A.; Wiberg, E. (2001) “Inorganic Chemistry”; Academic Press: Berlin, Germany; New York, NY, USA.

Hassan, A.M., Alrashdan, A., Hayajneh, M.T., and Mayyas, A.T. (2009) “Prediction of density, porosity and hardness in aluminum–copper-based composite materials using artificial neural network”, *Journal of Materials Processing Technology.*, 209, 894-899.

Hasting, H.S., Froseth, A.G., Andersen, S.J., Vissers, R., Walmsley, J.C., Marioara, C.D., Danoix, F., Lefebvre, W., and Holmestad, R. (2009) “Composition of beta precipitates in Al–Mg–Si alloys by atom probe tomography and first principles calculations”, *J. Appl. Phys.*, 106, 123–527.

Hitesh, Bansal. (2011) “Wear Behavior of Aluminium Based Metal Matrix Composites Reinforced With Red Mud, SiC and Al₂O₃”, *M. Tech. Thesis, Thapar University, India*

Ibrahim, I.A., Mohamed, F.A., and Lavernia, EJ. (1991) “Particulate reinforced metal matrix composites — a review”. *J Mater Sci.*, 26,1137–1156.

John, E. hatch (1984) “Aluminium properties and physical metallurgy”, *American society of metals (ASM) International*.

Jinmin Zhanga Robert, J., Pereza Catherine, R., Wong Enrique, and Laverniaa, J. (1994) “Effects of secondary phases on the damping behaviour of metals, alloys and metal matrix composites”, *Materials Science and Engineering: R: Reports.*, 13 (8),325-389.

Jacquesson, M., Girard, A., M.-H. Vidal-sétif, R. and Valle. (2004) “Tensile and fatigue behavior of Al-based metal matrix composites reinforced with continuous carbon or alumina fibers: Part I. Quasi-Unidirectional composites”, *Metall. Mater. Trans.*, A 35 3289-3305.

Jin, P., Xiao, B.L., Wang, Q.Z., Ma, Z.Y., Liu, Y., and Li, S. (2011) “Effect of solution temperature on aging behavior and properties of SiC_p/Al–Cu–Mg composites”, *Materials Science and Engineering.*, A528 ,1504-1511.

Jiang, W., Fan, Z., Dai, Y., and Li, C. (2014) “Effects of rare earth elements addition on microstructures tensile properties and fractography of A357 alloy”, *Mater. Sci. Eng.*, A 597 237-244.

Jiaqing, Z., Ya, L., Haoping, P., Jianhua, W., and Xuping, S. (2017) “Spheroidization of Si in Al–12.6wt.%Si at eutectic temperature and its tensile properties”, *Mater. Res. Express.*, (4)106505.

Johannes Herrmann., Torsten Kuhn., Tjorven Mullenstedt., Siham Mittelstedt., and Christian Mittelstedt. (2018) “Closed-form approximate solutions for the local

buckling behaviour of composite laminated beams based on third order shear deformation theory”, *Advances in Mechanics of Materials and Structural Analysis.*, 80,175-205.

Kashyap, K.T., Murali, S., Raman, K.S., and Murthy, K.S.S. (1993) “Casting and heat treatment variable of Al-7% Si-Mg alloy”, *Material Science and Technology.*, 9, 89–203.

Kassim, S., Al-Rubaie., Humberto, N., Yoshimura, and Jose Daniel Biasoli de Mello. (1999) “Two body abrasive wear of Al–SiC composites”, *Wear.*, 233–235 444–454.

Kaczmar, J.W., Pietrzak, K., and Wlosinski, W. (2000) “Production and Application of Metal Matrix Composite Materials”, *Journal of Materials Processing Technology.*, 106 58-67.

Kainer, K.U. (2006) “Custom-made Materials for Automotive and Aerospace Engineering”, Wiley-VCH Verlag GmbH & Co. KGaA, Weinheim”, *Metal Matrix Composites.*

Kaw, A.K. “ (2006) Mechanics of composite materials”, Second Edition, Taylor & Francis Group, LLC.

Kireitseu, M.V., Tomlinson, G.R., Ivanenko, A.V., and Bochkareva, L.V. (2007) “Dynamics and Vibration Damping Behavior of advanced meso/nanoparticle reinforced composites”, *Mechanics of Advanced Materials and Structures.*, 14 , 603-617.

Khalifa, T.A, and Mahmoud, T.S. (2009). “Elevated temperature mechanical properties of Al Alloy AA6063/SiCp MMCs”, London: *Proceedings of the World Congress on Engineering.*

Kaur, K., and Pandey, O.P. (2010) “Dry Sliding Wear Behavior of Zircon Sand Reinforced Al–Si Alloy”, *Tribology Letters* 38 377–387.

Kumar, S., Sharma, V., Panwar, R.S., and Pandey, O.P. (2012) “Wear behavior of dual particle size (DPS) zircon sand reinforced aluminum alloy”, *Tribol. Lett.* 47, 231-251.

Kumar, S., Panwar, R.S., and Pandey, O.P. (2013) “Wear Behavior at High Temperature of Dual-Particle Size Zircon-Sand-Reinforced Aluminum Alloy Composite”, *Metallurgical and Materials Transactions A.*, 44,1548-1565.

Kumar, S., Panwar, R.S., and Pandey, O.P. (2013) “Effect of dual reinforced ceramic particles on high temperature tribological properties of aluminum composites”, *Ceramics International.*, 39, 6333-6342.

Khosroshahi, N.B., Mousavian, R.T., Khosroshahi, R.A., and Brabazon, D. (2015) “Mechanical properties of rolled A356 based composites reinforced by Cu-coated bimodal ceramic particles”, *Materials & Design.*, 83,678-688.

Kumar, S.D., Mandal, A., and Chakraborty, M. (2015) “On the age hardening behavior of thixoformed A356-5TiB₂ in-situ composite” *Materials Science & Engineering A.*, 636 , 254-262. 33.

Kumar, T.S., Subramanian, R., Shalini, S., and Angelo, P.C. (2016) “Age hardening behaviour of Al-Si-Mg alloy matrix/zircon and alumina hybrid composite”, *Journal of Scientific and Industrial Research.*, 75,89-94.

Kandemir, S. (2017) “Microstructure and mechanical properties of A357/SiC nano composites fabricated by ultrasonic cavitation-based dispersion of ball-milled nanoparticles”, *J. Compos. Mater.*, 51, 3,395–404.

Kandpal, B.C., Kumar, J., and Singh, H. (2017) “Fabrication and characterization of Al₂O₃/aluminium alloy 6061 composites fabricated by Stir casting”, *Materials Today: Proceedings.*, 4 2783–2792.

Kheirifard, R., Khosroshahi, N.B., Khosroshahi, R.A., Mousavian, R.T., and Brabazon, D. (2018) “Fabrication of A356-based rolled composites reinforced by Ni-

P-coated bimodal ceramic particles”, Proceedings of the Institution of Mechanical Engineers, Part L: *Journal of Materials: Design and Applications.*, 232, 803-815.

Kumar, R.V., Keshavamurthy, R., Perugu, C.S., Koppad, P.G., and Alipour, M. (2018) “Influence of hot rolling on microstructure and mechanical behaviour of Al6061-ZrB₂ in-situ metal matrix composites,” *Mater. Sci. Eng. A.*, 738344–352.

Karuppusamy, T., Velmurugan, C., and Thirumalaimuthukumaran, M. (2019) “Experimental study on the mechanical properties of heat-treated aluminium composites” *Mater. Res. Express.*, 6 096552.

Lendvai, J., Ungar, T., and Kovacs, I. (1974) “The Effect of the Temperature of Solution Treatment and Quenching on the Zone Formation Process in Al-Mg-Si Alloys”, *Mater. Sci. Eng.*, 16,85–89.

Levi, C.G., Abbaschian, G.J., Mehrabian, R., R.D. French and F. S. Hodi, Eds (1977) “Rheocasting: Proceedings of a workshop held at the army materials and mechanics research centre”, p. 41, Metals and Ceramics Information Center, (MCIC), Columbus, OH, 78(35), 1-145.

Lloyd, D.J., Lagace, H., McLeod, A., and Morris, P.L. (January 1989) “Microstructural aspects of aluminium silicon carbide particulate composites produced by a casting method”, *Materials Science and Engineering: A.*, 107, 73-80.

Li, Q., Zhang, G.D., Blucher, J.T., and Cornie, J.A. (1990) “Microstructure of the interface and inter fiber regions in P-55 reinforced aluminum alloys manufactured by pressure infiltration Proceedings of the Third International Conference on Composite Interfaces (ICCI-III) held on May 21-24, in Cleveland, Ohio, USA, 131-145.

Leonard, A.J., Perrin, C., and Rainforth, W.M. (1997) “Microstructural changes induced by dry sliding wear of a A357/SiC metal matrix composite”, *Materials Science and Technology.*, 13, 41-48.

- Lados, D.A., Apelian, D., and Wan, L. (2011) "Solution treatment effects on microstructure and mechanical properties of Al-(1 to 13 pct.)Si-Mg cast alloys" *Metallurgical and Materials Transactions B.*, 42,171-180.
- Lei, Z.B., Zhao, K., Wang, Y.G., and An, L.N. (2013) "Thermal expansion of Al matrix composites reinforced with hybrid micro-/nano-sized Al₂O₃ particles", *J. Mater. Sci. Technology*, 40,1-4.
- Li, B., Luo, B., He, K., Zeng, L., Fan, W., and Bai, Z. (2015) "Effect of aging on interface characteristics of Al-Mg-Si/SiC composites", *J. Alloys Compd.*, 649, 495-499.
- Li, N., Yan, H., and Wang, Z.W. (2018) "Effects of heat treatment on the tribological properties of SiCp/Al-5Si-1Cu-0.5Mg composite processed by electromagnetic stirring method", *Appl. Sci.*, 8, 372.
- Liu, Z., Dong, Z., Cheng, X., Zheng, Q., Zhao, J., and Han, Q. (2018) "On the Supplementation of Magnesium and Usage of Ultrasound Stirring for Fabricating In Situ TiB₂/A356 Composites with Improved Mechanical Properties", *Metallurgical and Materials Transactions A.*, 49,5585-5598.
- Liu, C., Ma, P., Zhan, L., Huang, M., and Li, J. (2018) "Solute Sn-induced formation of composite β'/β "precipitates in Al-Mg-Si alloy", *Scr. Mater.*, 155, 68-72.
- Lakshmikanthan, A., Bontha, S., Krishna, M., Koppad, P.G., and Ramprabhu, T. (2019) "Microstructure, mechanical and wear properties of the A357 composites reinforced with dual sized SiC particles", *J. Alloys Compd.*, 786, 570-580.
- Lakshmikanthan, A, et al., (2020) "The effect of heat treatment on the mechanical and tribological properties of dual size SiC reinforced A357 matrix composites", *J Mater Res Technol. Volume 9, Issue 3, May-June 2020*, 6434-6452.

- Manoharan, M., and Lewandowski, J. (1989) “In-situ deformation studies of an aluminum metal-matrix composite in a scanning electron microscope”, *Scr. Metall.*, 23,10,1801–1804.
- Matthews, F.L., and Rawlings, R.D. (1994) “Composite materials engineering and science”, *Glasgow, UK: Chapman and Hall*.
- Miyajima, T., and Iwai, Y. (2003) “Effects of reinforcements on sliding wear behavior of aluminum matrix composites”, *Wear* 255,606–616.
- Miracle, D.B. (2005) “Metal Matrix Composites - from Science to Technological Significance”, *Composites Science and Technology.*, 65 2526-2540.
- Montoya-Davila, M., Pech-Canul, M.A., and Pech-Canul, M.I. (2007) “Effect of bi- and trimodal size distribution on the superficial hardness of Al/SiC_p composites prepared by pressure less infiltration”, *Powder Technology.*, 176, 66-71.
- Mutasher, S.A., Sahari, B.B., Hamouda, A.M.S., and Sapuan, S.M. (2007) “Static and dynamic characteristics of a hybrid aluminium/composite drive shaft”, *Journal of Materials Design and Applications.*, 221, 63-75.
- Möller, H., Govender, G., and Stumpf, W.E. (2008) “Investigation of the T4 and T6 Heat Treatment Cycles of Semi-Solid Processed Aluminium Alloy A356”, *Bentham Science Publishers Ltd.*, 2, 11-18.
- Möller, H., Govender, G., and Stumpf, W.E. (2008) “The T6 heat treatment of Semi-solid Metal Processed Alloy A356”, *Open Mater Sci J.*, 2: 6-10.
- Myriounis, D., Hasan, S., and Matikas, T. (2008) “Heat treatment and interface effects on the mechanical behavior of SiC-particle reinforced aluminium matrix composites”, *J. ASTM Int.*, 5, 7, 1–10.

Maleque, M.A., and Karim, M.R. (2008) “Tribological behavior of dual and triple particle size SiC reinforced Al-MMCs: a comparative study”, *Industrial Lubrication and Tribology.*, 60,189-194.

Mazahery, A., and Ostadshabani, M. (2011) “Investigation on mechanical properties of nano-Al₂O₃- reinforced aluminum matrix composites”, *J Compos Mater.*, 45, 2579–2586.

Mohamed, A.M.A., and Samuel, F.H. (2012) “A Review on the Heat Treatment of Al-Si-Cu/Mg Casting Alloys in Heat Treatment: Conventional and Novel Applications”, *ed. F. Czerwinski, Intech Open.*, 55-72.

Ma, K., Wen, H., Hu, T., Topping, T.D., Isheim, D., Seidman, D.N., Lavernia, E.J., and Schoenung, J.M. (2014) “Mechanical behavior and strengthening mechanisms in ultrafine grain precipitation-strengthened aluminum alloy”, *Acta Mater.*, 62, 141–155

Maube, S.E., Wangombe, D.N., Maranga, S.M., and Kihui, J. M. (2014) “Effect of cooling rate and heat treatment on the microstructure and impact resistance of recycled aluminium sand cast alloy”, *J. Sustain. Res. Eng.*, 1, 1.

Mizuuchi, K., Inoue, K., Agari, Y., Sugioka, M., Tanaka, M., Takeuchi, T., Tani, J., Kawahara, M., Makino, Y., and Ito, M. (2014) “Bimodal and monomodal diamond particle effect on the thermal conductivity of diamond particle dispersed Al matrix composite produced by SPS”, *Materials Science Forum.*, 783-786, 2462-2467.

Menargues, S., Martín, E., Baile, M.T., and Picas, J.A. (2015) “New short T6 heat treatments for aluminium silicon alloys obtained by semisolid forming”, *Materials Science & Engineering.*, A 621,236–242.

Matthew J. Donachie., (2015) "A Guide to Engineering Selection of Titanium Alloys for Design" Volume I. Materials and Engineering Mechanics, Part 1. Materials, First published: 20 February ,<https://doi.org/10.1002/9781118985960.meh105>.

Mirjavadi S. S. *et al.*, (2017) “Influence of TiO₂ nanoparticles incorporation to friction stir welded 5083 aluminum alloy on the microstructure, mechanical properties and wear resistance”, *J. Alloys Compd.*, 712,795–803.

Mirjavadi S. S. *et al.*, (2017) “Effect of multi-pass friction stir processing on the microstructure, mechanical and wear properties of AA5083/ZrO₂ nanocomposites”, *J. Alloys Compd.*, 726,1262–1273.

Mirjavadi S. S. *et al.*, (2018) “Effect of hot extrusion and T6 heat treatment on microstructure and mechanical properties of Al-10Zn-3.5 Mg-2.5 Cu nanocomposite reinforced with graphene nanoplatelets”, *J. Manuf. Process.*, 36, 264–271.

Mohamed, M., Dawoud., Hosam., and Saleh, M. (2018) “Introductory Chapter: Background on Composite Materials”, *IntechOpen*, DOI: 10.5772/intechopen.80960. 1-11.

Manu Sam., Radhika, N., and Katru Pavan Sai. (2020) “Effect of heat treatment on mechanical and tribological properties of aluminum metal matrix composites” *Proceedings of the Institution of Mechanical Engineers, Part C: Journal of Mechanical Engineering Science.*, 1–12.

Matweb.com.2020.Matweb-The Online Materials Information Resource.[online] Available at :<<http://www.matweb.com/search/DataSheet.aspx?>

Nick Tucker., and Kevin Lindsey. (2002) “Introduction to Automotive Composites”, *Rapra Technology Ltd.*

Natarajan, N., Vijayarangan, S., and Rajendran, I. (2006) “Wear behaviour of A356/25SiC_p aluminium matrix composites sliding against automobile friction material”, *Wear.*, 261, 812-822.

Nturanabo, F., Masu, L.M., and Govender, G. (Aug 1, 2015) “Automotive light-weighting using aluminium metal matrix composites”, *In: Materials Science Forum.*, 828. Switzerland: *Trans Tech Publications Ltd.*, 485.

Naveen, K., Mahenderkar, T., Ram Prabhu., and Anil Kumar. (2016) “Nanocomposites Potential for Aero Applications”, *Indian Institute of Metals Series, Springer*, 1,391-411

Pashley, D.W., Jacobs, M.H., and Vietz, J. T. (1967) “The basic processes affecting two-step aging in an Al alloy”, *Phil. Mag.*, 16, 51–76.

Polmear, I. J. (1995) “Light Alloys: Metallurgy of the Light Metals” Wiley, 3rd Edition.

Pedersen, L., and Arnberg, L. (2001) “The effect of solution heat treatment and quenching rates on mechanical properties and microstructures in AlSiMg foundry alloys”, *Metall. Mater. Trans., A*, 32, 3, 525–532.

Pavan Kumar., Sanjay Soni., Rana, R.S., and Alok Singh. (2014) “Mechanical behavior and dry sliding wear response of al-si-sic particulate composite”, *Proceedings of 02nd ITR International Conference*, 07th September-2014, Bhubaneswar, ISBN: 978-93-84209-50-6.

Prabhu, T.R., Varma, V.K., and Vedantam, S. (2014) “Effect of SiC volume fraction and size on dry sliding wear of Fe/SiC/Graphite hybrid composites for high sliding speed applications”, *wear.*, 309 1-10.

Prabhu, T.R., Varma, V.K., and Vedantam, S. (2014) “Effect of reinforcement type, size, and volume fraction on the tribological behavior of Fe matrix composites at high sliding speed conditions”, *Wear.*, 309,247-255.

Pushpendra, K., Kushwaha., and Jyoti vimal. (2014) “Study of Vibration Analysis of Laminated Composite Plates Using FEM”, *International Journal of Advanced Mechanical Engineering.*, 4 (6),675-680.

Prabhu, T. R. (2016) “Effect of bimodal size particles reinforcement on the wear, friction and mechanical properties of brake composites”, *Tribol.-Mater. Surf. Interfaces.*, 10, 4,163–171.

Prabhu, T.R., Basavarajappa, S., Santhosh, R.B., Ashwini, S.M. (2017) “Tribological and mechanical behaviour of dual-particle (nanoclay and CaSiO₃)-reinforced E-glass-reinforced epoxy nanocomposites”, *Bulletin of Materials Science.*, 40, 107-116.

Prabhu, T.R., (2017) “Effects of ageing time on the mechanical and conductivity properties for various round bar diameters of AA 2219 Al alloy”, *Eng. Sci. Technol. Int. J.*, 20, 1, 133–142.

Prasad Reddy, A., Vamsi Krishna, P., Narasimha Rao, R., and Murthy, N.V. (2017) “Silicon Carbide Reinforced Aluminium Metal Matrix Nano Composites-A Review” *Materials Today: Proceedings.*, 4 3959–3971.

Pramod, S.L., Ravikirana., Rao, A.K.P., Murty, B.S., and Bakshi, S.R. (2019) “Microstructure and mechanical properties of as-cast and T6 treated Sc modified A356-5TiB₂ in-situ composite”, *Materials Science & Engineering A.*, 739, 383-394.

Rong, C., Iwabuchi, A., and Shimizu, T. (2000) “The effect of a T6 heat treatment on the fretting wear of a SiC particle-reinforced A356 aluminum alloy matrix composite”, *Wear.*, 238(2):110–119.

Rajesh Sharma., Anesh Kumar., and Dwivedi, D.K. (2006) “Influence of Solution Temperature on Microstructure and Mechanical Properties of Two Cast Al–Si Alloys”, *Materials and Manufacturing Processes.*, 21:3, 309-314.

Rao, R., Das, S., Mondal, D., and Dixit, G. (2009) “Dry sliding wear behaviour of cast high strength aluminium alloy (Al–Zn–Mg) and hard particle composites”, *Wear.*, 267,9– 10, 1688–1695.

Rao, R.N. and Das, S. (2010) “Wear coefficient and reliability of sliding wear test procedure for high strength aluminium alloy and composite”, *Mater. Des.*, 31 3227-3233.

Rajeev, V., Dwivedi, D., and Jain, S. (2010) “Effect of load and reciprocating velocity on the transition from mild to severe wear behavior of Al–Si–SiCp composites in reciprocating conditions”, *Mater. Des.*, 31, 10, 4951–4959.

Rao, R.N. and Das, S. (2011) “Effect of SiC content and sliding speed on the wear behaviour of aluminium matrix composites”, *Mater. Des.* 32 1066-1071.

Rao, R.N. and Das, S. (2011) “Effect of sliding distance on the wear and friction behavior of as cast and heat-treated Al–SiCp composites”, *Mater. Des.*, 32 3051-3058.

Rao, C., Selvaraj, N., Veereshkumar, G. (2012) “Studies on mechanical and dry sliding wear of Al6061–SiC composites”, *Compos B Eng.*,43(3), 1185–1191.

Rajmohan, T., Palanikumar, K., and Ranganathan, S. (2013) “Evaluation of mechanical and wear properties of hybrid aluminium matrix composites”, *Trans. Nonferrous Met. Soc., China* 23 2509-2517.

Rahimipour, M.R., Tofigh, A.A., Shabani, M.O., and Davami, P. (2014) “The enhancement of Wear Properties of Compo-Cast A356 composites reinforced with Al₂O₃ nano particulates”, *Tribology in Industry.*, 36,220-227.

Ram Prabhu, T., Murugan, M., Chiranth, B.P., Mishra R.K., Rajini, N., Marimuthu, P., Dinesh Babu, P. and Suganya, G. (2019) “Effects of Dual-Phase Reinforcement Particles (Fly Ash + Al₂O₃) on the Wear and Tensile Properties of the AA 7075 Al Alloy Based Composites” *J. Inst. Eng. India Ser. D* 100, 29–35.

Robles-Hernandez, R.C., Herrera Ramírez, J.M., and Mackay, R. (2017) “Al-Si Alloys: Automotive, Aeronautical, and Aerospace Applications”, *Springer International Publishing AG*.

Ragab, K.A., Bouazara, M., and Chen, X.G. (2018) “Influence of Thermal Aging Parameters on the Characteristics of Aluminum Semi-Solid Alloys”, *Metals.*, 8,746.

Ravikumar, M. Reddappa, H. and Suresh, R. (2018), “Study on Mechanical and Tribological Characterization of Al₂O₃/SiCp Reinforced Aluminum Metal Matrix Composite”, *Silicon*, 10,6,2535–2545.

Radhika, N., Sasikumar, J., and Arulmozhivarman, J. (2020) “Tribo-Mechanical Behaviour of Ti-Based Particulate Reinforced As-Cast and Heat Treated A359 Composites”, *Silicon*.

Schoene, C., and Scala, E. 1 (1970) “Multiple necking phenomena in metal composites”, *Metallurgical Transactions.*, 3466-3469.

Suh, N.P. (1977) “An overview of the delamination theory of wear”, *Wear.*, 44, 1–16.
Shivkumar, S., Ricci, S., Steenhoff, B., Apelian, D., and Sigworth, G. (1989) “An experimental study to optimize the heat treatment of A356 alloy”, *Trans. Am. Found. Soc.*, 97, 791–800.

Shivkumar, S., Ricci, S., Jr, Keller, C., and Apelian, D. (1990) “Effect of solution treatment parameters on tensile properties of cast aluminum alloys”, *Journal of Heat Treating.*, 8: 63–70.

Shivkumar, S., Keller, C., Trazzera, M., and Apelian, D. (1990) “Precipitation hardening in A356 alloys”, in *Production, Refining, Fabrication and Recycling of Light Metals*, Elsevier., 264–278.

Samuel, A.M., Liu, H., and Samuel, F.H. (1993) “Effect of melt, solidification and heat treatment processing parameters on the properties of Al-Si-Mg/SiC(p) composites”, *Journal of Materials Science.*, 28 ,6785-6798.

Stephenson, T.F., Bell, J.A.E., Drew, R.A.L., and Mostaghaci, H. (Eds.), (1993) “Development and Applications of Ceramics and New Metal Alloys”, *CIM, Montreal.*, 51.

Song, W., Krauklis, P., Mouritz, A., and Bandyopadhyay, S. (1995) “The effect of thermal ageing on the abrasive wear behaviour of age-hardening 2014 Al/SiC and 6061 Al/SiC composites”, *wear.*, 185, 1–2, 125–130.

Stachowiak, G.W., and Batchelor, A.W. (2001) “Engineering Tribology”, 2nd Edition., Butterworth- Heinemann, Boston, MA, .740.

Surappa, M.K. (2003) “Aluminium matrix composites: Challenges and opportunities. *Sadhana*”. 28 (Parts 1 & 2):319-334.

Suresh, K.R., Niranjana, H.B., Martin Jebaraj, P., and Chowdiah, M.P. (2003) “Tensile and wear properties of aluminium composites”, *Wear* 225,638-642.

Shen, H.S. (2009) “Nonlinear bending of functionally graded carbon nanotube-reinforced composite plates in thermal environments”, *Composite Structures.*, 91, 9-19.

Sjolander, E., and Seifeddine, S. (2010) “The heat treatment of Al–Si–Cu–Mg casting alloys”, *J.Mater. Process. Technol.*, 210, 10, 1249–1259.

Suresha, S., Sridhara, B.K. (2010) “Effect of silicon carbide particulates on wear resistance of graphitic aluminium matrix composites”, *Mater Des.*, 31:4470–7.

Sankaranarayanan, S., Jayalakshmi, S., and Gupta, M. (2011) “Effect of addition of mutually soluble and insoluble metallic elements on the microstructure, tensile and compressive properties of pure magnesium”, *Mater. Sci. Eng. A.*, 530, 149–160.

Sanaty-Zadeh, A., and Rohatgi, P.K. (2012) “Corrigendum to: Comparison between current models for the strength of particulate-reinforced metal matrix nanocomposites with emphasis on consideration of Hall–Petch effect”, *Mater. Sci. Eng. A.*, 531 112–118.

- Sharma, V., Kumar, S., Panwar, R.S., and Pandey, O.P. (2012) “Microstructural and wear behavior of dual reinforced particle (DRP) aluminum alloy composite”, *J. Mater. Sci.*, 476633-6646.
- Shen, M., Wang, X., Li, C., Zhang, M., Hu, X., Zheng, M., and Wu, K. (2013) “Effect of bimodal size SiC Particulates on microstructure and mechanical properties of AZ31B magnesium matrix composites”, *Mater. Des.*, 52,1011-1017.
- Show, B.K. Mondal, D.K. and Maity, J. (2014) “Wear behavior of a novel aluminum-based hybrid composite”, *Mater. Trans.*, A 45 1027-1040.
- Sharma, A., Kumar, S., Singh, G., and Pandey, O.P. (2015) “Effect of Particle Size on Wear Behavior of Al–Garnet Composites”, *Particulate Science and Technology* 33, 234-239.
- Singh, R., Podder, D., and Singh, S. (2015) “Effect of Single, Double and Triple Particle Size SiC and Al₂O₃ Reinforcement on Wear Properties of AMC Prepared by Stir Casting in vacuum mould”, *Transactions of the Indian Institute of Metals.*, 68 , 791-797.
- Singh J., and Chauhan, A. (2016) “Overview of wear performance of aluminium matrix composites reinforced with ceramic materials under the influence of controllable variables”, *Ceram. Int.*, 42, 1, 56–81.
- Sardar, S., Karmakar, S.K. and, Das, D. (2018) “Tribological Properties of Al 7075 Alloy and 7075/Al₂O₃ Composite Under Two-Body Abrasion”, *A Statistical Approach, Journal of Tribology.*, 140 051602.
- Sethuram, D., Koppad, P.G., Shetty, H., Alipour, M., and Kord, S. (2018) “Characterization of graphene reinforced Al-Sn nanocomposite produced by mechanical alloying and vacuum hot pressing”, *Mater. Today Proc.*, 5, 11, 24505–24514.

Sharma, S., Nanda, T., and Pandey, O. (2018) “Effect of dual particle size (DPS) on dry sliding wear behaviour of LM30/sillimanite composites”, *Tribol. Int.*, 123, 142–154.

Subramanian R, Kannan G, Nanjappan N, and Vijayan K. (2018) “Analysis of temperature distribution in wire electrical discharge machine on hybrid Al-MMCs”, *Indian Journal of Engineering and Materials Sciences.*, 25,301-306.

Sardar, S., Pradhan, S.K., Karmakar, S.K. and Das, D. (2019) “Modeling of abraded surface Roughness and Wear Resistance of Aluminum matrix Composites”, *Journal of Tribology.*, 141, 071601.

Taya, M.R.J., Arsenault, (1989) “Metal Matrix Composites: Thermomechanical behavior”, Pergamon Press”, Inc., 1st Edition, New York.

Tan, Y.-H., Lee, S.-L., and Lin, Y.-L. (1995) “Effects of Be and Fe additions on the microstructure and mechanical properties of A357. 0 alloys”, *Metall. Mater. Trans. A.*, 26, 5, 1195–1205.

Thostenson, E.T., Ren, Z., and Chou, T-W. (2001) “Advances in the science and technology of carbon nanotubes and their composites”, A review. *Composites Science and Technology.*, 61(13),1899-1912.

M.L. Ted Guo, Chi.-Y.A. Tsao, (2002) “Tribological behavior of aluminum/SiC/nickel-coated graphite hybrid composites”, *Mater. Sci. Eng. A.*, 333 134-145.

Tekmen, C., and Cocen, U. (2003) “Role of cold work and SiC volume fraction on accelerated age hardening behavior of Al-Si-Mg/SiC composites”, *Journal of Materials Science Letters.*, 22 , 1247-1249.

Uthayakumar, M., Aravindan, S., and Rajkumar, K. (2013) “Wear performance of Al–SiC–B₄C hybrid composites under dry sliding conditions”, *Mater. Des.*, 47 456-464.

- Umaru, O., Abdulwahab, M., Tokan, A., Bello, A., and Umar, H. (2016) “Effect of double thermal ageing treatment on the mechanical properties of Al–Cu–Mg/3% rice husk ash composite”, *Results Phys.*, vol. 6, 342–345.
- Vennett, R.M., Wolf, S.M., and Levitt, A.P. (1970) “Multiple necking of tungsten fibers in a brass-tungsten composite”, *Metallurgical Transactions.*, 1 1569-1575.
- Vencl, A., Rac, A., and Bobić, I. (2004) “Tribological behaviour of Al-based MMCs and their application in automotive industry”, *Tribology in Industry.*, 26, 3-431-38.
- Villars, P.; Cenzual, K. Pearson’s (2007) “Crystal Data ®: Crystal Structure Database for Inorganic Compounds”; ASM International: Materials Park, OH, USA.
- Vieira, A.C., Sequeira, P.D., Gomes, J.R., and Rocha, L.A. (2009) “Dry sliding wear of Al alloy/SiCp functionally graded composites: influence of processing conditions”, *Wear* 267,585–592.
- Veeresh Kumar, G.B., Rao, C.S.P., and Selvaraj N. (2011) “Mechanical and tribological behavior of particulate reinforced aluminum metal matrix composites – a review”, *Journal of Minerals & Materials Characterization & Engineering.*, 10 (1), 59-91.
- Viswanatha, B.M., Prasanna Kumar, M., Basavarajappa, S., and Kiran, S. (2013) “Mechanical property evaluation of A356/SiCp/Gr metal matrix composites”, *Journal of Engineering Science and Technology.*, 8(6) 754 – 763.
- Wang, Q.G., and Davidson, C.J. “Solidification and precipitation behaviour of Al-Si-Mg casting alloys”, *Journal of Materials Science.*, 36, 739–750 (2001).
- Wang, Q., and Davidson, C. (2001) “Solidification and precipitation behaviour of Al-Si-Mg casting alloys”, *J. Mater. Sci.*, 36, 3, 739–750.

Wang, Q., Min, F., and Zhu, J. (2013) “Microstructure and thermo-mechanical properties of SiC_p/Al composites prepared by pressure less infiltration”, *J. Mater. Sci.: Mater. Elect.*, 24 , 1937-1940.

Wang, T., Zheng, Y., Chen, Z., Zhao, Y., and Kang, H. (2014) “Effects of Sr on the microstructure and mechanical properties of in situ TiB₂ reinforced A356 composite”, *Materials and Design.*, 64, 185-193.

Withers, P.J. “Metal matrix composite. In: Access Science”. United Kingdom: McGraw-Hill Education; 2014. DOI: 10.1036/1097-8542.418600.

Wang, T., Zhao, Y., Chen, Z., Zheng, Y., and Kang, H. (2015) “The bimodal effect of La on the microstructures and mechanical properties of in-situ A356–TiB₂ composites”, *Mater. Des.*, 85, 724–732.

Wang, C., Deng, K., Zhou, S., and Liang, W. (2016) “Dynamic recrystallization behavior of bimodal size SiC_p-reinforced Mg matrix composite during hot deformation”, *Acta Metallurgica Sinica (English Letters)*, 29 , 527-537.

Ye, H. (2003) “An overview of the development of Al-Si-Alloy based material for engine applications”, *J. of Materi Eng and Perform.*, 12, 288–297.

Yamanoglu, R., Karakulak, E., Zeren, A., and Zeren, M. (2013) “Effect of heat treatment on the tribological properties of Al–Cu–Mg/nanoSiC composites”, *Mater. Des.*, 49, 820– 825.

Yong, Hu., Tong Wu., Yue Guo., Wenyang Wang., Mingkai Song., Long Qian., Hongwei Zhao., and Maosen, Wang. (2019) “Effects of T6 Treatment, Tensile Temperature, and Mass Fraction of SiC on the Mechanical Properties of SiC_p/6061Al Composites”, *Materials.*, 12, 1602.

Zum Gahr K.H. (1987) “Microstructure and wear of materials, Elsevier”, Amsterdam, .8-17.

Zhou, W., and Xu, Z.M. (1997) “Casting of SiC Reinforced Metal Matrix Composites”, *Journal of Materials Processing Technology.*, 63, 358-363.

Zulfia, A., Atkinson, H.V., Jones, H., and King, S. (1999) “Effect of hot isostatic pressing on cast A357 aluminium alloy with and without SiC particle reinforcement”, *Journal of Materials Science* 34,4305-4310.

Zhu, H., Guo, J., and Jia, J. (2001) “Correlation of the aging characteristics and deformation behavior of A357 alloy”, *J. Mater. Eng. Perform.*, 10, 2,186–191.

H.M. Zakaria (2014) “Microstructural and corrosion behavior of Al/SiC metal matrix composites”, *Ain Shams Engineering Journal.*, 5, 831-838.

Zhang, L., Qiu, F., Wang, J., Wang, H., and Jiang, Q. (2015) “Microstructures and mechanical properties of the Al2014 composites reinforced with bimodal sized SiC particles”, *Materials Science & Engineering A.*, 637,70-74.

Zhu, J.B. and Yan, H. “Fabrication of an A356/fly-ash-mullite interpenetrating composite and its wear properties”, *Ceram. Int.*, 2017, 43, 12996–13003.

Zulfia, A., Zhakiah, T., Dhaneswara, D., and Sutopo. (2017) “Characteristics of Al-Si-Mg Reinforced SiC Composites produced by stir casting route”, *IOP Conf. Series: Materials Science and Engineering.*, 202 ,012089.

Zhang, W.Y., Du, Y.H., and Zhang, P. (2019) “Vortex-free stir casting of Al-1.5 wt% Si-SiC composite”, *Journal of Alloys and Compounds.*, 787, 206-215.

List of Publications based on Ph.D. Research Work

Sl. No.	Title of the paper	Authors (in the same order as in the paper. Underline the Research Scholar's name)	Name of the Journal/ Conference, Vol., No., Pages	Month, Year of Publication	Category *
1	The effect on the dry sliding wear behavior of gravity cast A357 reinforced with dual size silicon carbide particles	<u>L Avinash</u> , T Ram Prabhu, Srikanth Bontha	Applied-Mechanics-and-Materials Volume 829, March 2016, Pages 83-89 doi:10.4028/www.scientific.net/AMM.829.83 Online: 2016-03-30 © 2016 Trans Tech Publications, Switzerland	March ,2016	1
2	Microstructure, mechanical and wear properties of the A357 composites reinforced with dual sized SiC particles	<u>Avinash Lakshmikanthan</u> , Srikanth Bontha, M.Krishna, Praveennath G.Koppad T.Ramprabhu	Journal of Alloys and Compounds Volume 786, 25 May 2019, Pages 570-580. https://doi.org/10.1016/j.jallcom.2019.01.382 .(SCI, Scopus ,Impact Factor:4.650)	May, 2019	1
3	The effect of heat treatment on the mechanical and tribological properties of dual size SiC reinforced A357 matrix composites	<u>Avinash Lakshmikanthan</u> , T Ram Prabhu, Udayagiri Sai Babu, Praveennath G. Koppad, Manoj Gupta, M. Krishna, Srikanth Bontha	Journal of Materials Research and Technology-2020 ;9(3),Pages 6434-6452 https://doi.org/10.1016/j.jmrt.2020.04.027 (SCIE, Scopus ,Impact Factor:5.289)	May, 2020	1
4	Free Vibration Analysis of A357 Alloy Reinforced with Dual Particle Size Silicon Carbide Metal Matrix Composite Plates Using Finite Element Method	<u>A Lakshmikanthan</u> , V Mahesh, RT Prabhu, MGC Patil, S Bontha	Archives of Foundry Engineering , Volume 21, Issue 1/2021, 101 – 112, DOI: 10.24425/afe.2021.136085 (ESCI, Scopus ,Impact Factor:0.79)	March,2021	1

*Category: 1: Journal paper, full paper reviewed 2: Journal paper, Abstract reviews 3: Conference/Symposium paper, full paper reviewed.
4: Conference/Symposium paper, abstract reviewed 5: Others (including papers in Workshops, NITK Research Bulletins, Short notes etc.)

 03/06/2021

Avinash L
Research Scholar
Name & Signature, with Date

 (03/06/2021)

Dr. Srikanth Bontha
Research Guide
Name & Signature, with Date

BIO-DATA

Name: Avinash L
Father's Name: Lakshmikanthan M
Mother's Name: Hemalatha G
Date of Birth: 02 August 1988
Nationality: Indian
Marital Status: Married
Permanent Address: # 27 ,1st Main, Nanjappa Layout
Adjacent to Krishna Garden, Mylasandra
Bangalore-560059, Karnataka, India.
Mobile Number: +91-8951762147
Email ID: avinash.laks01@gmail.com

Educational Qualification:

Qualification	University/Board	Year of Passing
Ph.D. (Mechanical Engineering)	National Institute of Technology Karnataka (NIT-K)	Defended on June 3 rd , 2021
M. Tech. (Mechanical Engineering)	Acharya Institute of Technology, VTU, Bangalore, Karnataka, India.	2013
B.E. (Mechanical Engineering)	Bangalore Institute of Technology VTU, Bangalore, Karnataka, India	2010

Work Experience:

Name of the Employee	Designation	Duration
Nitte Meenakshi Institute of Technology	Assistant Professor	August 2014 to Present